AFCRL-69-0203

Scattering by a Spherical Shell with a Circular Aperture

by

Seichoong Chang and Thomas B. A. Senior
The University of Michigan
Radiation Laboratory
201 Catherine Street
Ann Arbor, Michigan 48108

April 1969

Scientific Report No. 5
Contract F19628-68-C-0071
Project 5635, Task 563502
Work Unit 56350201

Contract Monitor: Philipp Blacksmith
Microwave Physics Laboratory

Prepared For

Air Force Cambridge Research Laboratories
Office of Aerospace Research
L. G. Hanscom Field
Bedford, Massachusetts 01730

Submitted in partial fulfillment of the requirements for a Doctorate in Electrical Engineering at The University of Michigan.

ABSTRACT

The electromagnetic scattering behavior of a spherical shell with a circular aperture is studied. The shell is assumed to be perfectly conducting and infinitesimally thin, and is illuminated by a plane wave symmetrically incident upon the aperture. The application of the method of least square error, as well as of a modified version is fully discussed. The modification consists of the separating out of the appropriate surface field behavior near to the edge of the aperture, and was carried out to overcome the slow convergence and marginal accuracy of the original approach. The marked improvement provided by the modification is clearly evident.

The numerical study is limited to the frequency range corresponding to $0.8 \leq ka \leq 4.85$, where a is the radius of the spherical shell, and numerical values of the backscattering cross sections for the aperture angle $\theta_0=30^o$ and 90^o, as well as for the tangential field components over the boundary surface for $\theta_0=30^o$, are presented. To verify these results and to obtain more physical insight into the scattering behavior, experimental measurements of the backscattering cross sections for $\theta_0=15^o, 30^o, 45^o, 60^o$ and 90^o, and of the current components for $\theta_0=30^o$, are obtained using two sets of spherical shell models. It is observed that a spherical shell with aperture-on incidence has, in general, a higher backscattering cross section than a solid sphere except at values of ka near to the cavity resonances, where marked reductions occur. A comparison of the numerical and experimental results is made.

ACKNOWLEDGMENTS

The authors wish to thank Professor Chen-To Tai for his continuous advice and assistance and also express their appreciation to Mrs. Austra Liepa for computer programming. They also wish to thank Mr. Harold Hunter for the hand computations and Mr. August Antones for the technical illustrations.

TABLE OF CONTENTS

	Page No.
CHAPTER ONE: INTRODUCTION	1
CHAPTER TWO: THEORETICAL FORMULATION	5
2.1 Geometry and Field Expressions	5
2.2 Various Approaches	10
2.3 Method of Least Square Error	14
2.4 Modified Formulation	25
CHAPTER THREE: NUMERICAL RESULTS	37
3.1 Results of the Original Method	37
3.2 Results of the Modified Method	41
CHAPTER FOUR: EXPERIMENTAL RESULTS	67
4.1 Experimental Models and Facilities	67
4.2 Backscattering Measurements	69
4.3 Surface Field Measurements	71
CHAPTER FIVE: DISCUSSION	87
CHAPTER SIX: CONCLUSIONS	95
REFERENCES	96
APPENDIX A: EVALUATION OF $L_{mn}(\theta_o)$ AND $S_{mn}(\theta_o)$	99
APPENDIX B: APPLICATION OF THE GAUSS-SEIDEL ITERATIVE METHOD	104
APPENDIX C: SERIES REPRESENTATION OF EDGE SINGULARITY (Derivation of Eqs. (2.72) and (2.73)	110
APPENDIX D: COMPUTER PROGRAM	114

LIST OF ILLUSTRATIONS

Figure	Title	Page
2-1	Coordinate System.	6
3-1	Computed Backscattering Cross Sections of a Spherical Shell with $\theta_o = 30^o$.	38
3-2a	Computed Amplitude of the θ-Component of the Electric Field at R = a for ka = 2.0 with $\theta_o = 30^o$.	39
3-2b	Computed Amplitude of the ϕ-Component of the Electric Field at R = a for ka = 2.0 with $\theta_o = 30^o$.	40
3-3	Computed Backscattering Cross Sections of a Spherical Shell with $\theta_o = 30^o$.	42
3-4	Computed Backscattering Cross Sections of a Spherical Shell with $\theta_o = 90^o$.	43
3-5a	Computed Amplitude of the θ-Component of the Electric Field at R = a for ka = 2.0 with $\theta_o = 30^o$.	46
3-5b	Computed Amplitude of the ϕ-Component of the Electric Field at R = a for ka = 2.0 with $\theta_o = 30^o$.	47
3-6a	Computed Amplitude of the θ-Component of the Electric Field at R = a for ka = 2.5 with $\theta_o = 30^o$.	48
3-6b	Computed Amplitude of the ϕ-Component of the Electric Field at R = a for ka = 2.5 with $\theta_o = 30^o$.	49
3-7a	Computed Amplitude of the θ-Component of the Electric Field at R = a for ka = 2.75 with $\theta_o = 30^o$.	50
3-7b	Computed Amplitude of the ϕ-Component of the Electric Field at R = a for ka = 2.75 with $\theta_o = 30^o$.	51
3-8a	Computed Amplitude of the θ-Component of the Electric Field at R = a for ka = 4.0 with $\theta_o = 30^o$.	52
3-8b	Computed Amplitude of the ϕ-Component of the Electric Field at R = a for ka = 4.0 with $\theta_o = 30^o$.	53

Figure	Title	Page
3-9a	Computed $T_1^{II}(\theta)$ Component for ka = 2.0 with $\theta_o = 30^o$ (Using the Modified Least Square Method with M = 20), and $T_1(\theta)$ Component of a Solid Sphere.	54
3-9b	Computed $T_1^{II}(\theta)$ Component for ka = 2.0 with $\theta_o = 30^o$ (Using the Modified Least Square Method with M = 20), and $T_2(\theta)$ Component of a Solid Sphere.	55
3-10a	Computed $T_1^{II}(\theta)$ Component for ka = 2.5 with $\theta_o = 30^o$ (Using the Modified Least Square Method with M = 20), and $T_1(\theta)$ Component of a Solid Sphere.	56
3-10b	Computed $T_1^{II}(\theta)$ Component for ka = 2.5 with $\theta_o = 30^o$ (Using the Modified Least Square Method with M = 20), and $T_2(\theta)$ Component of a Solid Sphere.	57
3-11a	Computed $T_1^{II}(\theta)$ Component for ka = 2.75 with $\theta_o = 30^o$ (Using the Modified Least Square Method with M = 20), and $T_1(\theta)$ Component of a Solid Sphere.	58
3-11b	Computed $T_1^{II}(\theta)$ Component for ka = 2.75 with $\theta_o = 30^o$ (Using the Modified Least Square Method with M = 20), and $T_2^{II}(\theta)$ Component of a Solid Sphere.	59
3-12a	Computed $T_1^{II}(\theta)$ Component for ka = 4.0 with $\theta_o = 30^o$ (Using the Modified Least Square Method), and $T_1(\theta)$ Component of a Solid Sphere.	60
3-12b	Computed $T_2^{II}(\theta)$ Component for ka = 4.0 with $\theta_o = 30^o$ (Using the Modified Least Square Method), and $T_2(\theta)$ Component of a Solid Sphere.	61
3-13a	Computed Bistatic Scattering Pattern of a Spherical Shell for ka = 2.5 with $\theta_o = 30^o$. Dashed Line is for a Solid Sphere. $\phi = 0$.	63
3-13b	Computed Bistatic Scattering Pattern of a Spherical Shell for ka = 2.5 with $\theta_o = 30^o$. Dashed Line is for a Solid Sphere. $\phi = \pi/2$.	64
3-14a	Computed Bistatic Scattering Pattern of a Spherical Shell for ka = 2.7 with $\theta_o = 30^o$. Dashed Line is for a Solid Sphere. $\phi = 0$.	65

Figure	Title	Page
3-14b	Computed Bistatic Scattering Pattern of a Spherical Shell for ka = 2.7 with $\theta_o = 30^o$. Dashed Line is for a Solid Sphere. $\phi = \pi/2$.	66
4-1	Experimental Models. a) Diameter D = 2.55", Aperture Angle $\theta_o = 30^o$, b) D = 2.55", $\theta_o = 90^o$, c) D = 3.09", $\theta_o = 30^o$, d) D = 3.09", $\theta_o = 90^o$.	68
4-2	Surface Field Measurement Facility as Viewed From the Position of the Illuminating Antenna.	70
4-3	Measured Backscattering Cross Section of a Spherical Shell with $\theta_o = 15^o$ (-*-) and Theoretical Backscattering Cross Section of a Solid Sphere (- - -).	72
4-4	Measured Backscattering Cross Section of a Spherical Shell with $\theta_o = 30^o$.	73
4-5	Measured Backscattering Cross Section of a Spherical Shell with $\theta_o = 45^o$.	74
4-6	Measured Backscattering Cross Section of a Spherical Shell with $\theta_o = 60^o$.	75
4-7	Measured Backscattering Cross Section of a Spherical Shell with $\theta_o = 90^o$.	76
4-8	Backscattering Patterns of a Spherical Shell with $\theta_o = 30^o$ (——) and a Solid Sphere (- - -). Horizontal Polarization.	77
4-9a	Measured and Computed $T_1^{II}(\theta)$ Component for ka = 2.0 with $\theta_o = 30^o$ and M = 20.	79
4-9b	Measured and Computed $T_2^{II}(\theta)$ Component for ka = 2.0 with $\theta_o = 30^o$ and M = 20.	80
4-10a	Measured and Computed $T_1^{II}(\theta)$ Component for ka = 2.75 with $\theta_o = 30^o$ and M = 20.	81
4-10b	Measured and Computed $T_2^{II}(\theta)$ Component for ka = 2.75 with $\theta_o = 30^o$ and M = 20.	82
4-11a	Measured and Computed $T_1^{II}(\theta)$ Component for ka = 3.0 with $\theta_o = 30^o$ and M = 20.	83
4-11b	Measured and Computed $T_2^{II}(\theta)$ Component for ka = 3.0 with $\theta_o = 30^o$ and M = 20.	84

Figure	Title	Page
4-12a	Measured and Exact $T_1(\theta)$ Component of a Solid Sphere for ka = 3.0.	85
4-12b	Measured and Exact $T_2(\theta)$ Component of a Solid Sphere for ka = 3.0.	86
5-1	Computed (—) and Measured (x x x) Backscattering Cross Sections of a Spherical Shell for $\theta_o = 30^o$. Dashed Line is for a Solid Sphere.	88
5-2	Computed (—) and Measured (x x x) Backscattering Cross Sections of a Spherical Shell for $\theta_o = 90^o$.	89

CHAPTER I

INTRODUCTION

In the general area of electromagnetic scattering, impedance loading has received much attention as one of the more promising techniques for radar cross section control, especially for the reduction of cross sections in the resonance region. This technique provides a wide degree of control over the scattering behavior by varying the loading impedance which is introduced over a restricted portion of the scattering surface by means of a cavity structure, lumped elements, or transmission line with associated loads.

The loading technique has been known since the early 1920's (O'Neil, 1928; Meissner, 1929), when it was common practice to use lumped inductors and capacitors to detune the supporting structures of a transmitting antenna and, hence, reduce the fields radiated from them. However, Iams (1950) in his patent of "Radio Wave Conducting Device" was the first to apply the impedance loading technique for the control of scattering properties at microwave frequencies. He used a coaxial loading together with a dielectric coating to effect a wide-band reduction of the scattering from metallic posts in a parallel-plate assembly. More recently, several investigators, Ås and Schmitt (1958), Gerbes and Kearns (1963), and Chen and Liepa (1964a, 1964b) have studied the scattering cross section of a thin center-loaded cylinder. Chen and Liepa presented a complete analysis of the back scattered fields for arbitrary angles of incidence on a thin cylinder of length ℓ, $0 < \ell < 2\lambda$, and fully demonstrated the capability of loading for cross section reduction. In fact, it was shown that for every value of ℓ/λ within the chosen range, a loading exists for which the cross section is almost zero.

For thick cylinders, Sletten et al (1964) have shown experimentally that impedance loading is still effective using center-loaded cylinders approximately $\lambda/2$ in length and $\lambda/8$ and $\lambda/4$ in diameter. A theoretical treatment of loading of moderately thick cylinders was later given by Chen (1965). Liepa and Senior (1966) have studied the scattering behavior of a metallic sphere loaded with a circumferential slot in a plane perpendicular to the direction of incidence. Later Chang and Senior (1967) extended the analysis to the general case of arbitrary angle of incidence.

In most applications so far, the loading technique employed has been the simple one of backing a slot with a cavity. From all of these previous studies, it would appear that the realization of the loading required to give (for example) zero back scattering cross section over a significant frequency range is very difficult to attain due to the peculiar frequency characteristics of the required loading. It was found that the susceptive components of the optimum loading (for zero back scattering) has primarily a negative frequency slope and is almost precisely opposite to the behavior characteristic of any passive network. As a result, any simple loading device such as a radial cavity-backed slot will be severly limited in its frequency bandwidth, and more sophisticated techniques, non-linear or active, would have to be employed in the synthesis of the loading to increase the bandwidth. This is the main reason why the impedance loading method has not yet found any operational application to radar camouflage. To increase the bandwidth, active circuit synthesis approaches, using NIC's (negative impedance converter) or operational amplifiers, seem to be attractive and are currently receiving attention. The use of a non-uniform transmission line, filled with a lossy dielectric or even ferrite meterials, could also be considered. Nevertheless, it is clear that the nature of the load required for zero back scattering is a function of the cavity design, and in order to obtain some

basic understanding of the impedance loading problem, it is desirable that the aperture-cavity aspect of the loading problem be studied in more detail.

The present work is directed at the problem of an infinitely thin, perfectly conducting spherical shell with a circular aperture of arbitrary angle cut into the shell. In fact, therefore, we have a sphere loaded with a spherical cavity coupled through a circular aperture. It was felt that the loading with a spherical cavity could be particularly appropriate to the sphere geometry since the fields inside and outside the spherical shell are separable in the same spherical coordinate system, suggesting that the natural resonances of the cavity could be convenient for manipulating the scattered field.

The problem of a perfectly conducting spherical shell with a conical hole, which degenerates to our case when the shell thickness approaches zero, has already been rigorously formulated by Uslenghi and Zich (1965). However, when the shell thickness approaches zero, the formulation breaks down due to the edge singularity at the edge of the aperture. For a spherical shell whose angular extent is less than π, so that the shell is less than a hemisphere, Blore and Musal (1965) and Raybin (1965) have estimated the back scattering cross sections for incidence on the convex side at or near to the direction of the symmetry. The procedure was a high frequency one in which the physical optics value of the specular contribution was modified by the addition of an edge diffracted contribution, and the results obtained were reasonably close to measured data. For the case of a hemispherical shell with an electric dipole at its center, Yen (1959) has obtained a low frequency solution by using an iterative process in solving the integral equation for the current density induced on the shell. To the authors' knowledge, however, the electromagnetic problem of a spherical shell which is larger than a hemisphere has not been treated in either an exact or approximate sense as far as concrete answers are concerned. The present work, therefore, has both practical and theoretical interest.

Electromagnetic scattering by separable bodies has been treated extensively in the literature with presentation of both exact and approximate solutions. However, when these bodies are cut so that only parts of them still remain -- such as a spherical shell segment -- the scattering mechanism is, in general, drastically changed, and difficulties also arise in the treatment. For the acoustic problem, Sommerfeld (1949) has used the method of least square error to obtain a system of linear equations for the diffraction coefficients; and more recently Thomas (1963) obtained a low frequency solution using an iteration method developed by Williams (1962).

In the analysis, we assume that a plane electromagnetic wave is incident symmetrically on the aperture, and several different approaches to the solution of this problem are discussed. The most promising one is the method of least square error. This is described in detail, and the method is then modified in order to separate out the correct surface field behavior at the edge of the aperture. The numerical results of the modified method are compared with those of the original method and a marked improvement is shown.

To obtain some insight into the scattering behavior of a spherical shell and also to confirm the theoretical results, a series of surface and backscattering measurements were made in the range $0.8 \leq ka \leq 4.85$ for the aperture angle $\theta_o = 15^o$, 30^o, 45^o, 60^o and 90^o. It was found that the spherical cavity plays quite a significant role in the modification of the scattering, especially at frequencies near to those of the cavity resonance. The numerical results are compared with the experimental results for $\theta_o = 30^o$ and 90^o, and good agreement is found.

CHAPTER II

THEORETICAL FORMULATION

2.1 Geometry and Field Expressions

Let us consider an infinitely thin, perfectly conducting spherical shell with its center at the origin, 0 and the spherical segment given by $R = a$, $\theta_0 < \theta \leq \pi$ as shown in Fig. 2-1. In Fig. 2-1 the spherical polar coordinates (R, θ, ϕ) are related to the Cartesian coordinates (x, y, z) by the usual transformation $x = R\sin\theta\cos\phi$, $y = R\sin\theta\sin\phi$, $z = R\cos\theta$. Assuming a linearly polarized plane electromagnetic wave is incident in the direction of the negative z-axis with its electric vector parallel to the x-axis, the incident field becomes

$$\begin{aligned} \underline{E}^i &= \hat{x} e^{jkz}, \\ \underline{H}^i &= -\hat{y} Y e^{jkz}, \end{aligned} \tag{2.1}$$

where k is the propagation constant, Y is the intrinsic admittance of free space, and a time factor $e^{j\omega t}$ has been suppressed.

The incident field of Eq. (2.1) can be expressed in terms of spherical vector wave functions as follows:

$$\underline{E}^i = \sum_{n=1}^{\infty} j^n \frac{2n+1}{n(n+1)} \left[\underline{M}_{o1n}^{(1)} - j\underline{N}_{e1n}^{(1)} \right],$$

$$\underline{H}^i = jY \sum_{n=1}^{\infty} j^n \frac{2n+1}{n(n+1)} \left[\underline{N}_{o1n}^{(1)} - j\underline{M}_{e1n}^{(1)} \right], \tag{2.2}$$

where $\underline{M}^{(1)}$ and $\underline{N}^{(1)}$ are the spherical wave functions (Stratton, 1941):

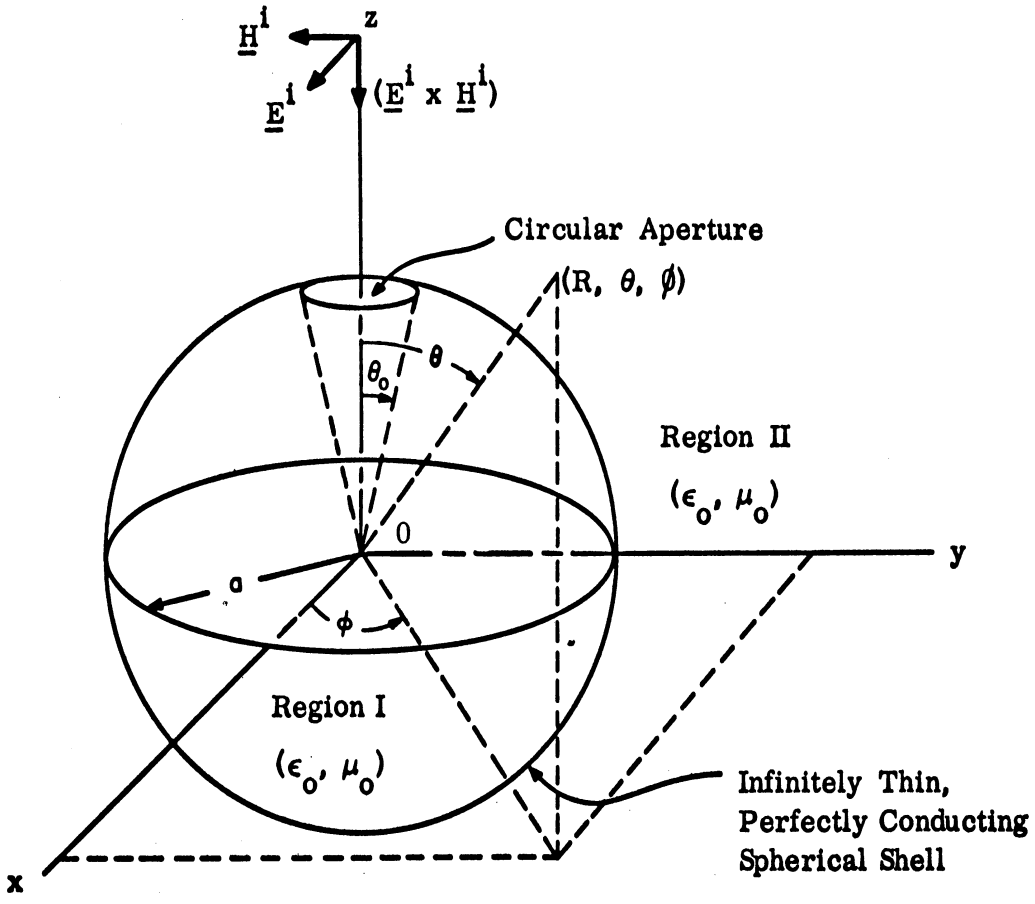

FIG. 2-1: COORDINATE SYSTEM

$$\underline{M}^{(1)}_{\substack{e\\o}mn} = \mp m \frac{\psi_n(kR)}{kR} \frac{P_n^m(\cos\theta)}{\sin\theta} \begin{matrix}\sin\\\cos\end{matrix} m\phi\,\hat{\theta} -$$

$$- \frac{\psi_n(kR)}{kR} \frac{\partial}{\partial\theta} P_n^m(\cos\theta) \begin{matrix}\cos\\\sin\end{matrix} m\phi\,\hat{\phi} \ ,$$

$$\underline{N}^{(1)}_{\substack{e\\o}mn} = n(n+1) \frac{\psi_n(kR)}{(kR)^2} P_n^m(\cos\theta) \begin{matrix}\cos\\\sin\end{matrix} m\phi\,\hat{R} +$$

$$+ \frac{\psi_n'(kR)}{kR} \frac{\partial}{\partial\theta} P_n^m(\cos\theta) \begin{matrix}\cos\\\sin\end{matrix} m\phi\,\hat{\theta} \mp$$

$$\mp m \frac{\psi_n'(kR)}{kR} \frac{P_n^m(\cos\theta)}{\sin\theta} \begin{matrix}\sin\\\cos\end{matrix} m\phi\,\hat{\phi} \ ,$$

with

$$\psi_n(kR) = kR\, j_n(kR) \ .$$

$j_n(kR)$ is the spherical Bessel function of order n, and the prime denotes differentiation with respect to the entire argument. $P_n^m(\cos\theta)$ is the Legendre function of degree n and order m as defined, for example, by Stratton.

The total field due to the presence of the spherical shell can now be expressed in forms similar to those for the incident field, but with unknown amplitude coefficients. Thus in region I ($R \leq a$):

$$\underline{E}^I = \sum_{n=1}^{\infty} \left[A_n \underline{M}^{(1)}_{oln} - jB_n \underline{N}^{(1)}_{eln} \right] ,$$

$$\underline{H}^I = jY \sum_{n=1}^{\infty} \left[A_n \underline{N}^{(1)}_{oln} - jB_n \underline{M}^{(1)}_{eln} \right] ; \qquad (2.3)$$

and in region II ($R \geq a$):

$$\underline{E}^{II} = \underline{E}^{i} + \underline{E}^{s} \quad , \quad \underline{H}^{II} = \underline{H}^{i} + \underline{H}^{s} \tag{2.4}$$

where

$$\underline{E}^{s} = \sum_{n=1}^{\infty} \left[C_n \underline{M}_{o1n}^{(4)} - jD_n \underline{N}_{e1n}^{(4)} \right] ,$$

$$\underline{H}^{s} = jY \sum_{n=1}^{\infty} \left[C_n \underline{N}_{o1n}^{(4)} - jD_n \underline{M}_{e1n}^{(4)} \right] . \tag{2.5}$$

Here, the subscript s designates the scattered field. From the requirement that the scattered field represent an outgoing wave at infinity, $\underline{M}^{(4)}$ and $\underline{N}^{(4)}$ differ from $\underline{M}^{(1)}$ and $\underline{N}^{(1)}$ in having $\psi_n(kR)$ replaced by $\zeta_n(kR) = kR\, h_n^{(2)}(kR)$, where $h_n^{(2)}(kR)$ is the spherical Hankel function of the second kind. The coefficients A_n, B_n, C_n and D_n are determined by the boundary conditions, which require the continuity of the field through the aperture and zero tangential electric field at the surface of the perfectly conducting spherical segment, and the edge condition (Meixner, 1949). Once those coefficients are obtained, all the field quantities are determined everywhere.

Since the surface current density on the spherical shell is directly related to the tangential magnetic field, H_θ and H_ϕ are of primary concern to us. They can be expressed, in a notation similar to that of Kazarinoff and Senior (1962) as follows:

at the inside shell surface:

$$H_\theta^I(a,\theta,\phi) = Y \sin\phi \; T_1^I(\theta) \quad , \tag{2.6}$$

$$H_\phi^I(a,\theta,\phi) = Y \cos\phi \; T_2^I(\theta) \quad , \tag{2.7}$$

where

$$T_1^I(\theta) = j \frac{1}{ka} \sum_{n=1}^{\infty} \left[A_n \psi_n'(ka) \frac{\partial}{\partial\theta} P_n^1(\cos\theta) + jB_n \psi_n(ka) \frac{P_n^1(\cos\theta)}{\sin\theta} \right] ,$$

(2.8)

$$T_2^I(\theta) = j\,\frac{1}{ka}\sum_{n=1}^{\infty}\left[A_n\psi_n'(ka)\,\frac{P_n^1(\cos\theta)}{\sin\theta} + jB_n\psi_n(ka)\frac{\partial}{\partial\theta}P_n^1(\cos\theta)\right], \tag{2.9}$$

and at the outside shell surface:

$$H_\theta^{II}(a,\theta,\phi) = Y\sin\phi\,T_1^{II}(\theta)\ , \tag{2.10}$$

$$H_\phi^{II}(a,\theta,\phi) = Y\cos\phi\,T_2^{II}(\theta)\ , \tag{2.11}$$

where

$$T_1^{II}(\theta) = j\,\frac{1}{ka}\sum_{n=1}^{\infty}\left\{\left[C_n\zeta_n'(ka) + j^n\frac{2n+1}{n(n+1)}\psi_n'(ka)\right]\frac{\partial}{\partial\theta}P_n^1(\cos\theta)\right.$$
$$\left. + j\left[D_n\zeta_n(ka) + j^n\frac{2n+1}{n(n+1)}\psi_n(ka)\right]\frac{P_n^1(\cos\theta)}{\sin\theta}\right\}, \tag{2.12}$$

$$T_2^{II}(\theta) = j\,\frac{1}{ka}\sum_{n=1}^{\infty}\left\{\left[C_n\zeta_n'(ka) + j^n\frac{2n+1}{n(n+1)}\psi_n'(ka)\right]\frac{P_n^1(\cos\theta)}{\sin\theta}\right.$$
$$\left. + j\left[D_n\zeta_n(ka) + j^n\frac{2n+1}{n(n+1)}\psi_n(ka)\right]\frac{\partial}{\partial\theta}P_n^1(\cos\theta)\right\}. \tag{2.13}$$

In the far zone the expressions for the scattered field can be obtained by replacing $\zeta_n(kR)$ and $\zeta_n'(kR)$ by the leading terms of their asymptotic expansions for large kR, viz.:

$$\zeta_n(kR) \sim j^{n+1}e^{-jkR}\ ,$$

$$\zeta_n'(kR) \sim j^n e^{-jkR}\ .$$

The transverse components of the scattered electric field in the far zone then become

$$E_\theta = j\cos\phi \frac{e^{-jkR}}{kR} S_1^s(\theta) \tag{2.14}$$

$$E_\phi^s = -j\sin\phi \frac{e^{-jkR}}{kR} S_2^s(\theta) \tag{2.15}$$

where $S_1^s(\theta)$ and $S_2^s(\theta)$ are defined as the far field scattering amplitudes and are given by

$$S_1^s(\theta) = \sum_{n=1}^{\infty} j^n \left[C_n \frac{P_n^1(\cos\theta)}{\sin\theta} - D_n \frac{\partial}{\partial\theta} P_n^1(\cos\theta) \right] \tag{2.16}$$

$$S_2^s(\theta) = \sum_{n=1}^{\infty} j^n \left[C_n \frac{\partial}{\partial\theta} P_n^1(\cos\theta) - D_n \frac{P_n^1(\cos\theta)}{\sin\theta} \right] . \tag{2.17}$$

The radar cross section is therefore

$$\sigma(\theta,\phi) = \sigma_\theta(\theta,\phi) + \sigma_\phi(\theta,\phi) , \tag{2.18}$$

where $\sigma_\theta(\theta,\phi)$ and $\sigma_\phi(\theta,\phi)$ are the component cross sections given by

$$\sigma_\theta(\theta,\phi) = \frac{\lambda^2}{\pi} \cos^2\phi \left| S_1^s(\theta) \right|^2 , \tag{2.19}$$

$$\sigma_\phi(\theta,\phi) = \frac{\lambda^2}{\pi} \sin^2\phi \left| S_2^s(\theta) \right|^2 . \tag{2.20}$$

2.2 Various Approaches

There are various ways of approaching this kind of boundary value problem. One of the common approaches is by means of integral equations in terms of the unknown aperture field. For our problem, if we introduce two unknown functions for the tangential components of the electric field in the aperture, we obtain two coupled integral equations involving infinite series. These integral equations can be converted to an infinite set of linear independent equations if we express each unknown function as a series

of functions orthogonal over the aperture ($0 \leq \theta \leq \theta_o$). The coefficients in the series are, of course, unknown and are to be determined. When in the course of numerical computation each infinite series is approximated by a finite series, the final (approximated) results depend on the choice of the orthogonal functions used for the series expansions for the aperture field components. For a good approximation a proper function with an unknown constant may be introduced to represent each unknown function, in addition to the series of the proper orthogonal functions; and by appropriate choice, it would appear that the resulting series could be made to converge rapidly. It is, however, not easy to find the optimum proper functions even though the method of trial and error might lead to ones which are adequate.

In the second method, we can apply the variational technique to obtain the backscattering cross section. The variational method has received a good deal of attention in antenna and scattering problems involving simple geometries such as a thin disc or wire, in which this method is capable of giving an accurate approximate solution with a minimum of computational labor (Schwinger, 1947; Tai, 1952).

We consider a scalar function U defined by

$$U = \iint_S \underline{E}^i \cdot \underline{J} \, dS \quad , \tag{2.21}$$

where $\underline{J}$ is the surface current density at the conducting surface S. The function U can then be expressed in the form (Mentzer, 1955)

$$U = \frac{Y}{jk} \frac{\left[\iint_S \underline{E}^i \cdot \underline{J} \, dS\right]^2}{\iint_S \iint_{S'} \underline{J} \cdot \overline{\overline{G}}_o \cdot \underline{J}' \, dS' \, dS} \quad , \tag{2.22}$$

where G_o is the free space Green's dyadic function given by

$$\overline{\overline{G}}_o(\underline{R}/\underline{R}') = \left(\overline{\overline{I}} + \frac{\nabla\nabla}{k^2}\right) \frac{1}{4\pi |\underline{R} - \underline{R}'|} e^{-jk|\underline{R} - \underline{R}'|} . \qquad (2.23)$$

It is easily shown that the expression for U in Eq. (2.22) is stationary with respect to variations of the surface current density, $\underline{J}$, about the correct value. The relation between the function U and the backscattering cross section can be written as

$$\sigma(o) = \frac{k^2}{4\pi Y^2} \frac{|U|^2}{|E^i|^4} , \qquad (2.24)$$

so that, for the computation of the backscattering cross section, it is sufficient to get an accurate determination of U.

For the case of the spherical shell segment, the total current density, $\underline{J}^t$ is expressed as a sum of the current densities inside and outside shell segment, and Eq. (2.22) then becomes

$$U = \frac{Y}{jk} \frac{\left[\int_o^{2\pi}\int_{\theta_o}^{\pi} \underline{E}^i \cdot \underline{J}^t \sin\theta \, d\theta \, d\phi\right]^2}{\int_o^{2\pi}\int_{\theta_o}^{\pi}\left[\int_o^{2\pi}\int_{\theta_o}^{\pi} \underline{J}^t \cdot \overline{\overline{G}}_o \, \underline{J}^{t'} \sin\theta' \, d\theta' \, d\phi'\right] \sin\theta \, d\theta \, d\phi} \qquad (2.25)$$

A variational solution can be obtained by writing the current density in the form

$$\underline{J}^t = \sum_{n=1}^{M} a_n \underline{\phi}_n \qquad (2.26)$$

where the functions $\underline{\phi}_n$ are independent of each other. The coefficients,

$a_1, a_2, \ldots a_M$, are determined from the linear system of M equations;

$$\frac{\partial U}{\partial a_i} = 0 \quad , \quad i = 1,2,\ldots M \quad . \tag{2.27}$$

As noted in connection with the integral equation approach, the accuracy of the approximation again depends on the choice of the functions, $\phi_1, \phi_2, \ldots \phi_n$.

Thus, either approach requires a careful study of the physics of the problem to guide the choice of a proper set of expansion functions, and it proved extremely difficult to find such functions for the present problem. The presence of the cavity is the main complicating factor, but other points which should be noted are:

1) In the integral equation approach the scattering coefficients are obtained indirectly after the aperture field is obtained. This requires additional computations.

2) Although the variational technique can lead to a good approximation to the backscattering cross section, the approximation of the near field quantities is, often, not reliable. Moreover, since the numerical solution of each approach mentioned above is carried out by reducing it to a matrix equation, it is rather convenient and preferable to obtain the matrix formulation directly from the physical characterization of the boundary value problem.

Such an approach has been followed by Uslenghi and Zich (1965) for the case of a perfectly conducting spherical shell with a conical hole. The problem has been rigorously formulated by applying the usual mode matching techniques. When the shell thickness approaches zero, the problem degenerates to our case, but the formulation, unfortunately, breaks down due to the edge effect of the aperture. As a similar but alternative approach, the method of least square error can be applied in matching modes through the

boundary. The method is, in a sense, somewhat akin to the variational method and provides the best approximated matching through the boundary in the sense of least squares. The application of the least square method will now be considered.

2.3 Method of Least Square Error

We here seek to find the scattering amplitude coefficients, C_n and D_n, in Eq. (2.5) by using the method of least square error. We shall proceed to the matrix formulation by imposing the boundary conditions directly to the field expressions given in Eqs. (2.3) through (2.5).

The condition of zero tangential electric field at the surface of the perfectly conducting sphere segment ($\hat{R} \times \underline{E}^I = \hat{R} \times \underline{E}^{II} = 0$ for $\theta_o < \theta \leq \pi$) requires that for $\theta_o < \theta \leq \pi$:

$$\sum_{n=1}^{\infty} \left[A_n \psi_n(ka) \frac{P_n^1(\cos\theta)}{\sin\theta} - jB_n \psi_n'(ka) \frac{\partial}{\partial\theta} P_n^1(\cos\theta) \right] = 0 , \qquad (2.28)$$

$$\sum_{n=1}^{\infty} \left[A_n \psi_n(ka) \frac{\partial}{\partial\theta} P_n^1(\cos\theta) - jB_n \psi_n'(ka) \frac{P_n^1(\cos\theta)}{\sin\theta} \right] = 0 , \qquad (2.29)$$

$$\sum_{n=1}^{\infty} \left[C_n \zeta_n(ka) \frac{P_n^1(\cos\theta)}{\sin\theta} - jD_n \zeta_n'(ka) \frac{\partial}{\partial\theta} P_n^1(\cos\theta) \right] = G_1(\theta) , \qquad (2.30)$$

$$\sum_{n=1}^{\infty} \left[C_n \zeta_n(ka) \frac{\partial}{\partial\theta} P_n^1(\cos\theta) - jD_n \zeta_n'(ka) \frac{P_n^1(\cos\theta)}{\sin\theta} \right] = G_2(\theta) , \qquad (2.31)$$

where

$$G_1(\theta) = -\sum_{n=1}^{\infty} j^n \frac{2n+1}{n(n+1)} \left[\psi_n(ka) \frac{P_n^1(\cos\theta)}{\sin\theta} - j\psi_n'(ka) \frac{\partial}{\partial\theta} P_n^1(\cos\theta) \right], \tag{2.32}$$

$$G_2(\theta) = -\sum_{n=1}^{\infty} j^n \frac{2n+1}{n(n+1)} \left[\psi_n(ka) \frac{\partial}{\partial\theta} P_n^1(\cos\theta) - j\psi_n'(ka) \frac{P_n^1(\cos\theta)}{\sin\theta} \right]. \tag{2.33}$$

Also, the continuity of the tangential components of the electric as well as the magnetic field through the aperture ($\hat{R} \times (\underline{E}^I - \underline{E}^{II}) = 0$, $\hat{R} \times (\underline{H}^I - \underline{H}^{II}) = 0$ for $0 \leq \theta < \theta_o$) requires that for $0 \leq \theta < \theta_o$:

$$\sum_{n=1}^{\infty} \left\{ \left[C_n \zeta_n(ka) - A_n \psi_n(ka) \right] \frac{P_n^1(\cos\theta)}{\sin\theta} - j \left[D_n \zeta_n'(ka) - B_n \psi_n'(ka) \right] \frac{\partial}{\partial\theta} P_n^1(\cos\theta) \right\}$$

$$= G_1(\theta) , \tag{2.34}$$

$$\sum_{n=1}^{\infty} \left\{ \left[C_n \zeta_n(ka) - A_n \psi_n(ka) \right] \frac{\partial}{\partial\theta} P_n^1(\cos\theta) - j \left[D_n \zeta_n'(ka) - B_n \psi_n'(ka) \right] \frac{P_n^1(\cos\theta)}{\sin\theta} \right\}$$

$$= G_2(\theta) , \tag{2.35}$$

$$\sum_{n=1}^{\infty} \left\{ \left[C_n \zeta_n'(ka) - A_n \psi_n'(ka) \right] \frac{\partial}{\partial\theta} P_n^1(\cos\theta) - j \left[D_n \zeta_n(ka) - B_n \psi_n(ka) \right] \frac{P_n^1(\cos\theta)}{\sin\theta} \right\}$$

$$= j\, G_1(\theta) , \tag{2.36}$$

$$\sum_{n=1}^{\infty} \left\{ \left[C_n \zeta_n'(ka) - A_n \psi_n'(ka) \right] \frac{P_n^1(\cos\theta)}{\sin\theta} - j \left[D_n \zeta_n(ka) - B_n \psi_n(ka) \right] \frac{\partial}{\partial\theta} P_n^1(\cos\theta) \right\}$$

$$= j\, G_2(\theta) . \tag{2.37}$$

From Eqs. (2.28) through (2.35), by making use of the orthogonal properties of the Legendre functions, it can be shown that the scattering amplitude coefficients C_n, D_n are directly related to the coefficients A_n, B_n by

$$C_n \zeta_n(ka) = \left[A_n - j^n \frac{2n+1}{n(n+1)}\right] \psi_n(ka) \quad , \tag{2.38}$$

$$D_n \zeta_n'(ka) = \left[B_n - j^n \frac{2n+1}{n(n+1)}\right] \psi_n'(ka) \quad . \tag{2.39}$$

$$(n = 1, 2, 3\ldots)$$

Hence, if we substitute Eqs. (2.38) and (2.39) into Eqs. (2.28) through (2.31) and (2.34) through (2.37), and eliminate the coefficients A_n and B_n, we obtain non-trivial equations for the scattering coefficients C_n and D_n as follows:

$$\sum_{n=1}^{\infty} \left[C_n \zeta_n(ka) \frac{P_n^1(\cos\theta)}{\sin\theta} - j D_n \zeta_n'(ka) \frac{\partial}{\partial\theta} P_n^1(\cos\theta)\right] = G_1(\theta) \quad , \tag{2.40}$$

$$\sum_{n=1}^{\infty} \left[C_n \zeta_n(ka) \frac{\partial}{\partial\theta} P_n^1(\cos\theta) - j D_n \zeta_n'(ka) \frac{P_n^1(\cos\theta)}{\sin\theta}\right] = G_2(\theta) \quad , \tag{2.41}$$

for $\theta_o < \theta \leq \pi$, and

$$\sum_{n=1}^{\infty} \left[\frac{C_n}{\psi_n(ka)} \frac{\partial}{\partial\theta} P_n^1(\cos\theta) - j \frac{D_n}{\psi_n'(ka)} \frac{P_n^1(\cos\theta)}{\sin\theta}\right] = 0 \quad , \tag{2.42}$$

$$\sum_{n=1}^{\infty} \left[\frac{C_n}{\psi_n(ka)} \frac{P_n^1(\cos\theta)}{\sin\theta} - j \frac{D_n}{\psi_n'(ka)} \frac{\partial}{\partial\theta} P_n^1(\cos\theta)\right] = 0 \quad , \tag{2.43}$$

for $0 \leq \theta < \theta_o$.

We now seek to solve for the unknown scattering amplitude coefficients C_n and D_n, starting from Eqs. (2.40) through (2.43) by applying the method of least square error. Two arbitrary weighting factors will be introduced and will later be replaced by quantities specifying the relative weights to be attached to the two boundary conditions -- one for the tangential components of the electric field on the conducting surface and the other for the tangential components of the magnetic field through the aperture.

By introducing weighting factors $W_1(>0)$ in Eqs. (2.40) and (2.41), and $W_2(>0)$ in Eqs. (2.42) and (2.43), and retaining only the first M terms, the total square error, $\mathcal{E}_M$ can be written as

$$\mathcal{E}_M = W_1 \int_{\theta_o}^{\pi} \left| G_1(\theta) - \sum_{n=1}^{M} \left[C_n \zeta_n(ka) \frac{P_n^1(\cos\theta)}{\sin\theta} - j D_n \zeta_n'(ka) \frac{\partial}{\partial\theta} P_n^1(\cos\theta) \right] \right|^2 \sin\theta d\theta$$

$$+W_1 \int_{\theta_o}^{\pi} \left| G_2(\theta) - \sum_{n=1}^{M} \left[C_n \zeta_n(ka) \frac{\partial}{\partial\theta} P_n^1(\cos\theta) - j D_n \zeta_n'(ka) \frac{P_n^1(\cos\theta)}{\sin\theta} \right] \right|^2 \sin\theta d\theta$$

$$+W_2 \int_{0}^{\theta_o} \left| \sum_{n=1}^{M} \left[C_n \frac{1}{\psi_n(ka)} \frac{\partial}{\partial\theta} P_n^1(\cos\theta) - j D_n \frac{1}{\psi_n'(ka)} \frac{P_n^1(\cos\theta)}{\sin\theta} \right] \right|^2 \sin\theta d\theta$$

$$+W_2 \int_{0}^{\theta_o} \left| \sum_{n=1}^{M} \left[C_n \frac{1}{\psi_n(ka)} \frac{P_n^1(\cos\theta)}{\sin\theta} - j D_n \frac{1}{\psi_n'(ka)} \frac{\partial}{\partial\theta} P_n^1(\cos\theta) \right] \right|^2 \sin\theta d\theta \,. \tag{2.44}$$

For least square error we require that

$$\frac{\partial \mathcal{E}_M}{\partial C_m} = 0 \qquad \text{and} \qquad \frac{\partial \mathcal{E}_M}{\partial D_m} = 0 \quad (m = 1, 2, 3 \ldots M) \tag{2.45}$$

from which we obtain

$$\sum_{n=1}^{M} \left\{ \frac{2m^2(m+1)^2}{2m+1} \psi_m(ka)\zeta_m(ka)\,\delta_{mn} - \left[\psi_m(ka)\zeta_n(ka) - \right.\right.$$

$$\left.\left. - \frac{W_2}{W_1} \frac{1}{\psi_n(ka)\zeta_m^*(ka)} \right] L_{mn}(\theta_o) \right\} C_n + j \sum_{n=1}^{M} \left[\psi_m(ka)\zeta_n'(ka) - \right.$$

$$\left. - \frac{W_2}{W_1} \frac{1}{\psi_n'(ka)\zeta_m^*(ka)} \right] S_{mn}(\theta_o)\, D_n = -\psi_m(ka) \sum_{n=1}^{\infty} j^n \frac{2n+1}{n(n+1)} \times$$

$$\times \left\{ \psi_n(ka) \left[\frac{2m^2(m+1)^2}{2m+1} \delta_{mn} - L_{mn}(\theta_o) \right] + j\psi_n'(ka)\zeta_{mn}(\theta_o) \right\}, \tag{2.46}$$

$$- \sum_{n=1}^{M} \left[\psi_m'(ka)\zeta_n(ka) - \frac{W_2}{W_1} \frac{1}{\psi_n(ka)\zeta_m'(ka)} \right] S_{mn}(\theta_o)\, C_n -$$

$$-j \sum_{n=1}^{M} \left\{ \frac{2m^2(m+1)^2}{2m+1} \psi_m'(ka)\zeta_m'(ka)\delta_{mn} - \left[\psi_m'(ka)\zeta_n'(ka) - \right.\right.$$

$$\left.\left. - \frac{W_2}{W_1} \frac{1}{\psi_n'(ka)\zeta_m'^*(ka)} \right] L_{mn}(\theta_o) \right\} D_n = \psi_m'(ka) \sum_{n=1}^{\infty} j^n \frac{2n+1}{n(n+1)} \times$$

$$\times \left\{ \psi_n(ka)\, S_{mn}(\theta_o) + j\psi_n'(ka) \left[\frac{2m^2(m+1)^2}{2m+1} \delta_{mn} - L_{mn}(\theta_o) \right] \right\}, \tag{2.47}$$

$$(m = 1, 2, 3, \ldots, M)$$

where the asterisk denotes the complex conjugate, δ_{mn} is the Kronecker delta and $L_{mn}(\theta_o)$ and $S_{mn}(\theta_o)$ are defined by

$$L_{mn}(\theta_o)=\int_0^{\theta_o}\left[\frac{\partial}{\partial\theta}P_m^1(\cos\theta)\frac{\partial}{\partial\theta}P_n^1(\cos\theta)+\frac{P_m^1(\cos\theta)}{\sin\theta}\frac{P_n^1(\cos\theta)}{\sin\theta}\right]\sin\theta d\theta, \tag{2.48}$$

$$S_{mn}(\theta_o)=\int_0^{\theta_o}\left[\frac{P_m^1(\cos\theta)}{\sin\theta}\frac{\partial}{\partial\theta}P_n^1(\cos\theta)+\frac{P_n^1(\cos\theta)}{\sin\theta}\frac{\partial}{\partial\theta}P_m^1(\cos\theta)\right]\sin\theta d\theta\,. \tag{2.49}$$

In order to arrive at weighting factors W_1 and W_2 having some physical significance, let us consider the following square error functions (by letting $C_n = D_n = 0$ for all $n > M$), normalized with respect to the corresponding incident field components. For the tangential electric field on the conducting surface ($R = a$, $\theta_o < \theta \leq \pi$):

$$\mathcal{E}_1=\frac{\int_0^{2\pi}\int_{\theta_o}^{\pi}\left|\underline{E}_t^i+\underline{E}_t^s\right|_{R=a}^2 a^2\sin\theta d\theta d\phi}{\int_0^{2\pi}\int_{\theta_o}^{\pi}\left|\underline{E}_t^i\right|_{R=a}^2 a^2\sin\theta d\theta d\phi} \tag{2.50}$$

and for the tangential magnetic field through the aperture ($R=a$, $0 \leq \theta < \theta_o$):

$$\mathcal{E}_2=\frac{\int_0^{2\pi}\int_0^{\theta_o}\frac{1}{Y^2}\left|\underline{H}_t^I-\underline{H}_t^{II}\right|_{R=a}^2 a^2\sin\theta d\theta d\phi}{\int_0^{2\pi}\int_0^{\theta_o}\frac{1}{Y^2}\left|\underline{H}_t^i\right|_{R=a}^2 a^2\sin\theta d\theta d\phi}\,. \tag{2.51}$$

It is clear that the smaller the quantities $\mathcal{E}_1$ and $\mathcal{E}_2$ become, the more accurate the solution. However, $\mathcal{E}_1$ and $\mathcal{E}_2$ cannot be minimized at the

same time. We here define the total (mean) square error $\mathcal{E}$, which we would like to minimize, as the ratio of sum of numerators to that of denominators in Eqs. (2.50) and (2.51), i.e.

$$\mathcal{E} = \frac{\int_0^{2\pi}\int_{\theta_o}^{\pi}\left|\underline{E}_t^i+\underline{E}_t^s\right|^2_{R=a}\sin\theta d\theta d\phi + \int_0^{2\pi}\int_0^{\theta_o}\frac{1}{Y^2}\left|\underline{H}_t^I-\underline{H}_t^{II}\right|^2_{R=a}\sin\theta d\theta d\phi}{\int_0^{2\pi}\int_{\theta_o}^{\pi}\left|\underline{E}_t^i\right|^2_{R=a}\sin\theta d\theta d\phi + \int_0^{2\pi}\int_0^{\theta_o}\frac{1}{Y^2}\left|\underline{H}_t^i\right|^2_{R=a}\sin\theta d\theta d\phi} . \tag{2.52}$$

Since

$$E_\theta^i\Big|_{R=a} = -\frac{1}{ka}\cos\phi\, G_1(\theta) = \cos\theta\cos\phi\, e^{jka\cos\theta} \tag{2.53}$$

$$E_\phi^i\Big|_{R=a} = \frac{1}{ka}\sin\phi\, G_2(\theta) = -\sin\phi\, e^{jka\cos\theta} \tag{2.54}$$

we have

$$\int_0^{2\pi}\int_{\theta_o}^{\pi}\left|\underline{E}_t^i\right|^2_{R=a}\sin\theta d\theta d\phi = \pi\left(\frac{4}{3}+\cos\theta_o+\frac{1}{3}\cos^3\theta_o\right) , \tag{2.55}$$

and also, from Eq. (2.5) with $C_n = D_n = 0$ for all $n > M$,

$$\int_0^{2\pi}\int_{\theta_o}^{\pi}\left|\underline{E}_t^i+\underline{E}_t^s\right|^2_{R=a}\sin\theta d\theta d\phi = \frac{\pi}{(ka)^2}\left\{\int_{\theta_o}^{\pi}\left|G_1(\theta)-\sum_{n=1}^{M}\left[C_n\zeta_n(ka)\frac{P_n^1(\cos\theta)}{\sin\theta}-\right.\right.\right.$$

$$\left.-jD_n\zeta_n'(ka)\frac{\partial}{\partial\theta}P_n^1(\cos\theta)\right]\Bigg|^2\sin\theta d\theta + \int_{\theta_o}^{\pi}\left|G_2(\theta)-\sum_{n=1}^{M}\left[C_n\zeta_n(ka)\frac{\partial}{\partial\theta}P_n^1(\cos\theta)-\right.\right.$$

$$\left.\left.\left.-jD_n\zeta_n'(ka)\frac{P_n^1(\cos\theta)}{\sin\theta}\right]\right|^2\sin\theta d\theta\right\} . \tag{2.56}$$

Similarly,

$$\int_0^{2\pi}\int_0^{\theta_o} \frac{1}{Y^2}\left|\underline{H}_t^i\right|_{R=a}^2 \sin\theta d\theta d\phi = \pi\left(\frac{4}{3} - \cos\theta_o - \frac{1}{3}\cos^3\theta_o\right) \tag{2.57}$$

and

$$\int_0^{2\pi}\int_0^{\theta_o} \frac{1}{Y^2}\left|\underline{H}_t^I - \underline{H}_t^{II}\right|_{R=a}^2 \sin\theta d\theta d\phi = \frac{\pi}{(ka)^2}\left\{\int_0^{\theta_o}\left|\sum_{n=1}^{M}\left[C_n \frac{1}{\psi_n(ka)} \frac{\partial}{\partial\theta} P_n^1(\cos\theta)\right.\right.\right.$$

$$\left.\left.\left. - jD_n \frac{1}{\psi_n'(ka)} \frac{P_n^1(\cos\theta)}{\sin\theta}\right]\right|^2 \sin\theta d\theta +$$

$$\left. + \int_0^{\theta_o}\left|\sum_{n=1}^{M}\left[C_n \frac{1}{\psi_n(ka)} \frac{P_n^1(\cos\theta)}{\sin\theta} - jD_n \frac{1}{\psi_n'(ka)} \frac{\partial}{\partial\theta} P_n^1(\cos\theta)\right]\right|^2 \sin\theta d\theta\right\} . \tag{2.58}$$

Substituting Eqs. (2.55) through (2.58) into Eq. (2.52), and letting $\mathcal{E} = \mathcal{E}_M$, we obtain

$$W_1 = W_2 = \frac{3}{8}\frac{1}{(ka)^2} , \tag{2.59}$$

$$\mathcal{E}_M = \mathcal{E}_E + \mathcal{E}_H , \tag{2.60}$$

where

$$\mathcal{E}_E = \frac{3}{8}\frac{1}{(ka)^2}\left\{\int_{\theta_o}^{\pi}\left|G_1(\theta) - \sum_{n=1}^{M}\left[C_n\zeta_n(ka)\frac{P_n^1(\cos\theta)}{\sin\theta} - jD_n\zeta_n'(ka)\frac{\partial}{\partial\theta}P_n^1(\cos\theta)\right]\right|^2 \sin\theta d\theta\right.$$

$$\left. + \int_{\theta_o}^{\pi}\left|G_2(\theta) - \sum_{n=1}^{M}\left[C_n\zeta_n(ka)\frac{\partial}{\partial\theta}P_n^1(\cos\theta) - jD_n\zeta_n'(ka)\frac{P_n^1(\cos\theta)}{\sin\theta}\right]\right|^2 \sin\theta d\theta\right\} , \tag{2.61}$$

$$\mathcal{E}_H = \frac{3}{8}\frac{1}{(ka)^2}\left\{\int_0^{\theta_o}\left|\sum_{n=1}^{M}\left[C_n\frac{1}{\psi_n(ka)}\frac{\partial}{\partial\theta}P_n^1(\cos\theta) - jD_n\frac{1}{\psi_n'(ka)}\frac{P_n^1(\cos\theta)}{\sin\theta}\right]\right|^2\sin\theta d\theta\right.$$

$$\left.+\int_0^{\theta_o}\left|\sum_{n=1}^{M}\left[C_n\frac{1}{\psi_n(ka)}\frac{P_n^1(\cos\theta)}{\sin\theta} - jD_n\frac{1}{\psi_n'(ka)}\frac{\partial}{\partial\theta}P_n^1(\cos\theta)\right]\right|^2\sin\theta d\theta\right\}. \tag{2.62}$$

$\mathcal{E}_E$ and $\mathcal{E}_H$ are square errors related to the electric and magnetic field components respectively. The weighting factors given by Eq. (2.59) are convenient since we are dealing with the total mean square error function $\mathcal{E}_M$ and only a single constant need be given to determine the number of modes, M, regardless of the values of ka and θ_o, for the same degree of error.

If we substitute Eq. (2.59) into Eqs. (2.46) and (2.47), and re-arrange, we obtain the matrix equation

$$\left[b_{pq}\right]\left[y_q\right] = \left[g_p\right], \quad (p,q = 1,2,\ldots,2M) \tag{2.63}$$

where the following notations have been introduced:

$$b_{2m-1,2n-1} = \frac{2m^2(m+1)^2}{2m+1}\left[\psi_m(ka)\right]^2\delta_{mn} + \left[\frac{1}{\zeta_n(ka)\zeta_m^*(ka)} - \psi_n(ka)\psi_m(ka)\right]L_{mn}(\theta_o), \tag{2.64}$$

$$b_{2m-1,2n} = \left[\frac{1}{\zeta_n'(ka)\zeta_m^*(ka)} - \psi_n'(ka)\psi_m(ka)\right]S_{mn}(\theta_o), \tag{2.65}$$

$$b_{2m,2n} = \frac{2m^2(m+1)^2}{2m+1}\left[\psi_m'(ka)\right]^2\delta_{mn} + \left[\frac{1}{\zeta_n'(ka)\zeta_m'^*(ka)} - \psi_n'(ka)\psi_m'(ka)\right]L_{mn}(\theta_o), \tag{2.66}$$

$$b_{2m,2n-1} = \left[\frac{1}{\zeta_n(ka)\,\zeta'^{*}_m(ka)} - \psi_n(ka)\,\psi'_m(ka) \right] S_{mn}(\theta_o) \quad , \tag{2.67}$$

$$y_{2n-1} = \frac{\zeta_n(ka)}{\psi_n(ka)} \; C_n \quad , \tag{2.68}$$

$$y_{2n} = -j \, \frac{\zeta'_n(ka)}{\psi'_n(ka)} \; D_n \quad , \tag{2.69}$$

$$g_{2m-1} = -\psi_m(ka) \sum_{n=1}^{\infty} j^n \, \frac{2n+1}{n(n+1)} \left\{ \psi_n(ka) \left[\frac{2m^2(m+1)^2}{2m+1} \, \delta_{mn} - L_{mn}(\theta_o) \right] + j\psi'_n(ka) \, S_{mn}(\theta_o) \right\} , \tag{2.70}$$

$$g_{2m} = \psi'_m(ka) \sum_{n=1}^{\infty} j^n \, \frac{2n+1}{n(n+1)} \left\{ \psi_n(ka) \, S_{mn}(\theta_o) + j\psi'_n(ka) \left[\frac{2m^2(m+1)^2}{2m+1} \, \delta_{mn} - L_{mn}(\theta_o) \right] \right\} \tag{2.71}$$

It should be noted that for the special case in which $\psi_r(ka) = 0$, Eq. (2.38) gives $C_r = 0$ and the expression $\left[\zeta_r(ka) / \psi_r(ka)\right] C_r$ in Eq. (2.68) must be replaced by

$$\left[A_r - i^r \, \frac{2r+1}{r(r+1)} \right] .$$

Similarly, if $\psi'_r(ka) = 0$, we have $D_r = 0$, and $\left[\zeta'_r(ka) / \psi'_r(ka)\right] D_r$ in Eq. (2.69) must be replaced by

$$\left[B_r - i^r \, \frac{2r+1}{r(r+1)} \right] .$$

The 2M unknown scattering amplitude coefficients, C_n and D_n $(n = 1, 2, \ldots M)$ can now be approximated in the least square sense by solving the 2M x 2M

matrix equation (2.63) obtained by imposing the boundary conditions and letting $C_n = D_n = 0$ for all $n > M$. The coefficients, C_n and D_n do not enjoy the property of finality. However, this approximation converges to the exact solution as M approaches infinity. In actual computation, therefore, the number M must be large enough to give sufficient accuracy, but small enough to keep the computation time reasonable. It is well known that in solving large systems of linear equations, matrix iterative methods (Varga, 1962; Cole et al, 1967) give distinct advantages, most notably with respect to the speed of execution, over conventional matrix inversion methods, provided the corresponding iterative matrix has a reasonable rate of convergence. Fortunately, the matrix b_{pq} in Eq. (2.63) is Hermitian and also positive definite if $\theta_o \neq 0$, and it therefore guarantees that the Gauss-Seidel iteration will always converge when applied to Eq. (2.63) (Appendix B).

The number M can be determined according to the accuracy we require. For example, we may require the total square error $\mathcal{E}_M$ to be less than a given small positive quantity δ. It is known that the accuracy of the solution improves as $\mathcal{E}_M$ approaches zero, and if we have $\mathcal{E}_M = 0$, the expression becomes exact, except at the points where it has a discontinuity or singularity. Nevertheless, $\mathcal{E}_M$ is not a measure of the error in the customary sense since an accurate computation of the error would require a knowledge of the tangential components of the electric and/or magnetic fields over the entire boundary surface. However, it should be noted that $\mathcal{E}_M$ provides at least a valid measure of error for the tangential electric field at the conducting spherical shell where we know $R \times \underline{E}^I = R \times \underline{E}^{II} = 0$.

It is expected that the solution of Eq. (2.63) will converge only slowly to the exact answer as M increases due to the field singularity at the edge of the aperture. From the edge condition it is readily seen that at the boundary surface the θ-component of the electric field for $\theta_o < \theta$ and also

the θ-component of the magnetic field for $\theta < \theta_o$ vary as the inverse square root of the distance from the edge, while the ϕ-components have no singularity at all. Consequently, the infinite series involving the scattering amplitude coefficients, C_n and D_n in Eqs. (2.40) and (2.42), which are respectively related to the θ-components of the electric and magnetic field at the boundary, introduce significant errors near the edge when the series are approximated by the first M modes even if the number M is chosen large. To overcome the slow convergence of the solution due to the edge effect, the above least square method can be modified by separating out the correct surface field behavior at the edge of the aperture. This modified method is presented in the following section.

2.4 Modified Formulation

To separate out the field having the edge behavior from the total field expression, we should first of all determine functions which satisfy not only the edge condition but Maxwell's equations as well. It is in general extremely difficult (if not impossible) to obtain such functions explicitly. But since the general formulation of solution presented in Section 2.1 is in terms of spherical vector wave functions (and therefore each term satisfies Maxwell's equation), and must contain the edge singularity, a possible approac is to pinpoint those terms which can become infinite at $\theta = \theta_o$ and thereby separate out the singular point.

Let us therefore examine Eqs. (2.40), (2.41), (2.42) and (2.43) which are related to E^s_θ, E^s_ϕ, $H^I_\theta - H^{II}_\theta$ and $H^I_\phi - H^{II}_\phi$ at R=a, respectively. We know from the edge condition that both functions E^s_θ and $H^I_\theta - H^{II}_\theta$ satisfy Dirichlet's conditions with $|\theta - \theta_o|^{-1/2}$ singularity, and hence the terms in the series expansion of each function are $O\left(\frac{1}{\sqrt{n}}\right)$ for n large (Carslow, 1930). On the other hand E^s_ϕ and $H^I_\phi - H^{II}_\phi$ are bounded and otherwise

satisfy Dirichlet's conditions, and hence the terms in the series expansion of each function are at least $O\left(\frac{1}{n}\right)$ for n large. Therefore, together with the asymptotic forms, for large n,

$$\zeta_n(ka) \sim i \frac{1}{(ka)^n}\left[(2n-1) \ldots . 5\cdot 3\cdot 1\right]$$

$$\zeta_n'(ka) \sim -i \frac{1}{(ka)^{n+1}} n \left[(2n-1) \ldots . 5\cdot 3\cdot 1\right]$$

$$\frac{1}{\psi_n(ka)} \sim \frac{1}{(ka)^{n+1}} \left[(2n+1)(2n-1) \ldots . 5\cdot 3\cdot 1\right]$$

$$\frac{1}{\psi_n'(ka)} \sim \frac{1}{(ka)^n} \frac{1}{n+1} \left[(2n+1)(2n-1) \ldots . 5\cdot 3\cdot 1\right]$$

$$P_n^1(\cos\theta) \sim -\sqrt{\frac{2n}{\pi \sin\theta}} \cos\left\{\left(n+\frac{1}{2}\right)\theta + \frac{\pi}{4}\right\}, \quad n >> \frac{1}{\sin\theta}$$

$$\frac{\partial}{\partial\theta} P_n^1(\cos\theta) \sim n\sqrt{\frac{2n}{\pi \sin\theta}} \sin\left\{\left(n+\frac{1}{2}\right)\theta + \frac{\pi}{4}\right\}, \quad n >> \frac{1}{\sin\theta},$$

a close examination of each term in Eqs. (2.40) through (2.43) reveals that

$$C_n \frac{1}{\psi_n(ka)} \frac{\partial}{\partial\theta} P_n^1(\cos\theta) \sim O\left(\frac{1}{\sqrt{n}}\right),$$

$$D_n \zeta_n'(ka) \frac{\partial}{\partial\theta} P_n^1(\cos\theta) \sim O\left(\frac{1}{\sqrt{n}}\right),$$

and only the series

$$\sum_{n=1}^{\infty} C_n \frac{1}{\psi_n(ka)} \frac{\partial}{\partial\theta} P_n^1(\cos\theta) \quad \text{and} \quad \sum_{n=1}^{\infty} D_n \zeta_n'(ka) \frac{\partial}{\partial\theta} P_n^1(\cos\theta)$$

have $\left|\theta - \theta_o\right|^{-1/2}$ singularity at the edge.

Since, from Appendix C

$$\sum_{n=1}^{\infty} \gamma_n \frac{\partial}{\partial\theta} P_n^1(\cos\theta) = \begin{cases} 0 & 0 < \theta < \theta_o \\ \cos\theta \sqrt{2(\cos\theta_o - \cos\theta)} + \dfrac{\sin^2\theta}{\sqrt{2(\cos\theta_o - \cos\theta)}}, & \theta_o < \theta < \pi \end{cases} \tag{2.72}$$

$$\sum_{n=1}^{\infty} \delta_n \frac{\partial}{\partial\theta} P_n^1(\cos\theta) = \begin{cases} -\cos\theta \sqrt{2(\cos\theta - \cos\theta_o)} + \dfrac{\sin^2\theta}{\sqrt{2(\cos\theta - \cos\theta_o)}}, & 0 < \theta < \theta_o \\ 0, & \theta_o < \theta < \pi \end{cases} \tag{2.73}$$

where

$$\gamma_n = \mathrm{Re}\left\{a_n\right\}, \tag{2.74}$$

$$\delta_n = \mathrm{Im}\left\{a_n\right\}, \tag{2.75}$$

$$a_n = \frac{2}{(2n-1)(2n+3)} b_n - \frac{1}{(2n+5)(2n+3)} b_{n+2} - \frac{1}{(2n-3)(2n+1)} b_{n-2}, \tag{2.76}$$

$$b_n = e^{i(n+1/2)\theta_o}, \tag{2.77}$$

we notice that Eqs. (2.72) and (2.73) behave the same as the θ-components of the magnetic and electric field respectively in the neighborhood of the edge. Now, introducing some constants K_1 and K_2, if we let

$$C_n = c_n + K_1 \psi_n(ka)\, \gamma_n, \tag{2.78}$$

$$D_n = d_n + K_2 \frac{1}{\xi_n'(ka)} \delta_n, \tag{2.79}$$

Eqs. (2.40) through (2.43) can be rewritten as

$$\sum_{n=1}^{\infty}\left[c_n\zeta_n(ka)\frac{P_n^1(\cos\theta)}{\sin\theta}-jd_n\zeta_n'(ka)\frac{\partial}{\partial\theta}P_n^1(\cos\theta)\right]+K_1\sum_{n=1}^{\infty}\gamma_n\psi_n(ka)\zeta_n(ka)\frac{P_n^1(\cos\theta)}{\sin\theta}-$$

$$-jK_2\sum_{n=1}^{\infty}\delta_n\frac{\partial}{\partial\theta}P_n^1(\cos\theta)=G_1(\theta)\ ,\ \theta_o<\theta<\pi \qquad (2.80)$$

$$\sum_{n=1}^{\infty}\left[c_n\zeta_n(ka)\frac{\partial}{\partial\theta}P_n^1(\cos\theta)-jd_n\zeta_n'(ka)\frac{P_n^1(\cos\theta)}{\sin\theta}\right]+K_1\sum_{n=1}^{\infty}\gamma_n\psi_n(ka)\zeta_n(ka)\frac{\partial}{\partial\theta}P_n^1(\cos\theta)-$$

$$-jK_2\sum_{n=1}^{\infty}\delta_n\frac{P_n^1(\cos\theta)}{\sin\theta}=G_2(\theta)\ ,\ \theta_o<\theta<\pi \qquad (2.81)$$

$$\sum_{n=1}^{\infty}\left[c_n\frac{1}{\psi_n(ka)}\frac{\partial}{\partial\theta}P_n^1(\cos\theta)-jd_n\frac{1}{\psi_n'(ka)}\frac{P_n^1(\cos\theta)}{\sin\theta}\right]+K_1\sum_{n=1}^{\infty}\gamma_n\frac{\partial}{\partial\theta}P_n^1(\cos\theta)-$$

$$-jK_2\sum_{n=1}^{\infty}\frac{\delta_n}{\psi_n'(ka)\zeta_n'(ka)}\frac{P_n^1(\cos\theta)}{\sin\theta}=0\ ,\ 0<\theta<\theta_o \qquad (2.82)$$

$$\sum_{n=1}^{\infty}\left[c_n\frac{1}{\psi_n(ka)}\frac{P_n^1(\cos\theta)}{\sin\theta}-jd_n\frac{1}{\psi_n'(ka)}\frac{\partial}{\partial\theta}P_n^1(\cos\theta)\right]+K_1\sum_{n=1}^{\infty}\gamma_n\frac{P_n^1(\cos\theta)}{\sin\theta}-$$

$$-jK_2\sum_{n=1}^{\infty}\frac{\delta_n}{\psi_n'(ka)\zeta_n'(ka)}\frac{\partial}{\partial\theta}P_n^1(\cos\theta)=0\ ,\ 0<\theta<\theta_o. \qquad (2.83)$$

We again apply the least square method to Eqs. (2.80) through (2.83) retaining only the first M terms for the coefficients c_n and d_n. Since the series having the coefficient K_2 in Eqs. (2.80) and (2.81) and having the coefficient K_1 in

Eqs. (2.82) and (2.83) vanish according to Eqs. (2.72) and (2.73), the total square error, $\mathcal{E}_M$ is given by

$$\mathcal{E}_M = \frac{3}{8}\frac{1}{(ka)^2}\left\{\int_{\theta_o}^{\pi}\left|G_1(\theta) - \sum_{n=1}^{M}\left[c_n\zeta_n(ka)\frac{P_n^1(\cos\theta)}{\sin\theta} - jd_n\zeta_n'(ka)\frac{\partial}{\partial\theta}P_n^1(\cos\theta)\right]\right.\right.$$

$$\left. - K_1\sum_{n=1}^{\infty}\gamma_n\psi_n(ka)\zeta_n(ka)\frac{P_n^1(\cos\theta)}{\sin\theta}\right|^2\sin\theta d\theta +$$

$$+\int_{\theta_o}^{\pi}\left|G_2(\theta) - \sum_{n=1}^{M}\left[c_n\zeta_n(ka)\frac{\partial}{\partial\theta}P_n^1(\cos\theta) - jd_n\zeta_n'(ka)\frac{P_n^1(\cos\theta)}{\sin\theta}\right]\right.$$

$$\left. - K_1\sum_{n=1}^{\infty}\gamma_n\psi_n(ka)\zeta_n(ka)\frac{\partial}{\partial\theta}P_n^1(\cos\theta)\right|^2\sin\theta d\theta +$$

$$+\int_0^{\theta_o}\left|\sum_{n=1}^{M}\left[c_n\frac{1}{\psi_n(ka)}\frac{\partial}{\partial\theta}P_n^1(\cos\theta) - jd_n\frac{1}{\psi_n'(ka)}\frac{P_n^1(\cos\theta)}{\sin\theta}\right]\right.$$

$$\left. - jK_2\sum_{n=1}^{\infty}\frac{\delta_n}{\psi_n'(ka)\zeta_n'(ka)}\frac{P_n^1(\cos\theta)}{\sin\theta}\right|^2\sin\theta d\theta +$$

$$+\int_0^{\theta_o}\left|\sum_{n=1}^{M}\left[c_n\frac{1}{\psi_n(ka)}\frac{P_n^1(\cos\theta)}{\sin\theta} - jd_n\frac{1}{\psi_n'(ka)}\frac{\partial}{\partial\theta}P_n^1(\cos\theta)\right]\right.$$

$$\left.\left. - jK_2\sum_{n=1}^{\infty}\frac{\delta_n}{\psi_n'(ka)\zeta_n'(ka)}\frac{\partial}{\partial\theta}P_n^1(\cos\theta)\right|^2\sin\theta d\theta\right\}, \qquad (2.84)$$

where we have used the same weighting factors W_1 and W_2 given in Eq. (2.59). The requirement that

$$\frac{\partial \mathcal{E}_M}{\partial c_m} = \frac{\partial \mathcal{E}_M}{\partial d_m} = 0 \ , \qquad (m = 1, 2, \ldots M)$$

and

$$\frac{\partial \mathcal{E}_M}{\partial K_1} = \frac{\partial \mathcal{E}_M}{\partial K_2} \ ,$$

leads to a linear system of 2(M+1) equations in the 2(M+1) unknown coefficients $c_1, c_2, \ldots c_M, \ d_1, d_2, \ldots d_M, \ K_1, K_2$. After some manipulation those equations can be written in matrix form as

$$\left[a_{pq}\right] x_q\right] = f_p\right] \ , \qquad (p, q = 1, 2, \ldots 2(M+1)) \tag{2.85}$$

where the following notations have been introduced:

$$a_{2m-1,\,2n-1} = \frac{2m^2(m+1)^2}{2m+1} \psi_m(ka)\zeta_m(ka)\delta_{mn} + \left[\frac{1}{\psi_m(ka)\zeta_m^*(ka)} - \psi_n(ka)\zeta_n(ka)\right] L_{mn}(\theta_o) \ , \tag{2.86}$$

$$a_{2m-1,\,2n} = \left[\frac{1}{\psi_m(ka)\zeta_m^*(ka)} - \psi_n'(ka)\zeta_n'(ka)\right] S_{mn}(\theta_o) \ , \tag{2.87}$$

$$a_{2m,\,2n} = \frac{2m^2(m+1)^2}{2m+1} \psi_m'(ka)\zeta_m'(ka)\delta_{mn} + \left[\frac{1}{\psi_m'(ka)\zeta_m'^*(ka)} - \psi_n'(ka)\zeta_n'(ka)\right] L_{mn}(\theta_o) \ , \tag{2.88}$$

$$a_{2m,\,2n-1} = \left[\frac{1}{\psi_m'(ka)\zeta_m'^*(ka)} - \psi_n(ka)\zeta_n(ka)\right] S_{mn}(\theta_o) \ , \tag{2.89}$$

$$a_{2m-1,\,2M+1} = \frac{1}{\psi_m(ka)\,\zeta_m^*(ka)}\; a^*_{2M+1,\,2m-1}$$

$$= \frac{2m^2(m+1)^2}{2m+1}\,\gamma_m\psi_m(ka)\,\zeta_m(ka) - \sum_{\ell=1}^{\infty}\gamma_\ell\psi_\ell(ka)\,\zeta_\ell(ka)\,L_{m\ell}(\theta_o), \tag{2.90}$$

$$a_{2m,\,2M+1} = \frac{1}{\psi'_m(ka)\,\zeta'^*_m(ka)}\; a_{2M+1,\,2m}$$

$$= -\sum_{\ell=1}^{\infty}\gamma_\ell\psi_\ell(ka)\,\zeta_\ell(ka)\,S_{\ell m}(\theta_o)\ , \tag{2.91}$$

$$a_{2M+2,\,2m-1} = \psi_m(ka)\,\zeta_m(ka)\; a^*_{2m-1,\,2M+2}$$

$$= \sum_{\ell=1}^{\infty}\frac{\delta_\ell}{\psi'_\ell(ka)\,\zeta'^*_\ell(ka)}\; S_{\ell m}(\theta_o)\ , \tag{2.92}$$

$$a_{2M+2,\,2m} = \psi'_m(ka)\,\zeta'_m(ka)\; a_{2m,\,2M+2}$$

$$= \sum_{\ell=1}^{\infty}\frac{\delta_\ell}{\psi'_\ell(ka)\,\zeta'^*_\ell(ka)}\; L_{\ell m}(\theta_o)\ , \tag{2.93}$$

$$a_{2M+1,\,2M+2} = a_{2M+2,\,2M+1} = 0 \tag{2.94}$$

$$a_{2M+1,\,2M+1} = \sum_{\ell=1}^{\infty}\frac{2\ell^2(\ell+1)^2}{2\ell+1}\left|\gamma_\ell\psi_\ell(ka)\,\zeta_\ell(ka)\right|^2 -$$

$$-\sum_{i=1}^{\infty}\sum_{\ell=1}^{\infty}\gamma_i\psi_i(ka)\,\zeta_i(ka)\,\gamma^*_\ell\psi_\ell(ka)\,\zeta^*_\ell(ka)\,L_{i\ell}(\theta_o)\ , \tag{2.95}$$

$$b_{2M+2,2M+2} = \sum_{i=1}^{\infty} \sum_{\ell=1}^{\infty} \frac{\delta_i}{\psi_i'(ka)\zeta_i'(ka)} \frac{\delta_\ell^*}{\psi_\ell'(ka)\zeta_\ell'^*(ka)} L_{i\ell}(\theta_o) , \quad (2.96)$$

$$x_{2n-1} = \frac{1}{\psi_n(ka)} c_n , \quad (2.97)$$

$$x_{2n} = -j \frac{1}{\psi_n'(ka)} d_n , \quad (2.98)$$

$$x_{2M+1} = K_1 , \quad (2.99)$$

$$x_{2M+2} = -jK_2 , \quad (2.100)$$

$$f_{2m-1} = -\sum_{\ell=1}^{\infty} j^\ell \frac{2\ell+1}{\ell(\ell+1)} \left\{ \psi_\ell(ka) \left[\frac{2m^2(m+1)^2}{2m+1} \delta_{\ell m} - L_{\ell m}(\theta_o) \right] + \right.$$

$$\left. + j\psi_\ell'(ka) S_{\ell m}(\theta_o) \right\} , \quad (2.101)$$

$$f_{2m} = \sum_{\ell=1}^{\infty} j^\ell \frac{2\ell+1}{\ell(\ell+1)} \left\{ \psi_\ell(ka) S_{\ell m}(\theta_o) + j\psi_\ell'(ka) \left[\frac{2m^2(m+1)^2}{2m+1} \delta_{\ell m} - L_{\ell m}(\theta_o) \right] \right\} \quad (2.102)$$

$$f_{2M+1} = -\sum_{i=1}^{\infty} \gamma_i \psi_i(ka) \zeta_i^*(ka) \sum_{\ell=1}^{\infty} j^\ell \frac{2\ell+1}{\ell(\ell+1)} \left\{ \psi_\ell(ka) \left[\frac{2i^2(i+1)^2}{2i+1} \delta_{\ell i} - \right. \right.$$

$$\left. \left. - L_{\ell i}(\theta_o) \right] + j\psi_\ell'(ka) S_{\ell i}(\theta_o) \right\} \quad (2.103)$$

$$f_{2M+2} = 0 . \quad (2.104)$$

$$(m, n: 1, 2, \ldots, M)$$

Although some of the above matrix coefficients are more complicated in nature than those appearing in Eq. (2.63), the solution of Eq. (2.85) gives rise to

less error than that of Eq. (2.63) if the dimensions of the matrix equations are taken equal. The labor involved in obtaining a solution to a specified degree of accuracy is therefore less if Eq. (2.85) is used rather than Eq. (2.63).

At the surface, R=a, the scattered tangential electric field can be written in terms of the solution of Eq. (2.85) as

$$E_\theta^s(a,\theta,\phi) \sim \frac{1}{ka} \left\{ \sum_{n=1}^{M} \left[x_{2n-1} \psi_n(ka) \zeta_n(ka) \frac{P_n^1(\cos\theta)}{\sin\theta} + \right.\right.$$

$$\left. + x_{2n} \psi_n'(ka) \zeta_n'(ka) \frac{\partial}{\partial\theta} P_n^1(\cos\theta) \right] + x_{2M+1} \sum_{n=1}^{\infty} \gamma_n \psi_n(ka) \zeta_n(ka) \frac{P_n^1(\cos\theta)}{\sin\theta} +$$

$$\left. + x_{2M+2} \Gamma_{1,\theta}(\theta) \right\} \cos\phi \qquad (2.105)$$

$$E_\phi^s(a,\theta,\phi) \sim -\frac{1}{ka} \left\{ \sum_{n=1}^{M} \left[x_{2n-1} \psi_n(ka) \zeta_n(ka) \frac{\partial}{\partial\theta} P_n^1(\cos\theta) + \right.\right.$$

$$\left. + x_{2n} \psi_n'(ka) \zeta_n'(ka) \frac{P_n^1(\cos\theta)}{\sin\theta} \right] + x_{2M+1} \sum_{n=1}^{\infty} \gamma_n \psi_n(ka) \zeta_n(ka) \frac{\partial}{\partial\theta} P_n^1(\cos\theta) +$$

$$\left. + x_{2M+2} \Gamma_{1,\phi}(\theta) \right\} \sin\phi \qquad (2.106)$$

where $\Gamma_{1,\theta}(\theta)$ and $\Gamma_{1,\phi}(\theta)$ are, for convenience, defined as

$$\Gamma_{1,\theta}(\theta) = \begin{cases} \dfrac{\sin^2\theta}{\sqrt{2(\cos\theta - \cos\theta_o)}} - \cos\theta \sqrt{2(\cos\theta - \cos\theta_o)}, & \text{for } 0 \le \theta < \theta_o \\ 0, & \text{for } \theta_o < \theta \le \pi \end{cases}$$

$$\Gamma_{1,\phi}(\theta) = \begin{cases} -\sqrt{2(\cos\theta - \cos\theta_o)} \quad , & \text{for } 0 \le \theta < \theta_o \\ \\ 0 \quad , & \text{for } \theta_o < \theta \le \pi \end{cases}$$

Also, the surface current components are, at the inside shell surface,

$$T_1^I(\theta) \sim -\cos\theta\, e^{jka\cos\theta} + \frac{j}{ka} \left\{ \sum_{n=1}^{M} \left[x_{2n-1} \psi_n'(ka) \zeta_n(ka) \frac{\partial}{\partial\theta} P_n^1(\cos\theta) - \right.\right.$$

$$\left. - x_{2n} \psi_n(ka) \zeta_n'(ka) \frac{P_n^1(\cos\theta)}{\sin\theta} \right] + x_{2M+1} \sum_{n=1}^{\infty} \gamma_n \psi_n'(ka) \zeta_n(ka) \frac{\partial}{\partial\theta} P_n^1(\cos\theta) -$$

$$\left. - x_{2M+2} \sum_{n=1}^{\infty} \delta_n \frac{\psi_n(ka)}{\psi_n'(ka)} \frac{P_n^1(\cos\theta)}{\sin\theta} \right\} , \qquad (2.107)$$

$$T_2^I(\theta) \sim -e^{jka\cos\theta} + \frac{j}{ka} \left\{ \sum_{n=1}^{M} \left[x_{2n-1} \psi_n'(ka) \zeta_n(ka) \frac{P_n^1(\cos\theta)}{\sin\theta} - \right.\right.$$

$$\left. - x_{2n} \psi_n(ka) \zeta_n'(ka) \frac{\partial}{\partial\theta} P_n^1(\cos\theta) \right] + x_{2M+1} \sum_{n=1}^{\infty} \gamma_n \psi_n'(ka) \zeta_n(ka) \frac{P_n^1(\cos\theta)}{\sin\theta}$$

$$\left. - x_{2M+2} \sum_{n=1}^{\infty} \delta_n \frac{\psi_n(ka)}{\psi_n'(ka)} \frac{\partial}{\partial\theta} P_n^1(\cos\theta) \right\} , \qquad (2.108)$$

and, at the outside shell surface,

$$T_1^{II}(\theta) \sim -\cos\theta\, e^{jka\cos\theta} + \frac{j}{ka}\left\{\sum_{n=1}^{M}\left[x_{2n-1}\psi_n(ka)\zeta_n'(ka)\frac{\partial}{\partial\theta}P_n^1(\cos\theta)\right.\right.$$

$$\left. - x_{2n}\psi_n'(ka)\zeta_n(ka)\frac{P_n^1(\cos\theta)}{\sin\theta}\right] + x_{2M+1}\sum_{n=1}^{\infty}\gamma_n\psi_n(ka)\zeta_n'(ka)\frac{\partial}{\partial\theta}P_n^1(\cos\theta) -$$

$$\left. - x_{2M+2}\sum_{n=1}^{\infty}\delta_n\frac{\zeta_n(ka)}{\zeta_n'(ka)}\frac{P_n^1(\cos\theta)}{\sin\theta}\right\}, \qquad (2.109)$$

$$T_2^{II}(\theta) \sim -e^{jka\cos\theta} + \frac{j}{ka}\left\{\sum_{n=1}^{M}\left[x_{2n-1}\psi_n(ka)\zeta_n'(ka)\frac{P_n^1(\cos\theta)}{\sin\theta}\right.\right.$$

$$\left. - x_{2n}\psi_n'(ka)\zeta_n(ka)\frac{\partial}{\partial\theta}P_n^1(\cos\theta)\right] + x_{2M+1}\sum_{n=1}^{\infty}\gamma_n\psi_n(ka)\zeta_n'(ka)\frac{P_n^1(\cos\theta)}{\sin\theta} -$$

$$\left. - x_{2M+2}\sum_{n=1}^{\infty}\delta_n\frac{\zeta_n(ka)}{\zeta_n'(ka)}\frac{\partial}{\partial\theta}P_n^1(\cos\theta)\right\}. \qquad (2.110)$$

In the far zone, the scattering amplitudes are, from Eqs. (2.16) and (2.17),

$$S_{11}^{s}(\theta) \sim \sum_{n=1}^{M} j^n\left[x_{2n-1}\psi_n(ka)\frac{P_n^1(\cos\theta)}{\sin\theta} - j\,x_{2n}\psi_n'(ka)\frac{\partial}{\partial\theta}P_n^1(\cos\theta)\right] +$$

$$+ x_{2M+1}\sum_{n=1}^{\infty} j^n\gamma_n\psi_n(ka)\frac{P_n^1(\cos\theta)}{\sin\theta} - j\,x_{2M+2}\sum_{n=1}^{\infty} j^n\delta_n\frac{1}{\zeta_n'(ka)}\frac{\partial}{\partial\theta}P_n^1(\cos\theta), \qquad (2.111)$$

$$S_2^s(\theta) \sim \sum_{n=1}^{M} j^n \left[x_{2n-1} \psi_n(ka) \frac{\partial}{\partial\theta} P_n^1(\cos\theta) - j x_{2n} \psi_n'(ka) \frac{P_n^1(\cos\theta)}{\sin\theta} \right]$$

$$+ x_{2M+1} \sum_{n=1}^{\infty} j^n \gamma_n \psi_n(ka) \frac{\partial}{\partial\theta} P_n^1(\cos\theta) - j x_{2M+2} \sum_{n=1}^{\infty} j^n \delta_n \frac{1}{\zeta_n'(ka)} \frac{P_n^1(\cos\theta)}{\sin\theta} \quad . \tag{2.112}$$

It should be noted that Eq. (2.85) can also be solved by the Gauss-Seidel iterative method. This is easily shown by associating Eq. (2.85) with a positive definite Hermitian matrix after some matrix transformations (Appendix B). Even though we have overcome the slow convergence due to the edge behavior of the field, the order of the matrix $[a_{pq}]$ has to be increased, as ka increases, to maintain a given accuracy of solution. In consequence, the use of the Gauss-Seidel iterative method is both convenient and desirable if ka is large.

CHAPTER III

NUMERICAL RESULTS

3.1 Results of the Original Method

A computer program with double-precision mode (about seventeen significant decimal digits) was written for the University of Michigan IBM 360 computer to calculate the surface and far fields. The scattering amplitude coefficients, C_n and D_n (n=1, 2, . . . M), were first computed from Eqs. (2.63) through (2.71), obtained by the unmodified least square method (we will henceforth refer to this as the original method). From these, all the field quantities were then computed.

The backscattering cross sections of the spherical shell with the aperture angle, $\theta_o = 30^o$ were computed with various values of M (= number of modes incorporated), and they are given in Fig. 3-1. The results indicate that the solution converges slowly as M increases except in the region where ka is small (less than about 1.2). This is further confirmed by comparison with the experimental results given in Fig. 4-4, Chapter IV. Even with a fairly large M, say M=40, the computed results differ considerably from the experimental results in the region of $ka > 2.0$.

In order to examine the accuracy of the solution over the boundary region, the tangential components of the total electric field were computed from the approximate scattering amplitude coefficients, C_n and D_n (n=1, 2, . . . M) for M=30 and 50 with ka=2.0 and $\theta_o = 30^o$. Their amplitudes are plotted in Figs. 3-2a and 3-2b. From the edge condition, we know that the field E_θ at the edge, $\theta=30^o$, of the aperture has a singularity of order $\rho^{-1/2}$, where ρ is the distance from the edge. Also, knowing that the exact tangential components of the total electric field must vanish at the conducting surface, R=a and $30^o < \theta \leq 180^o$, we see that the results give a poor approximation to the exact field near the edge of the spherical shell.

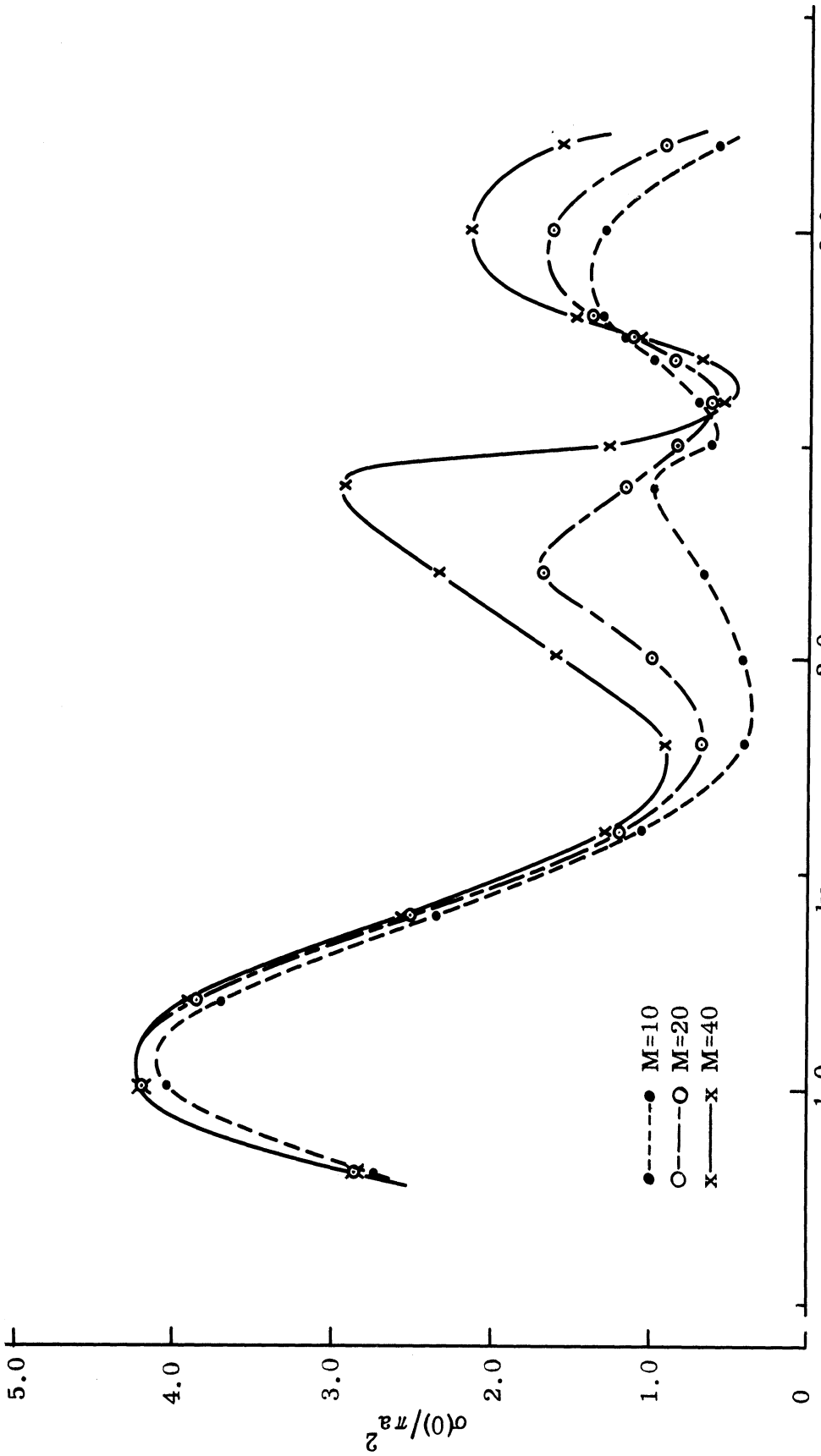

FIG. 3-1: COMPUTED BACKSCATTERING CROSS SECTIONS OF A SPHERICAL SHELL WITH $\theta_o = 30^o$ (USING THE ORIGINAL LEAST SQUARE METHOD).

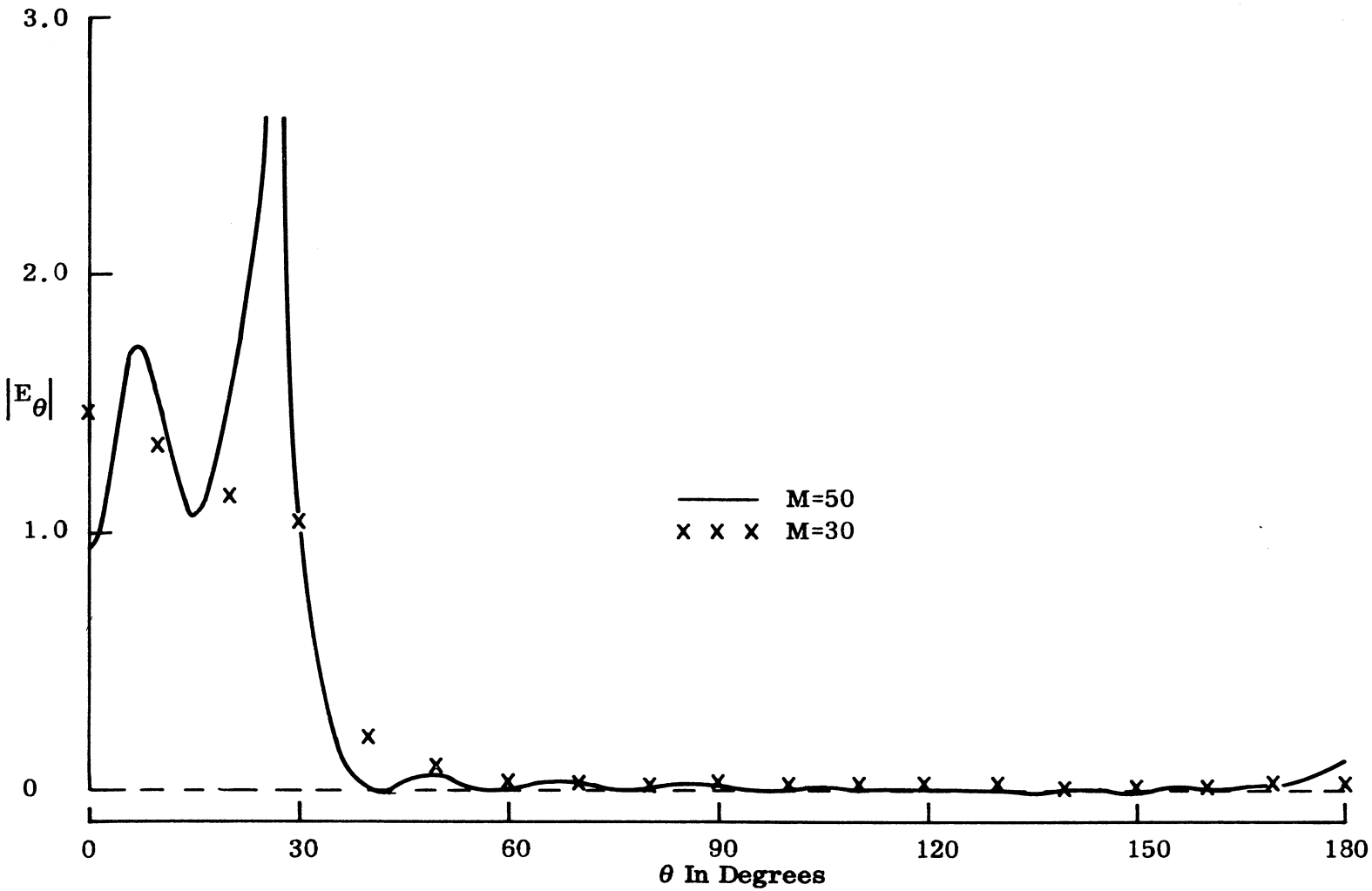

FIG. 3-2a: COMPUTED AMPLITUDE OF THE θ-COMPONENT OF THE ELECTRIC FIELD AT R=a FOR ka=2.0 WITH $\theta_o = 30^o$ (USING THE ORIGINAL LEAST SQUARE METHOD). ϕ=0.

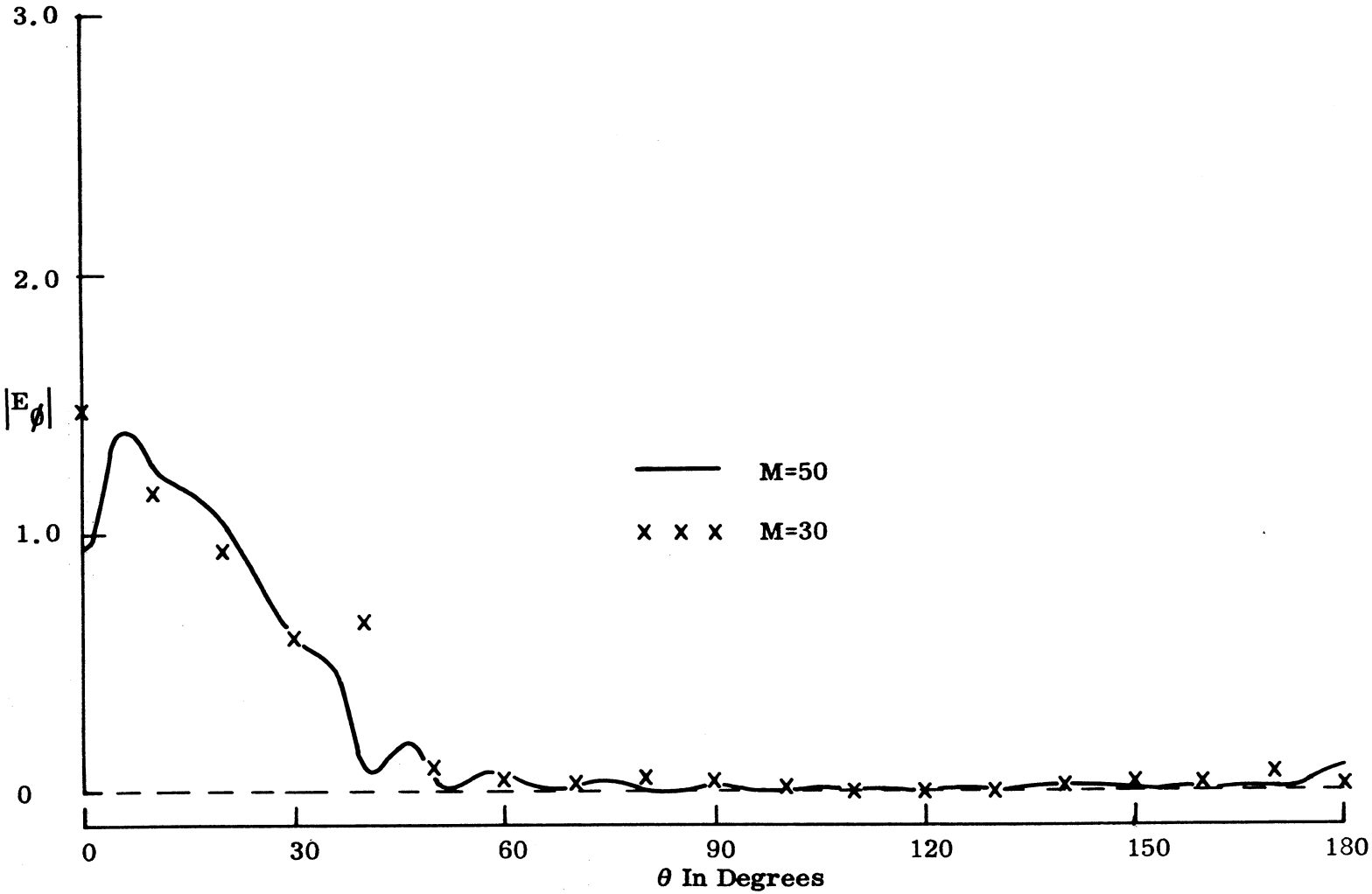

FIG. 3-2b: COMPUTED AMPLITUDE OF THE ϕ-COMPONENT OF THE ELECTRIC FIELD AT R=a FOR ka=2.0 WITH $\theta_o = 30^o$ (USING THE ORIGINAL LEAST SQUARE METHOD). $\phi=\pi/2$.

Although the results for M=50 are an improvement over those for M=30 and also give some indication of the field singularity at the edge, it is believed that the rapid oscillations appearing in E_θ over the aperture do not represent the actual field characteristics. Since only a finite number of modes (=M) is retained in approximating the field having the edge singularity, these oscillations are believed due to Gibb's phenomenon which occurs whenever a discontinuous function is approximated by a finite series. In order to overcome the difficulties arising from the edge singularity, the original formulation has been modified, and all subsequent computations were carried out using this modified method.

3.2 Results of the Modified Method

The original computer program was modified to compute the scattering amplitude coefficients from Eqs. (2.85) through (2.104), derived by using the modified least square method. In this programming, considerable care was taken in the computation of functions such as $\psi_n(ka)$, $\zeta_n(ka)$ and $P_n^1(\cos\theta)$ for large n. A brief description and listing of the main program and related subroutines are given in Appendix D.

The backscattering cross sections of the spherical shell with $\theta_o = 30^o$ and 90^o were computed for $0.8 \leq ka \leq 4.8$ and plotted in Figs. 3-3 and 3-4 respectively. The numbers M=10 for $ka \leq 1.1$ and M=20 for $1.1 < ka \leq 4.8$ were used in the computation except in the vicinity of ka values where a sharp peak in the scattering cross section was expected, where M=30 was chosen. The results near this peak appear somewhat less accurate than those further away for the same number of modes retained in the computation. It is, however, believed that the number M=30 is large enough to give a reasonable approximation to the exact cross section in the region we are interested in. To show the rate of convergence of the solution near this peak, the backscattering cross sections and the error $\mathcal{E}_M$ (see Eq.(2.84)) for ka = 2.4, 3.4, 4.0 and 4.7, with various

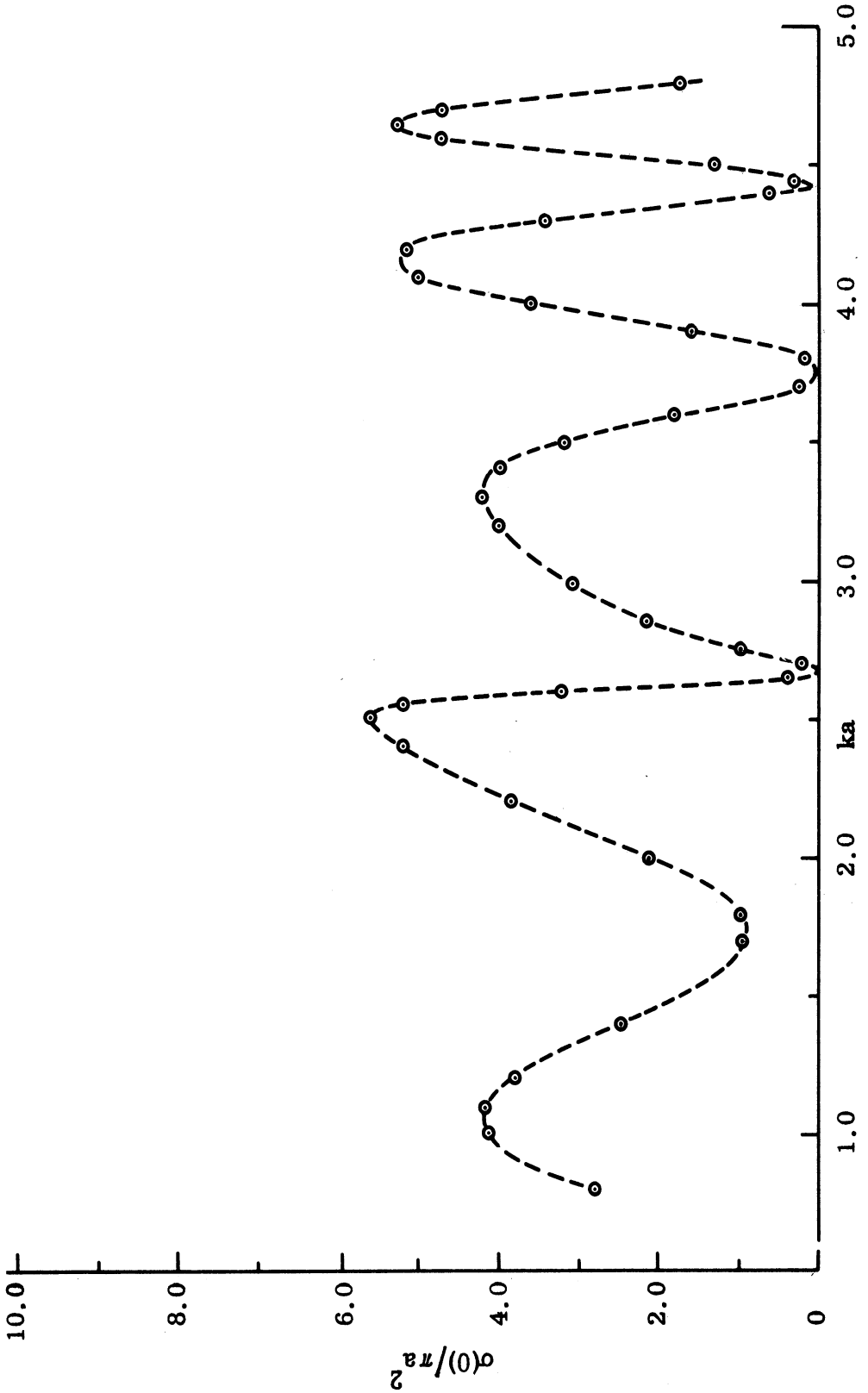

FIG. 3-3: COMPUTED BACKSCATTERING CROSS SECTIONS OF A SPHERICAL SHELL WITH $\theta_o = 30^o$ (USING THE MODIFIED LEAST SQUARE METHOD).

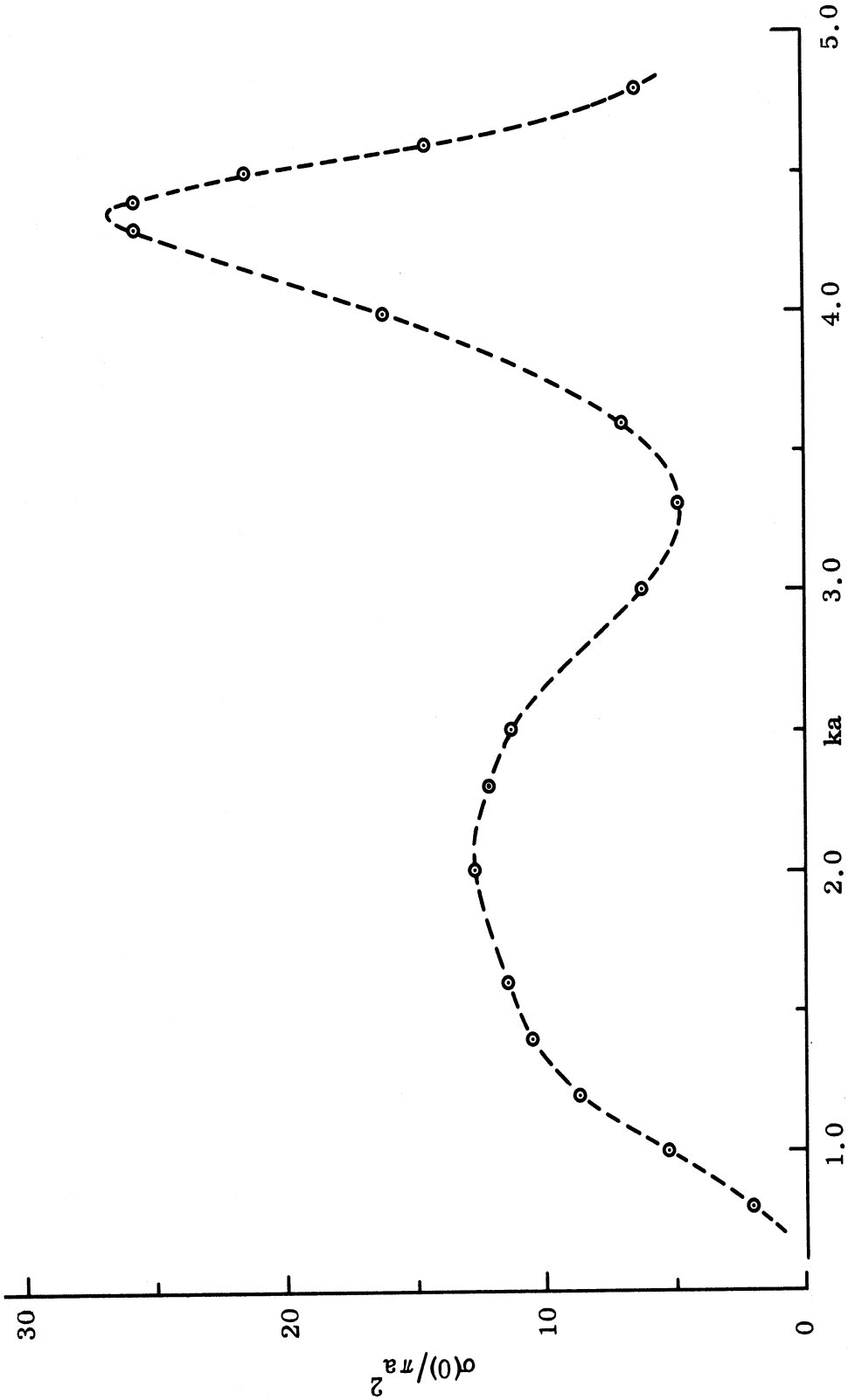

FIG. 3-4: COMPUTED BACKSCATTERING CROSS SECTIONS OF A SPHERICAL SHELL WITH $\theta_o = 90^o$
(USING THE MODIFIED LEAST SQUARE METHOD).

values of M are tabulated in Table 3-1. The results obtained from the original computation was also included to show the significant improvement achieved by the modified method. Although the value of ε_M cannot be explicitly related to the error in the backscattering cross section, an error ε_M less than about 0.4×10^{-2} seems to provide an adequate criterion for the computation of the backscattering cross section. The computed cross sections are compared with the experimental results in Figs. 5-1 and 5-2, Chapter V, and a detailed discussion will be given in Chapter V.

The tangential components of the near field were computed at R=a for ka = 2.0, 2.5, 2.75 and 4.0 with $\theta_o = 30^o$ to compare with either the exact answers or experimental results and possibly to obtain some insight into the scattering behavior of a spherical shell. In Figs. 3-5 through 3-8, the amplitude of each tangential electric field components, and in Figs. 3-9 through 3-12 the amplitude and phase of $T_1^{II}(\theta)$ and $T_2^{II}(\theta)$ are plotted with theoretical values for a solid sphere with the same ka. A close examination of Figs. 3-5 through 3-8 reveals that the larger the amplitude of the tangential electric field in the aperture becomes, the larger the error near to the edge of the conducting surface and also the larger the amplitude of the oscillations in the aperture. Separate computations for M=20 and M=30 in Fig. 3-8a and 3-8b show quite a close agreement between them except for different shapes of small oscillations over the aperture. Very similar behavior can also be observed in $T_1^{II}(\theta)$ and $T_2^{II}(\theta)$. For ka=2.5 (Figs. 3-10a and 3-10b) rapid but small oscillations appear in the amplitude and phase of $T_1^{II}(\theta)$ while the amplitudes of $T_1^{II}(\theta)$ and $T_2^{II}(\theta)$ suddenly become small over the aperture. On the other hand, for ka=2.75 (Figs. 3-11a and 3-11b) the amplitude and phase of $T_1^{II}(\theta)$ as well as $T_2^{II}(\theta)$ show no such rapid oscillations, and apart from the singular discontinuity at the edge of the aperture, the variations

M / ka	M=5	M=10	M=20	M=30	M=40
2.4		0.99816* (0.6237×10^{-1})	1.1673* (0.4329×10^{-1})		2.9314* (0.2708×10^{-1})
	2.3053 (0.2768×10^{-1})	4.6119 (0.7552×10^{-2})	5.1721 (0.3298×10^{-2})	5.1839 (0.2417×10^{-2})	
3.4		2.7291 (0.1287×10^{-1})	3.9029 (0.5047×10^{-2})	4.0281 (0.4239×10^{-2})	4.0196 (0.4033×10^{-2})
4.0			3.6001 (0.5064×10^{-3})	3.6107 (0.3226×10^{-3})	
4.7		2.9714 (0.1142×10^{-1})	4.5605 (0.4581×10^{-2})	4.7177 (0.3594×10^{-2})	4.7331 (0.3441×10^{-2})

TABLE 3-1: COMPUTED BACKSCATTERING CROSS SECTIONS $\sigma(0)/\pi a^2$ FOR $\theta_o = 30^o$

( ): Computed values of the Error Function $\mathcal{E}_M$.

*: Results from the Original least square method.

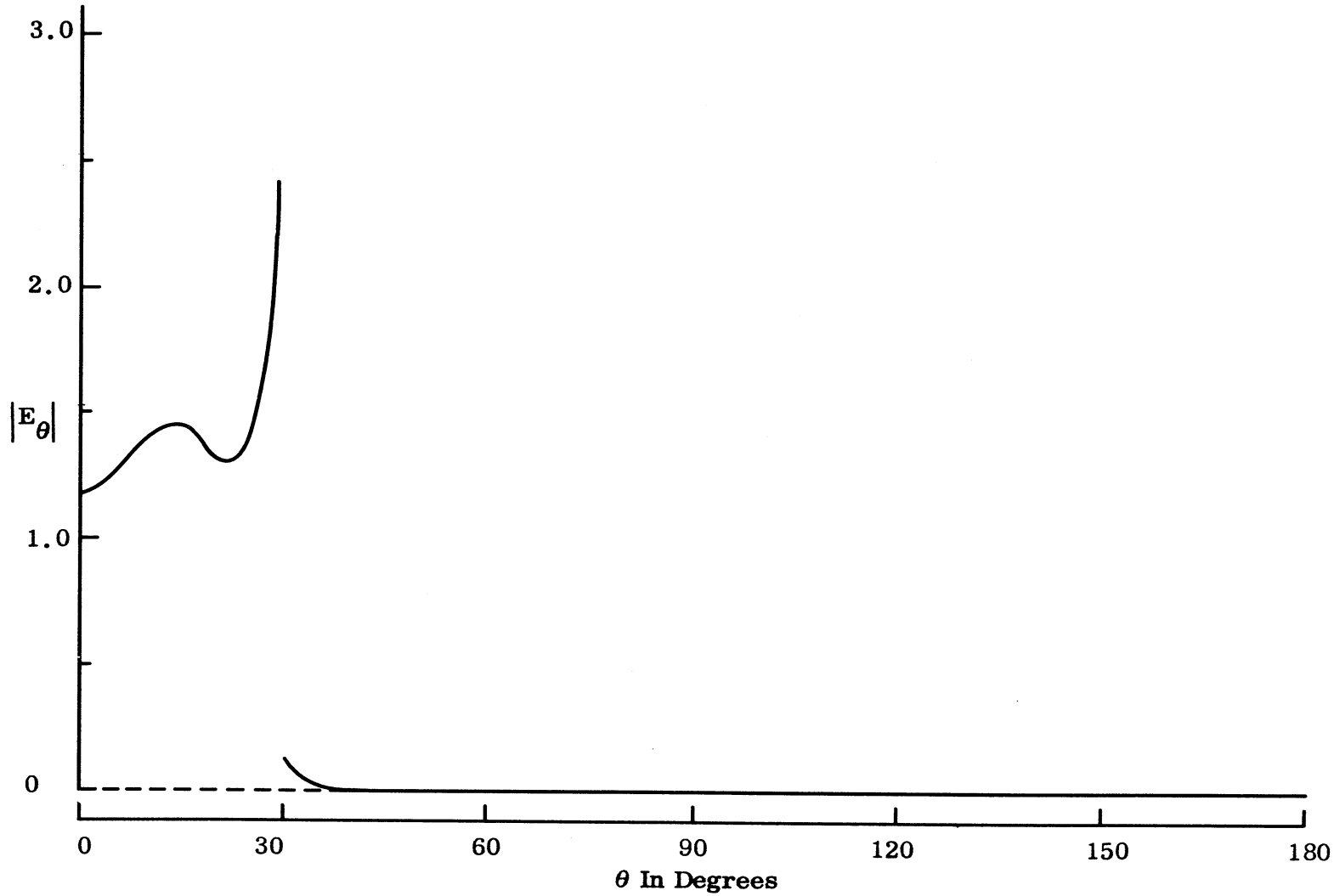

FIG. 3-5a: COMPUTED AMPLITUDE OF THE θ-COMPONENT OF THE ELECTRIC FIELD AT R=a FOR ka=2.0 WITH $\theta_o = 30^o$ (USING THE MODIFIED LEAST SQUARE METHOD WITH M=20). $\phi = 0$.

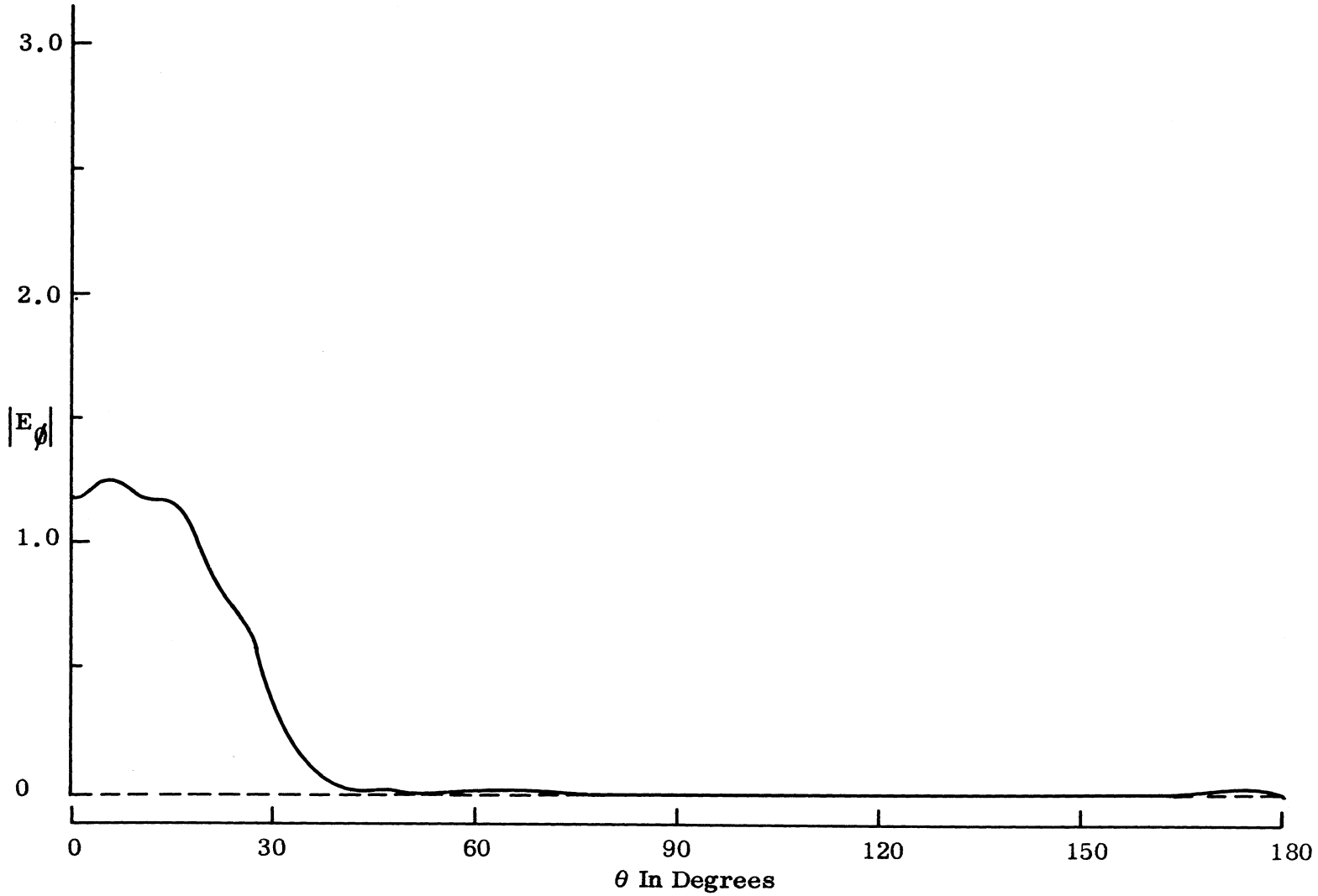

FIG. 3-5b: COMPUTED AMPLITUDE OF THE ϕ-COMPONENT OF THE ELECTRIC FIELD AT R=a FOR ka=2.0 WITH $\theta_o = 30^o$ (USING THE MODIFIED LEAST SQUARE METHOD WITH M=20). $\phi = \pi/2$.

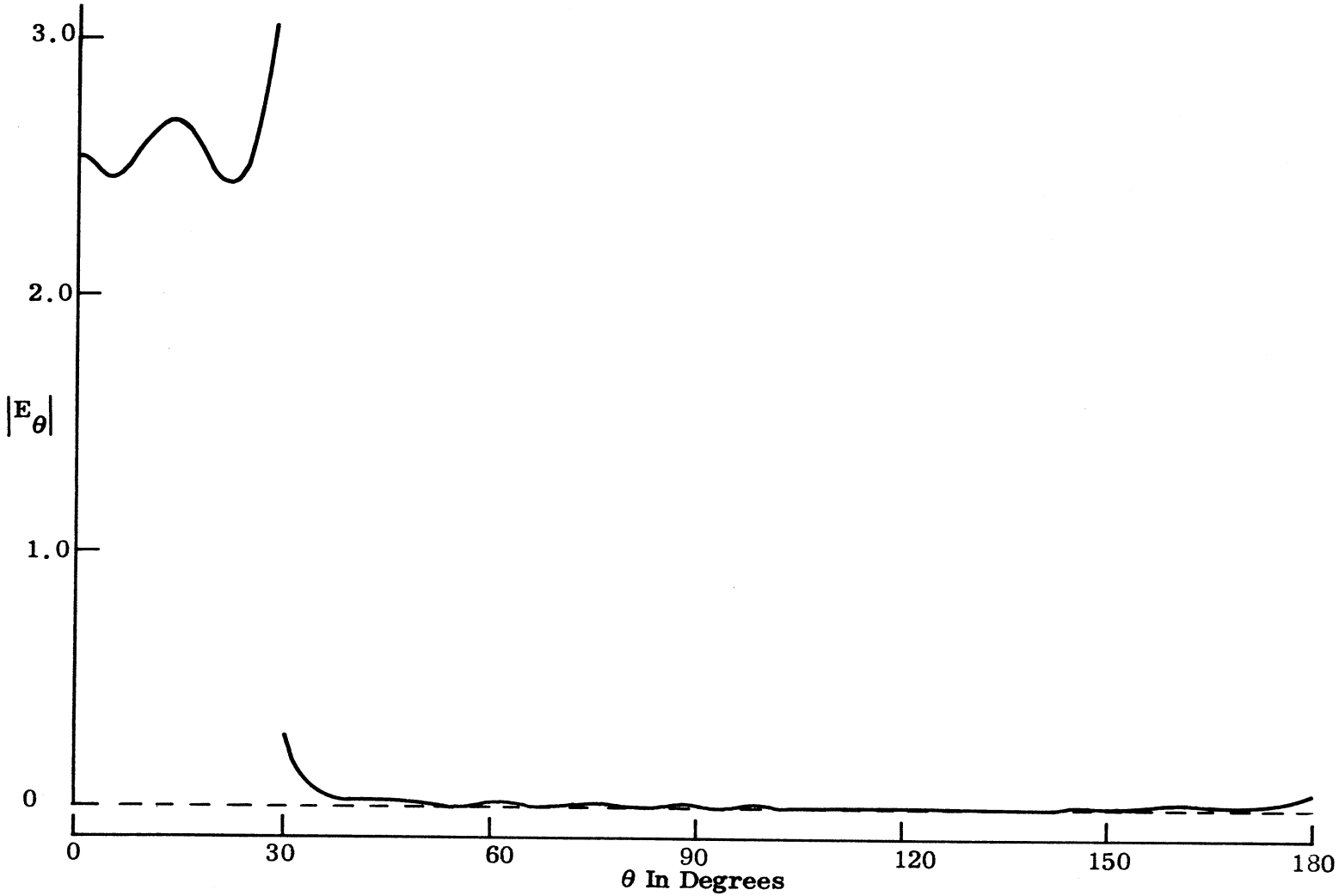

FIG. 3-6a: COMPUTED AMPLITUDE OF THE θ-COMPONENT OF THE ELECTRIC FIELD AT R=a FOR ka=2.5 WITH $\theta_o = 30^o$ (USING THE MODIFIED LEAST SQUARE METHOD WITH M=20). ϕ=0.

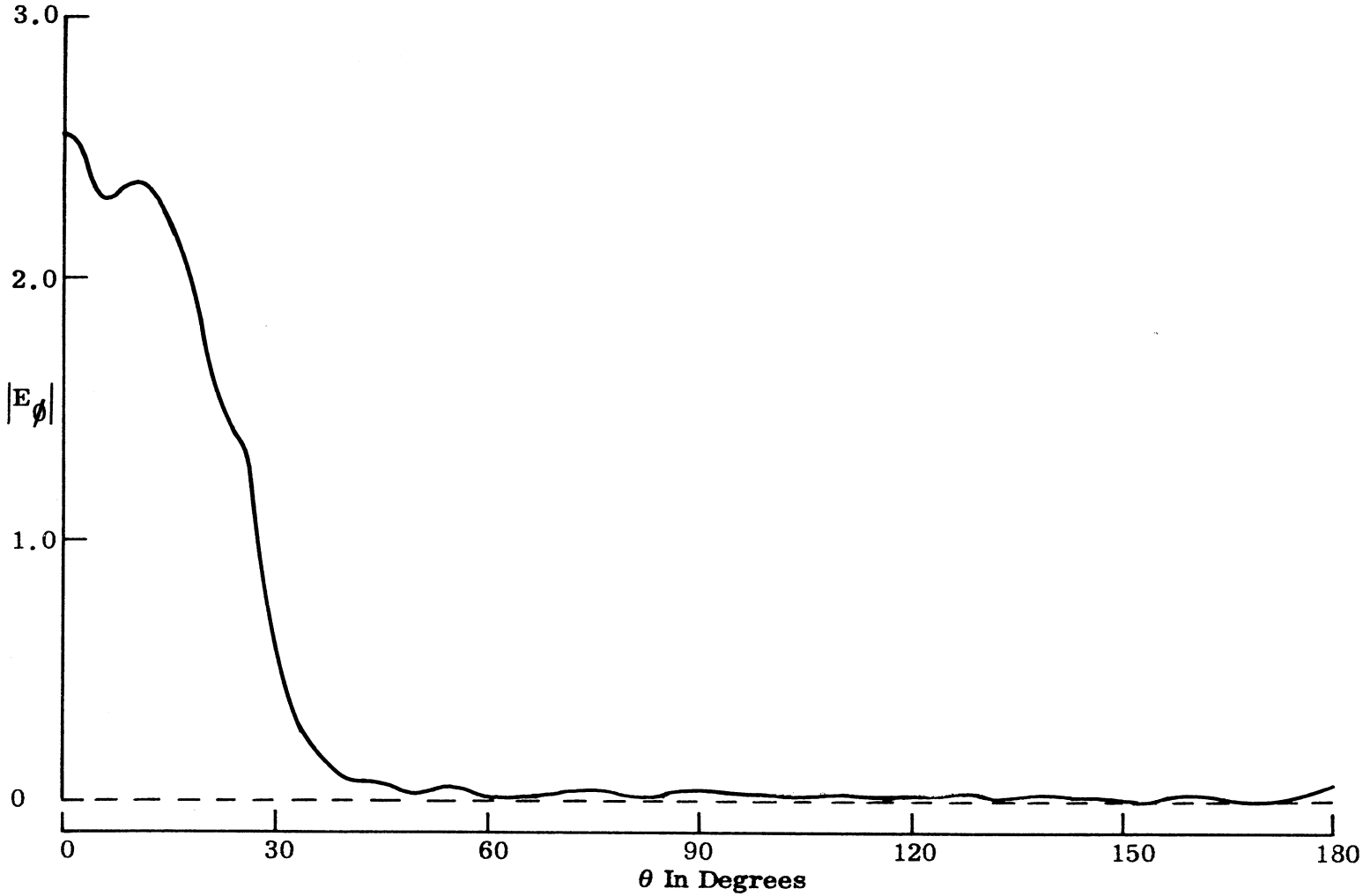

Fig. 3-6b: COMPUTED AMPLITUDE OF THE ϕ-COMPONENT OF THE ELECTRIC FIELD AT R=a FOR ka =2.5 WITH $\theta_o = 30^o$ (USING THE MODIFIED LEAST SQUARE METHOD WITH M=20). $\phi = \pi/2$.

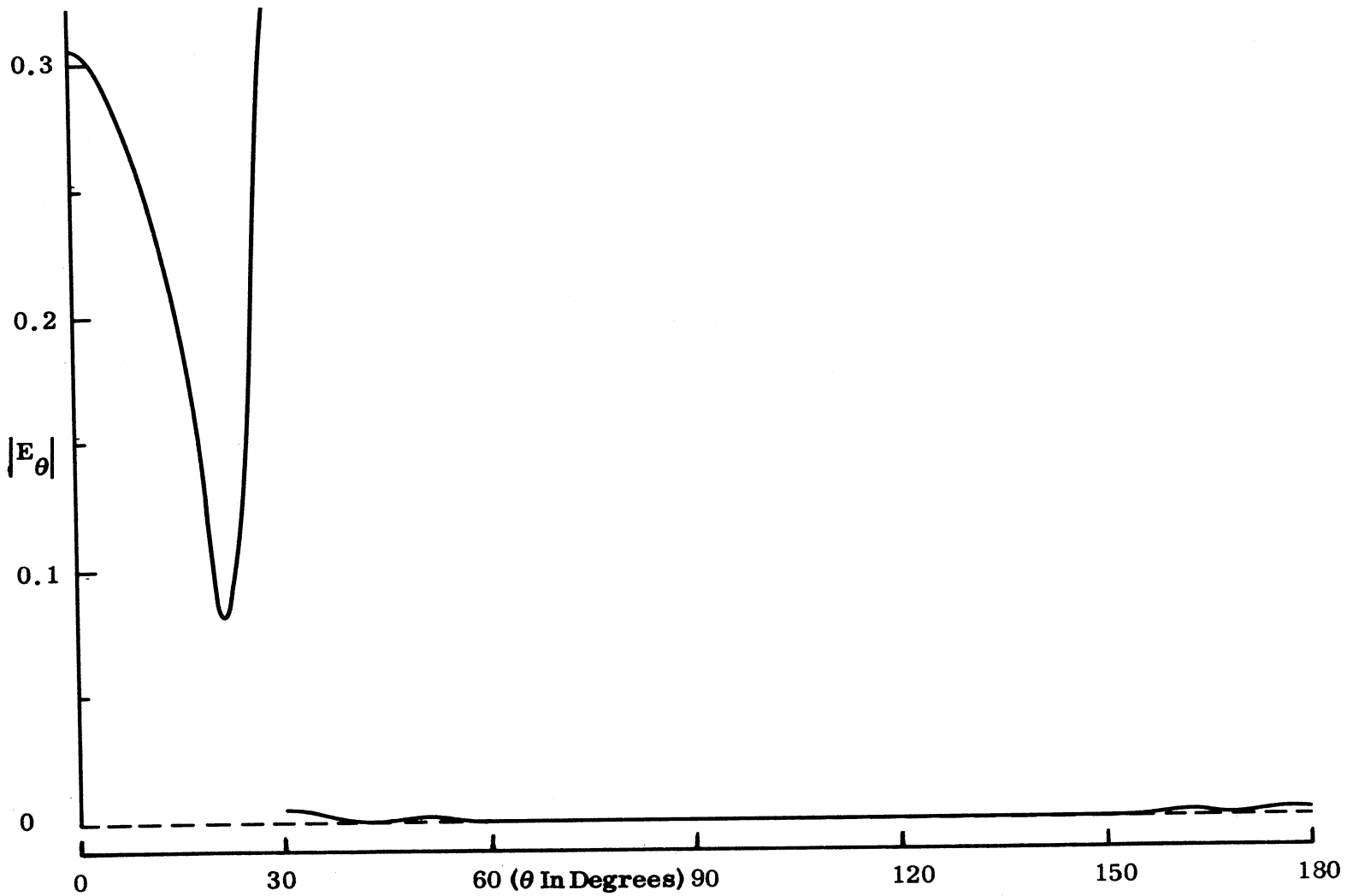

FIG. 3-7a: COMPUTED AMPLITUDE OF THE θ-COMPONENT OF THE ELECTRIC FIELD AT R=a FOR ka=2.75 WITH θ_o=30° (USING THE MODIFIED LEAST SQUARE METHOD WITH M=20). ϕ=0.

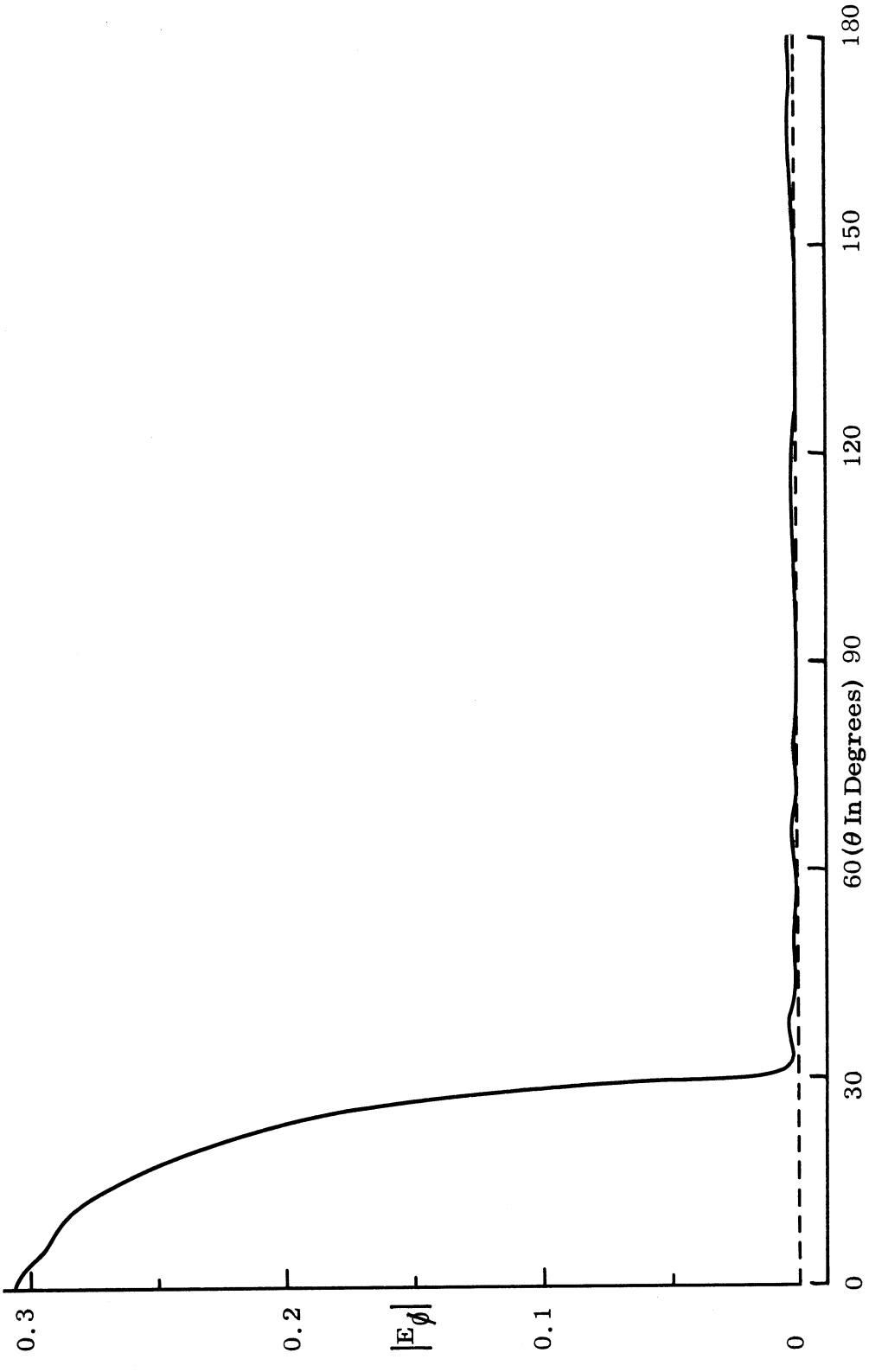

FIG. 3-7b: COMPUTED AMPLITUDE OF THE ϕ-COMPONENT OF THE ELECTRIC FIELD AT R=a FOR ka=2.75 WITH $\theta_o = 30^o$ (USING THE MODIFIED LEAST SQUARE METHOD WITH M=20). $\phi=\pi/2$.

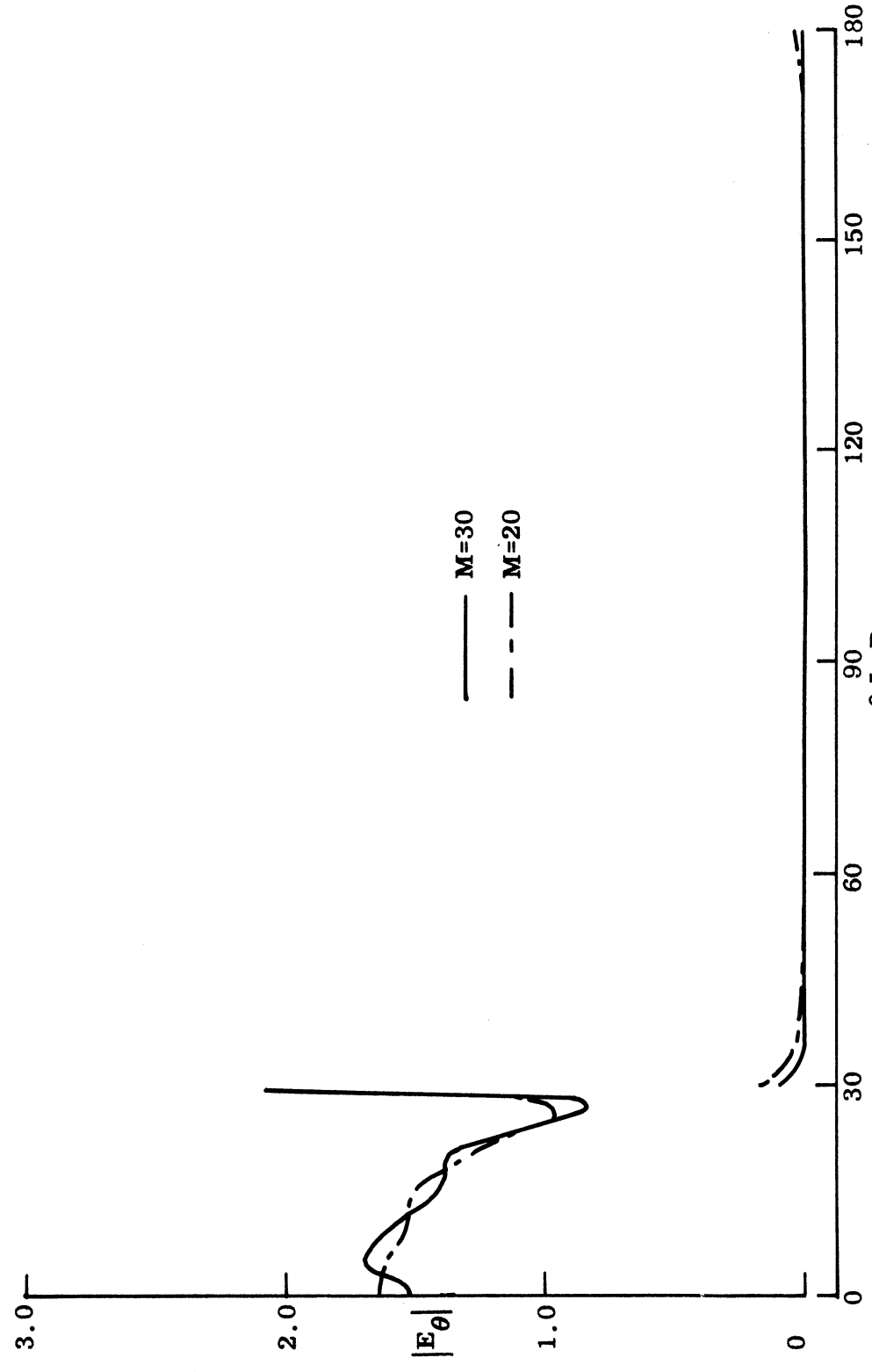

FIG. 3-8a: COMPUTED AMPLITUDE OF THE θ-COMPONENT OF THE ELECTRIC FIELD AT R=a FOR ka=4.0 WITH $\theta_o = 30^o$ (USING THE MODIFIED LEAST SQUARE METHOD). ϕ=0.

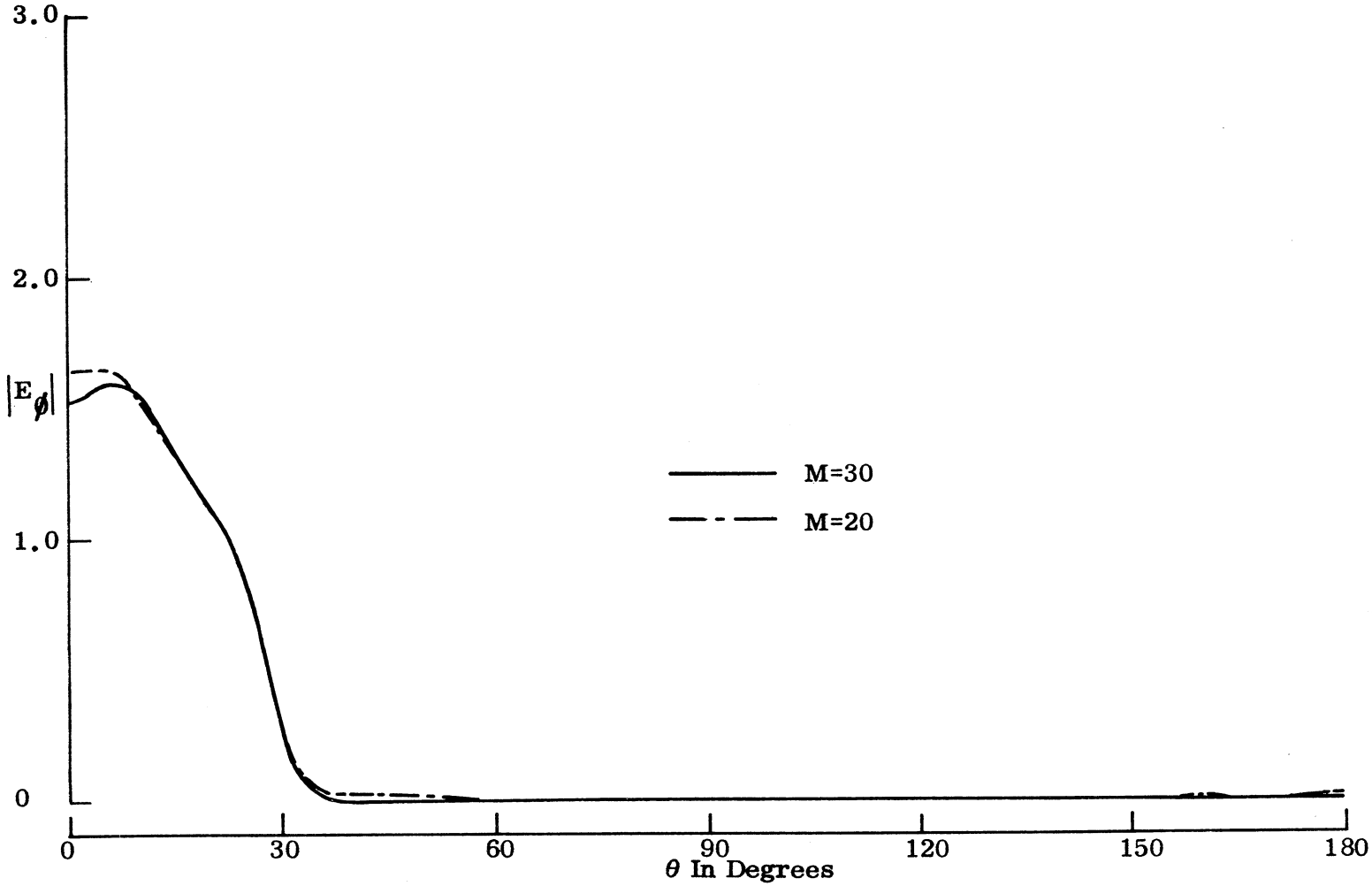

FIG. 3-8b: COMPUTED AMPLITUDE OF THE ϕ-COMPONENT OF THE ELECTRIC FIELD AT R=a FOR ka=4.0 WITH θ_o=30° (USING THE MODIFIED LEAST SQUARE METHOD). $\phi = \pi/2$.

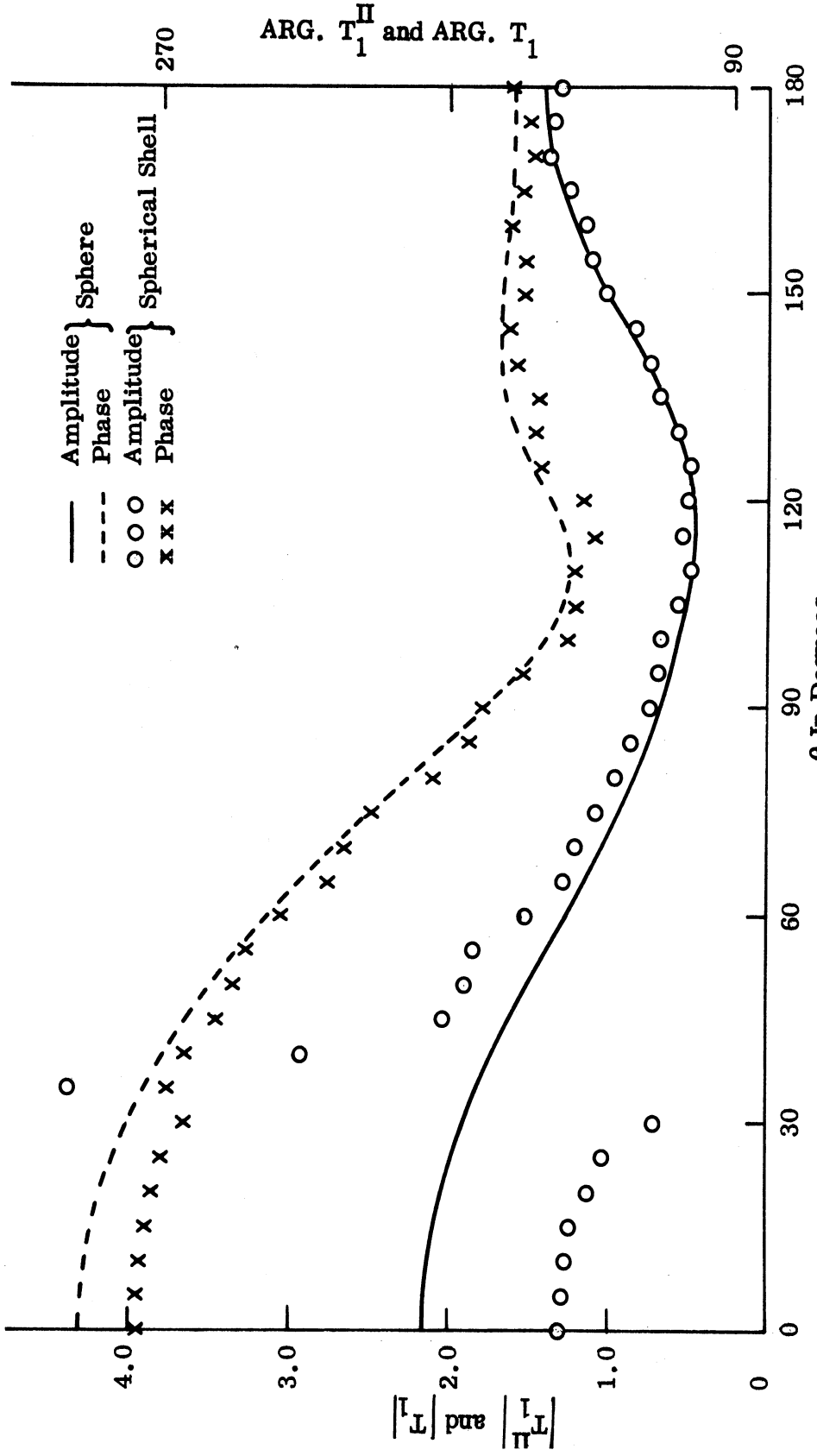

FIG. 3-9a: COMPUTED $T_1^{II}(\theta)$ COMPONENT FOR ka=2.0 WITH $\theta_o = 30^o$ (USING THE MODIFIED LEAST SQUARE METHOD WITH M=20), AND $T_1(\theta)$ COMPONENT OF A SOLID SPHERE.

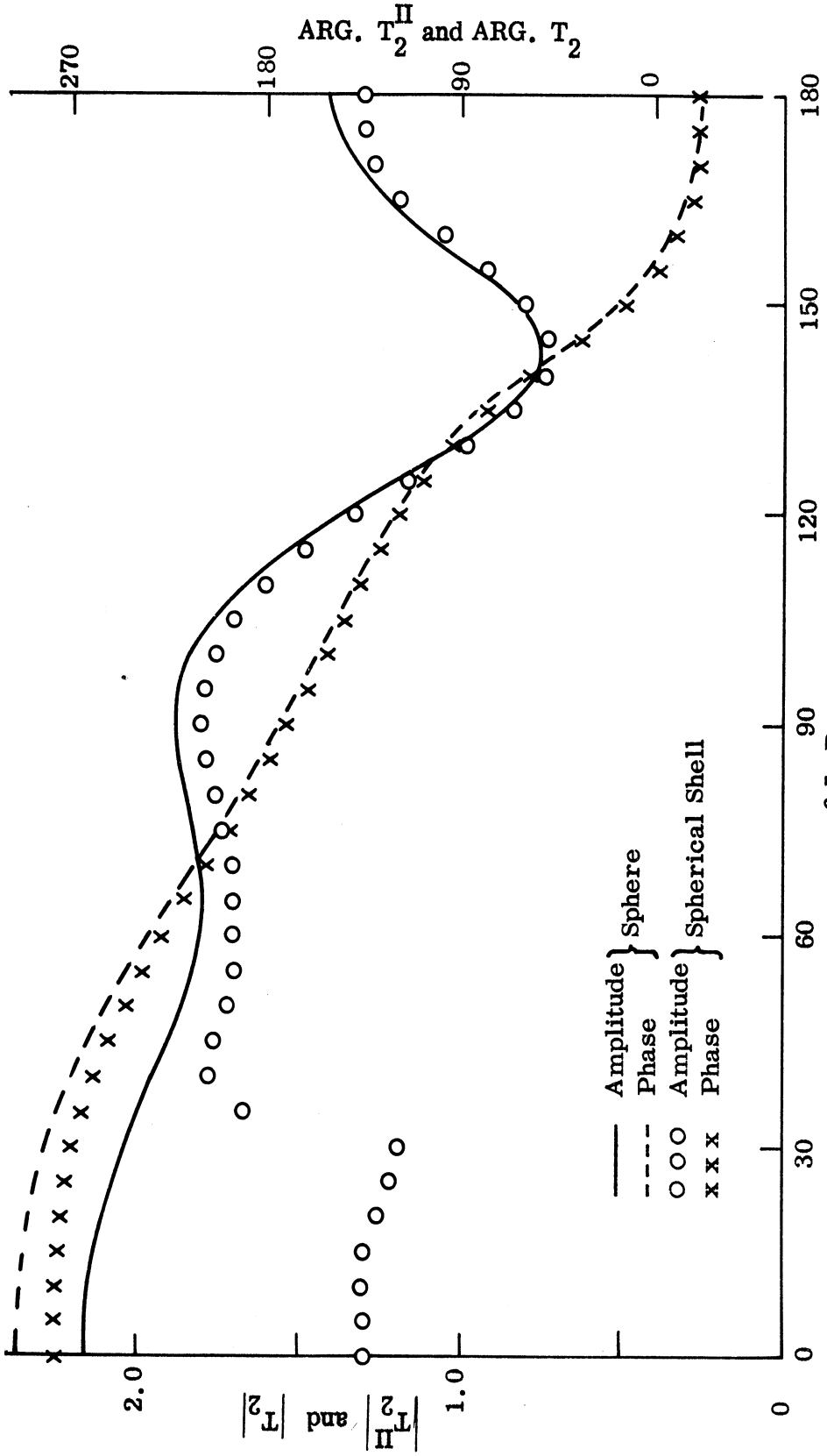

FIG. 3-9b: COMPUTED $T_2^{II}(\theta)$ COMPONENT FOR ka=2.0 WITH $\theta_o = 30^o$ (USING THE MODIFIED LEAST SQUARE METHOD WITH M=20), AND $T_2(\theta)$ COMPONENT OF A SOLID SPHERE.

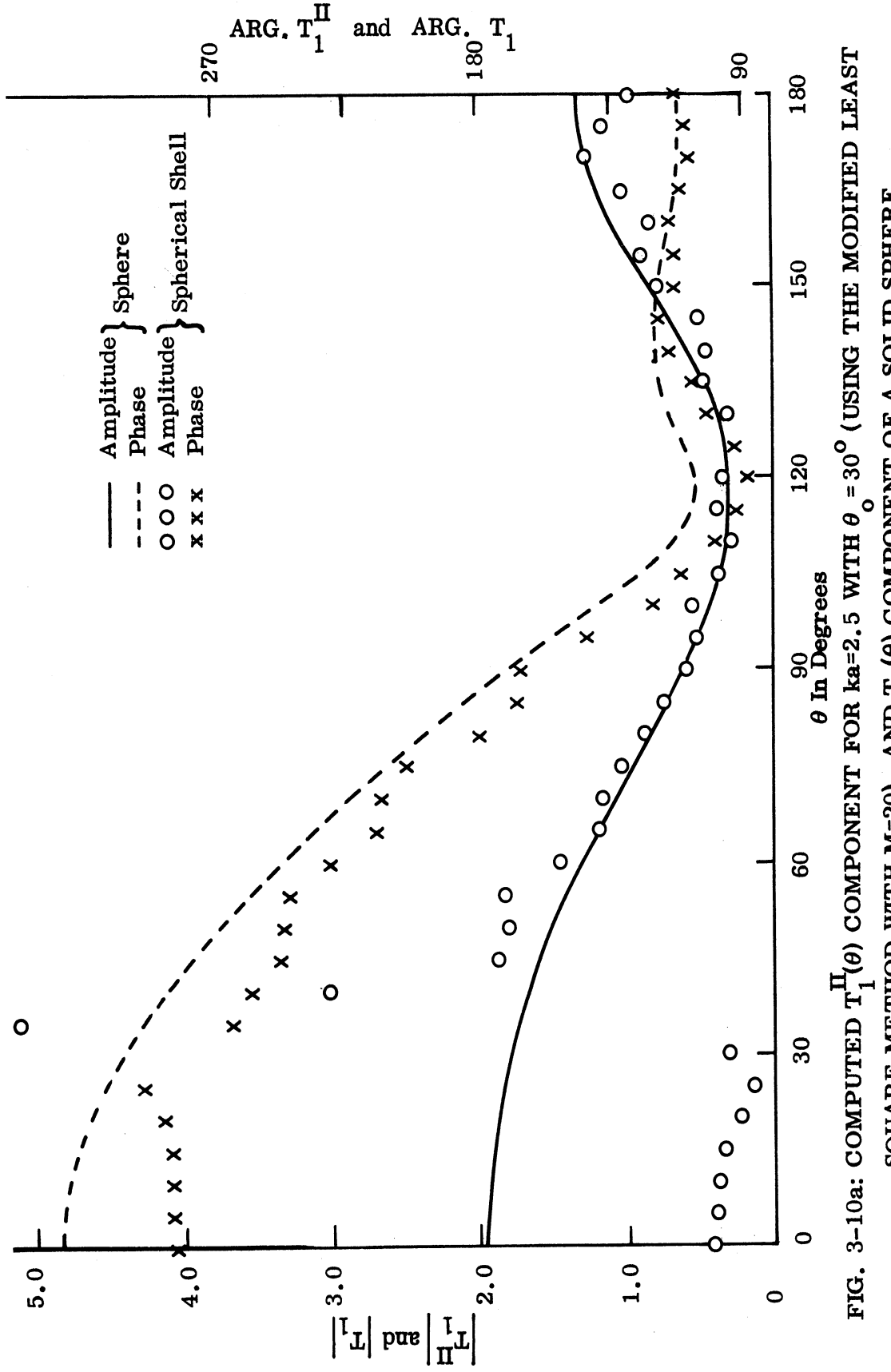

FIG. 3-10a: COMPUTED $T_1^{II}(\theta)$ COMPONENT FOR ka=2.5 WITH $\theta_o = 30^o$ (USING THE MODIFIED LEAST SQUARE METHOD WITH M=20), AND $T_1(\theta)$ COMPONENT OF A SOLID SPHERE.

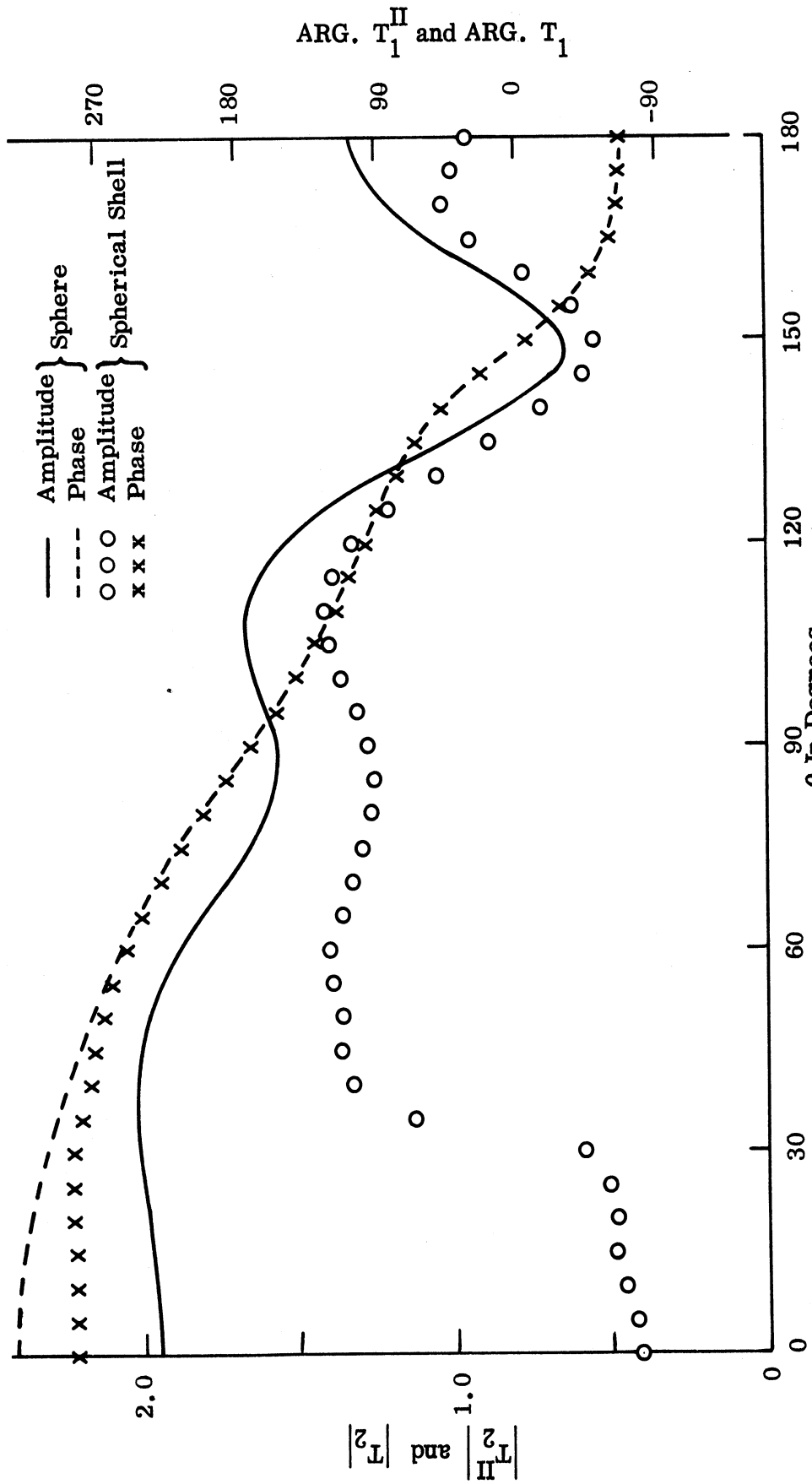

FIG. 3-10b: COMPUTED $T_2^{II}(\theta)$ COMPONENT FOR ka=2.5 WITH $\theta_o = 30^o$ (USING THE MODIFIED LEAST SQUARE METHOD WITH M=20), AND $T_2(\theta)$ COMPONENT OF A SOLID SPHERE.

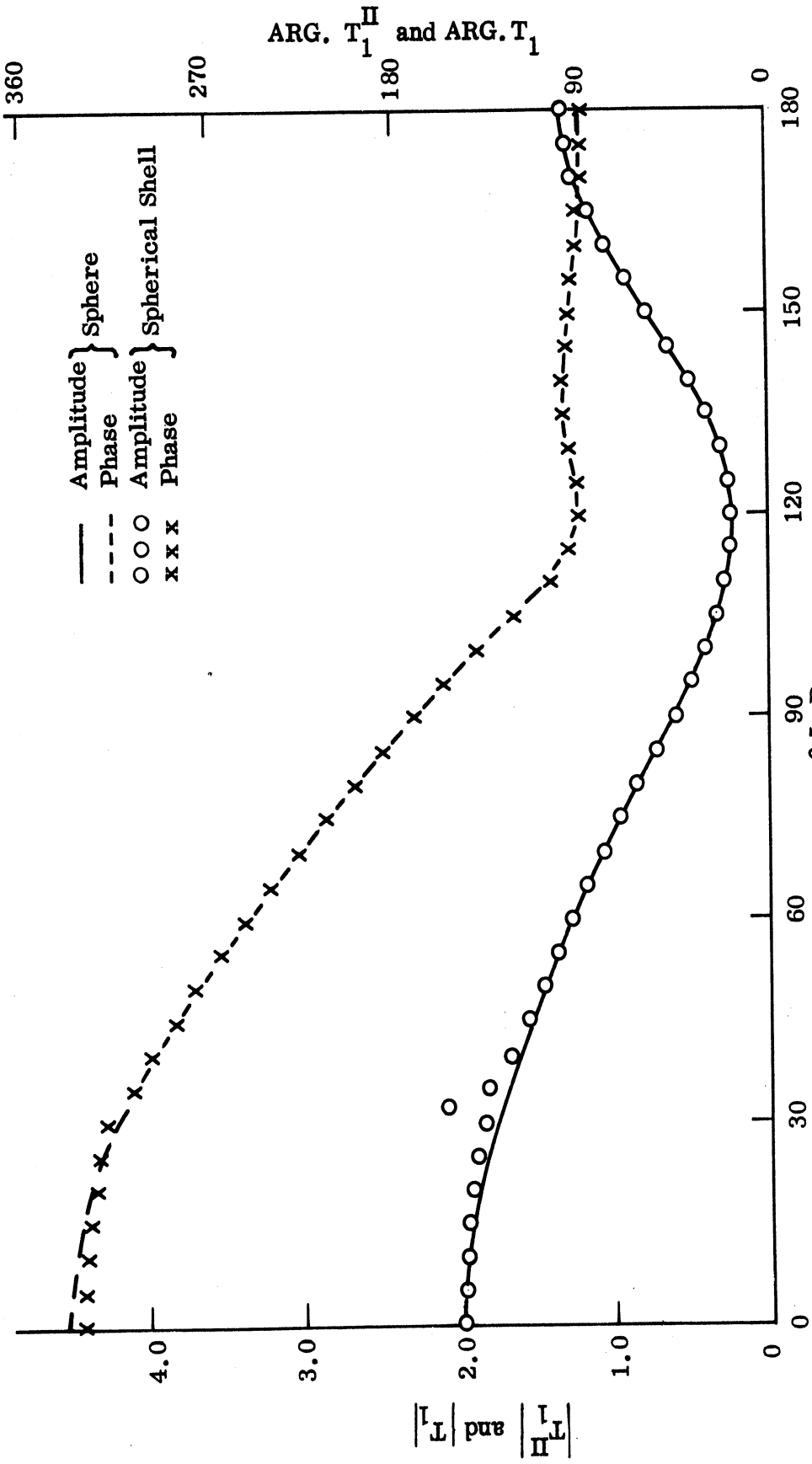

FIG. 3-11a: COMPUTED $T_1^{II}(\theta)$ COMPONENT FOR ka=2.75 WITH $\theta_o = 30^o$ (USING THE MODIFIED LEAST SQUARE METHOD WITH M=20), AND $T_1(\theta)$ COMPONENT OF A SOLID SPHERE.

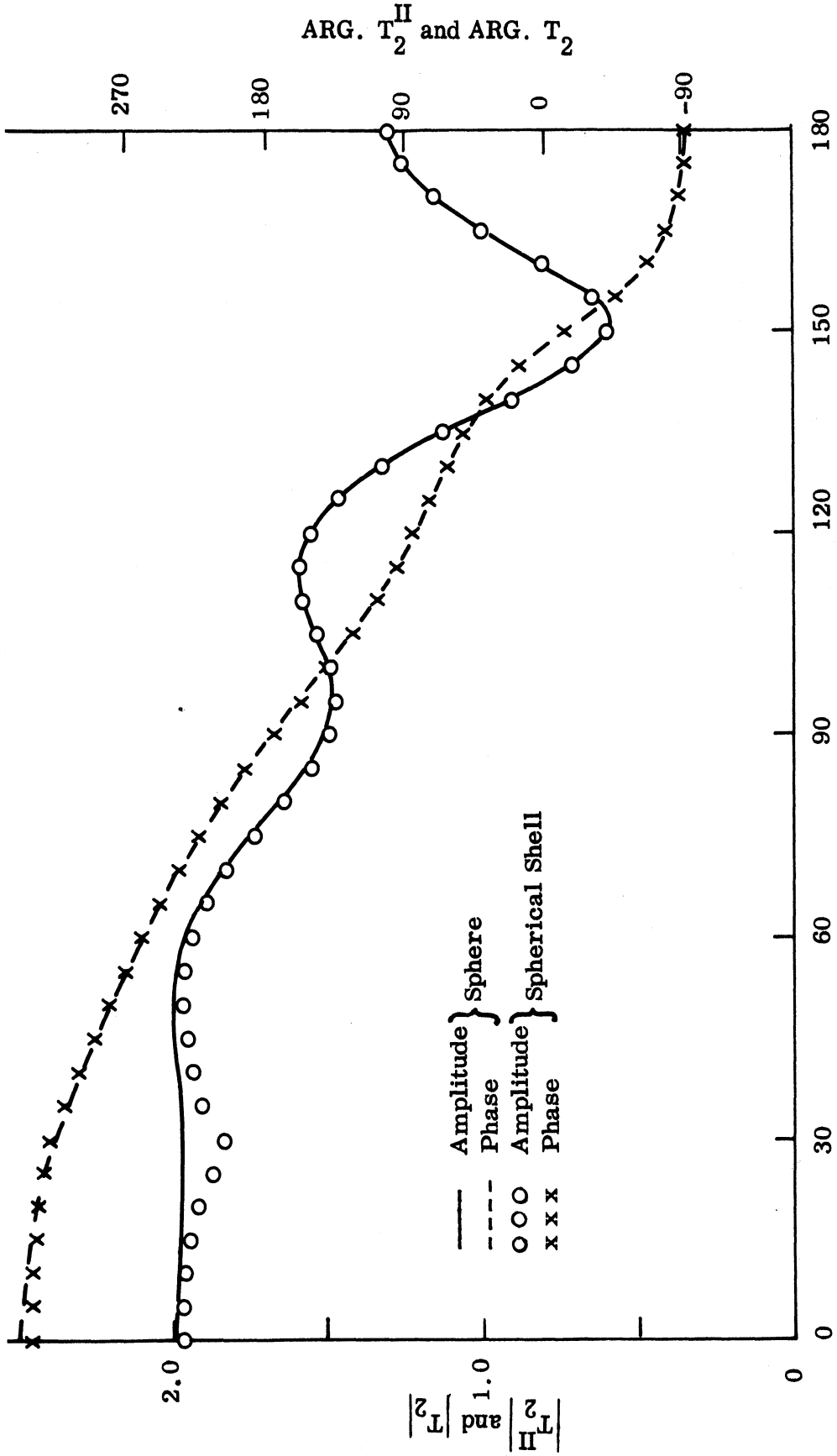

FIG. 3-11b: COMPUTED $T_2^{II}(\theta)$ COMPONENT FOR ka=2.75 WITH $\theta_o = 30^o$ (USING THE MODIFIED LEAST SQUARE METHOD WITH M=20), AND $T_2^{II}(\theta)$ COMPONENT OF A SOLID SPHERE.

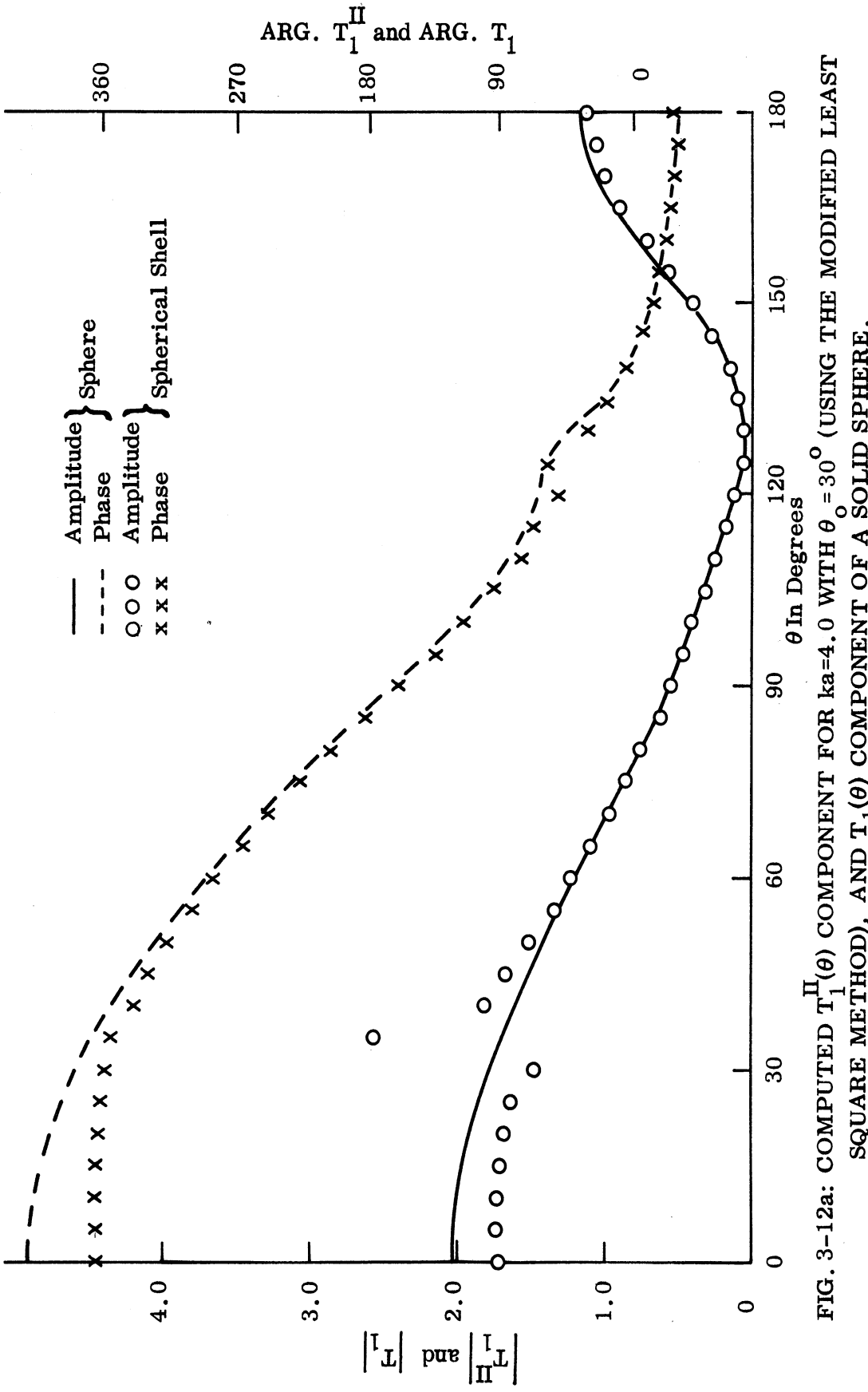

FIG. 3-12a: COMPUTED $T_1^{II}(\theta)$ COMPONENT FOR ka=4.0 WITH $\theta_o = 30^o$ (USING THE MODIFIED LEAST SQUARE METHOD), AND $T_1(\theta)$ COMPONENT OF A SOLID SPHERE.

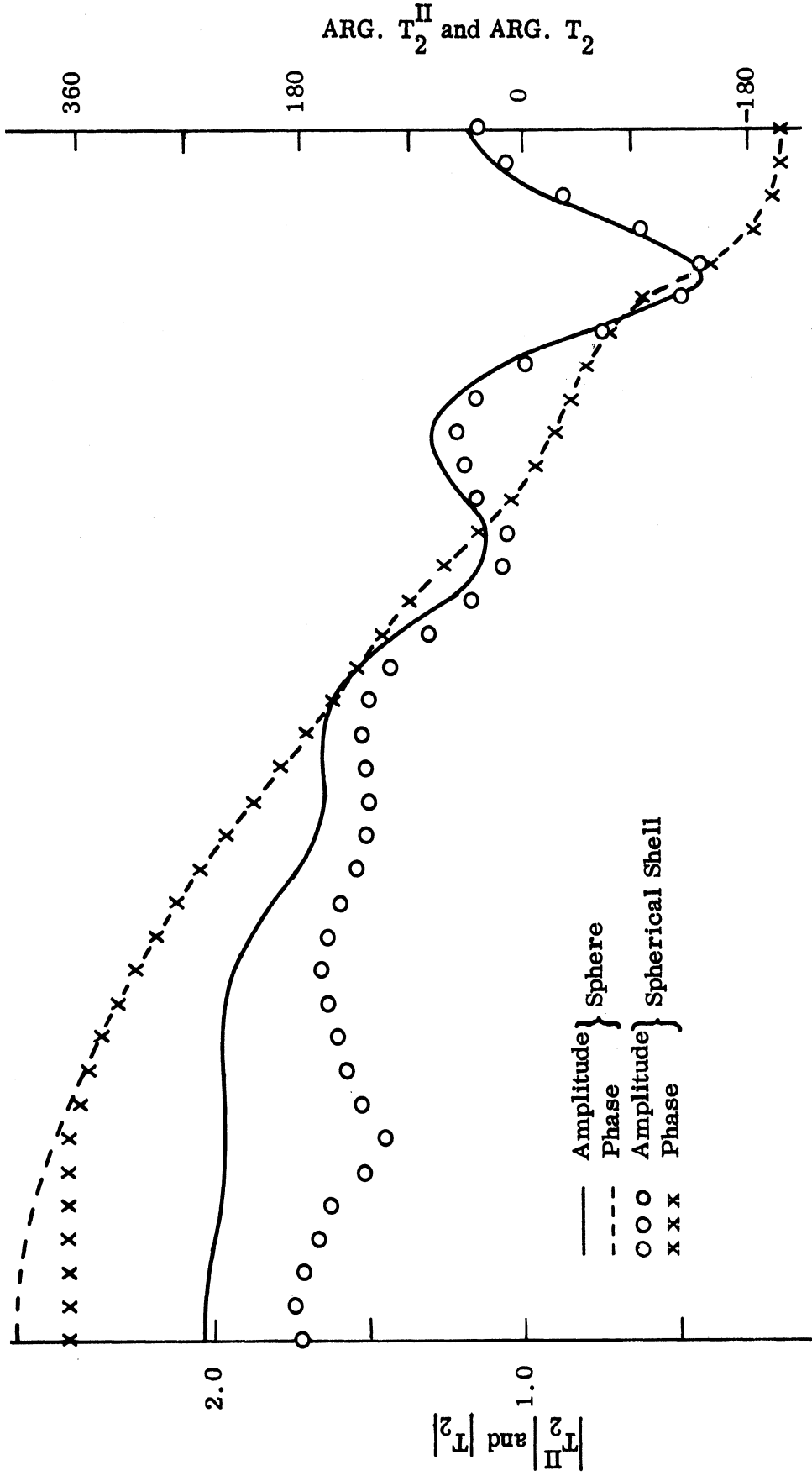

FIG. 3-12b: COMPUTED $T_2^{II}(\theta)$ COMPONENT FOR ka=4.0 WITH $\theta_o = 30^o$ (USING THE MODIFIED LEAST SQUARE METHOD), AND $T_2(\theta)$ COMPONENT OF A SOLID SPHERE.

across the aperture are quite smooth. The computed results of the surface field components are believed very close to the exact solution, apart from small oscillations observed above. The results will be confirmed by comparing with the experimental results in Chapter IV.

The bistatic cross sections have also been computed for $\theta_o = 30^o$ and ka=2.5 and 2.7, corresponding approximately to the frequencies for maximum and minimum backscattering cross section, respectively. The results for $\phi=0$ (E-plane) and $\phi=\pi/2$ (H-plane) are plotted in Figs. 3-13 and 3-14 in which the curves are normalized with respect to the backscattering cross section of a solid sphere for the same ka. Near the forward- and back-scattering directions, the cross section of the spherical shell is enhanced for ka=2.5 and reduced for ka=2.7, but in all other directions there seems to be no significant difference between a spherical shell and a sphere in the bistatic pattern.

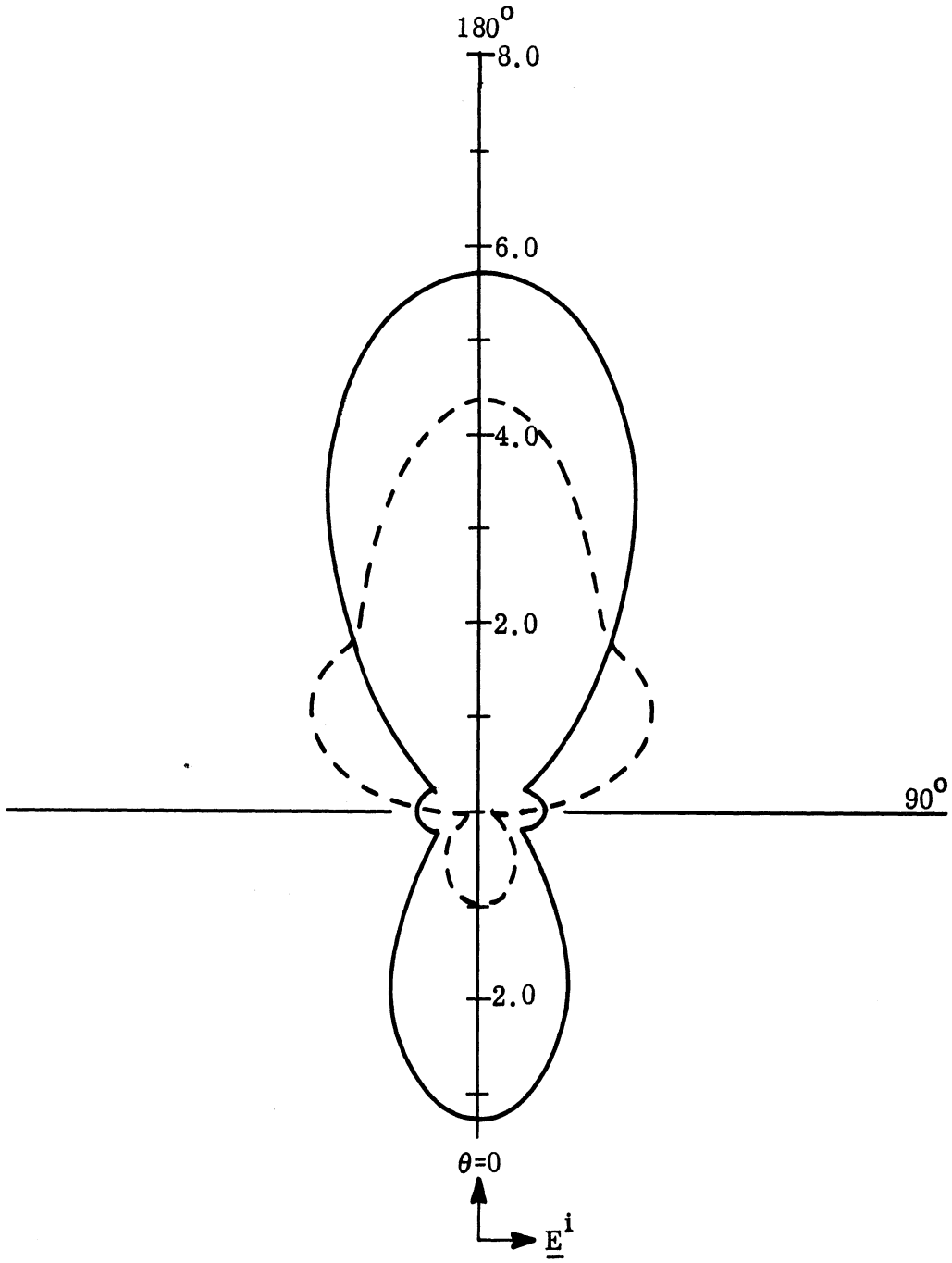

FIG. 3-13a: COMPUTED BISTATIC SCATTERING PATTERN OF A SPHERICAL SHELL FOR ka=2.5 WITH $\theta_o = 30^o$. DASHED LINE IS FOR A SOLID SPHERE. ϕ=0.

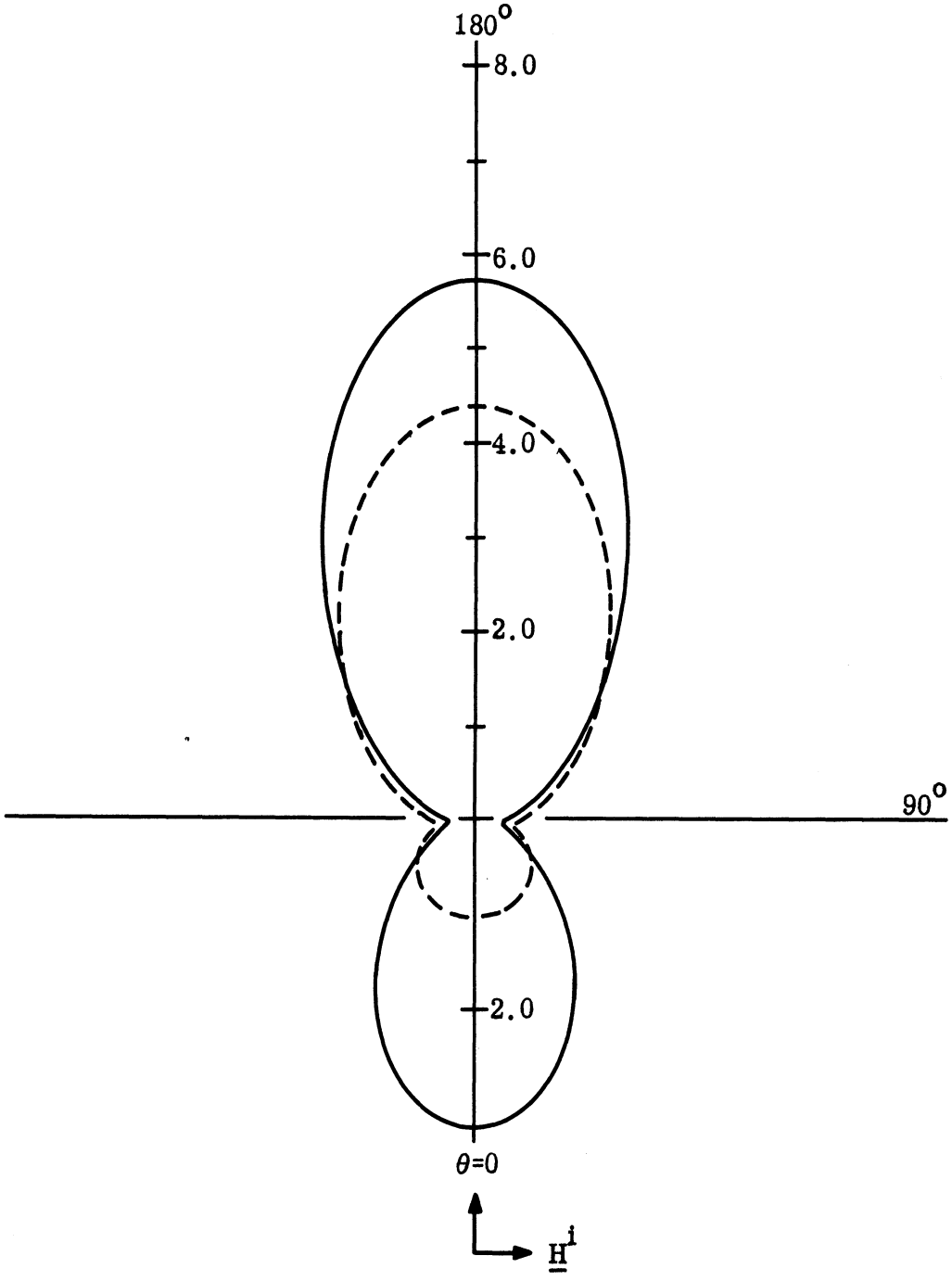

H-PLANE

FIG. 3-13b: COMPUTED BISTATIC SCATTERING PATTERN OF A SPHERICAL SHELL FOR ka=2.5 WITH $\theta_o = 30^o$. DASHED LINE IS FOR A SOLID SPHERE. $\phi = \pi/2$.

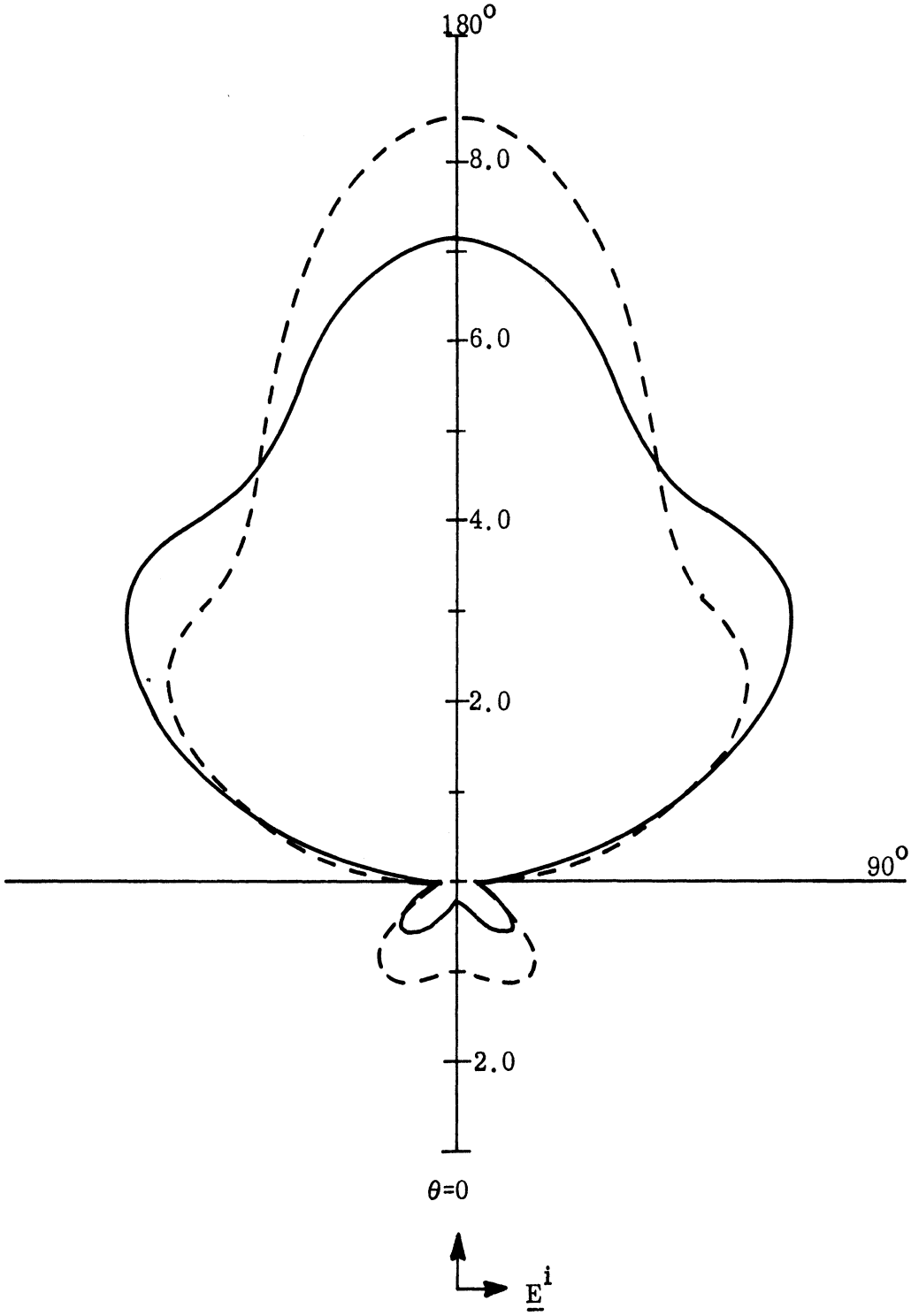

FIG. 3-14a: COMPUTED BISTATIC SCATTERING PATTERN OF A SPHERICAL SHELL FOR ka=2.7 WITH $\theta_o = 30^o$. DASHED LINE IS FOR A SOLID SPHERE. ϕ=0.

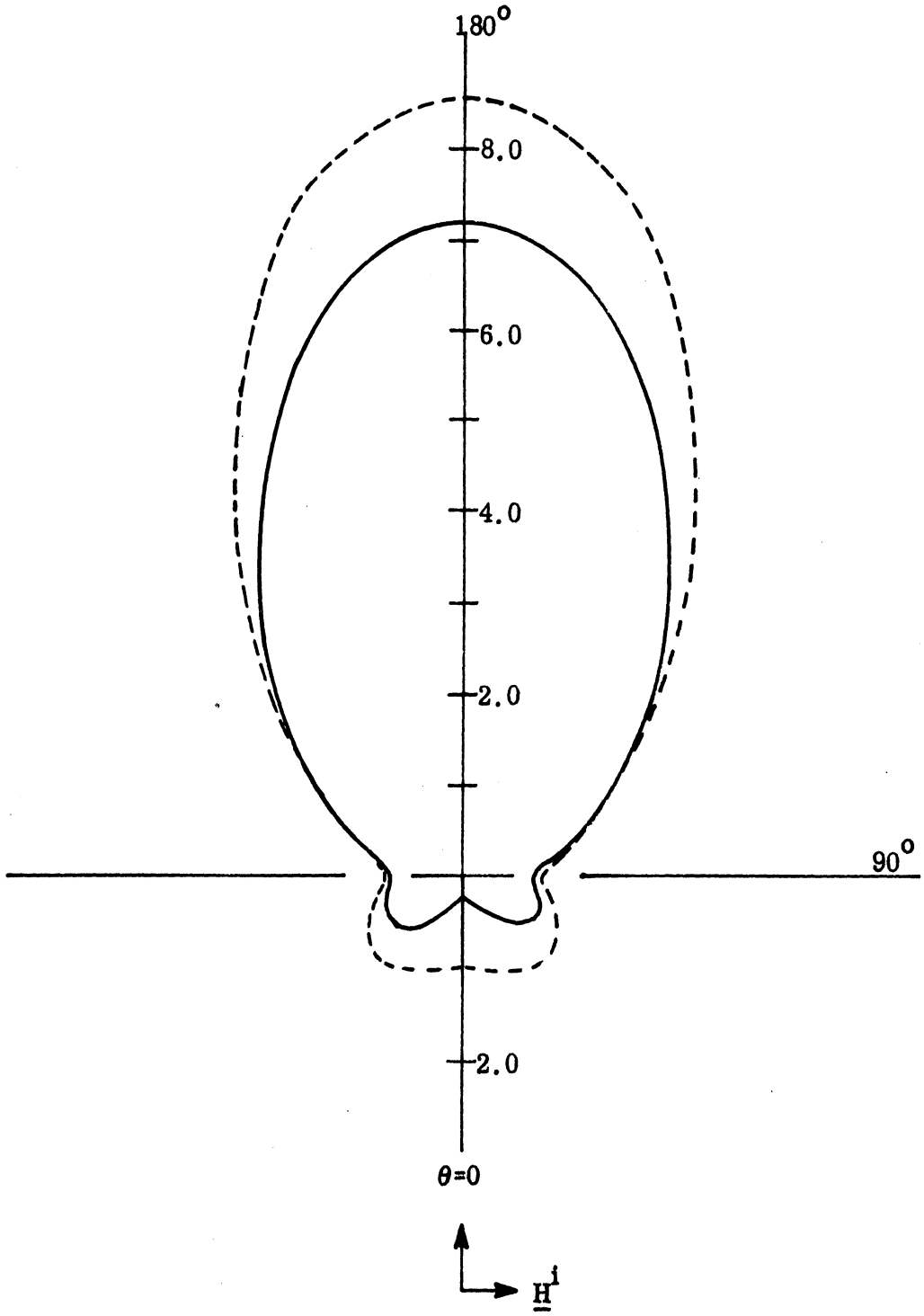

FIG. 3-14b: COMPUTED BISTATIC SCATTERING PATTERN OF A SPHERICAL SHELL FOR ka=2.7 WITH $\theta_o = 30^o$. DASHED LINE IS FOR A SOLID SPHERE. $\phi = \pi/2$.

CHAPTER IV

EXPERIMENTAL RESULTS

4.1 Experimental Models and Facilities

To obtain some physical insight into the scattering behavior of a spherical shell and to confirm the numerical results, a series of measurements was carried out on spherical shells with various aperture angles, θ_o. All the backscattering and surface field measurements were made within the L-, S- and C- band regions. Since frequencies between these bands were not available, two different sets of spherical shell models, about 2.55 and 3.09 inches in (outside) diameter, were used to span the entire range, $0.7 \leq ka \leq 4.85$. Each spherical shell was made by joining two hemispherical shells (cold drawn from thin steel sheet) and then cutting a hole of appropriate size in the top of one of the hemispheres. A photograph of some of the models is shown in Fig. 4-1. Altogether, eleven such models were constructed; five models in each (diameter) set with $\theta_o = 15^o$, 30^o, 45^o, 60^o and 90^o, and a complete shell (sphere) of 3.09 inch diameter. The sphere was used for calibrating all the measured data. The shell thicknesses were somewhat non-uniform varying from 0.015 to 0.020 inches for the 2.55 inch models and from 0.030 to 0.040 inches for the 3.09 inch models.

The backscattering measurements were made using conventional c.w. equipment in an anechoic room, where the complete backscattering patterns for both horizontal and vertical polarizations could be taken. The surface field measurements were performed in a tapered anechoic chamber specifically designed for such measurements. A probe traversing mechanism is mounted above the chamber and the probe, with its coaxial lead supported

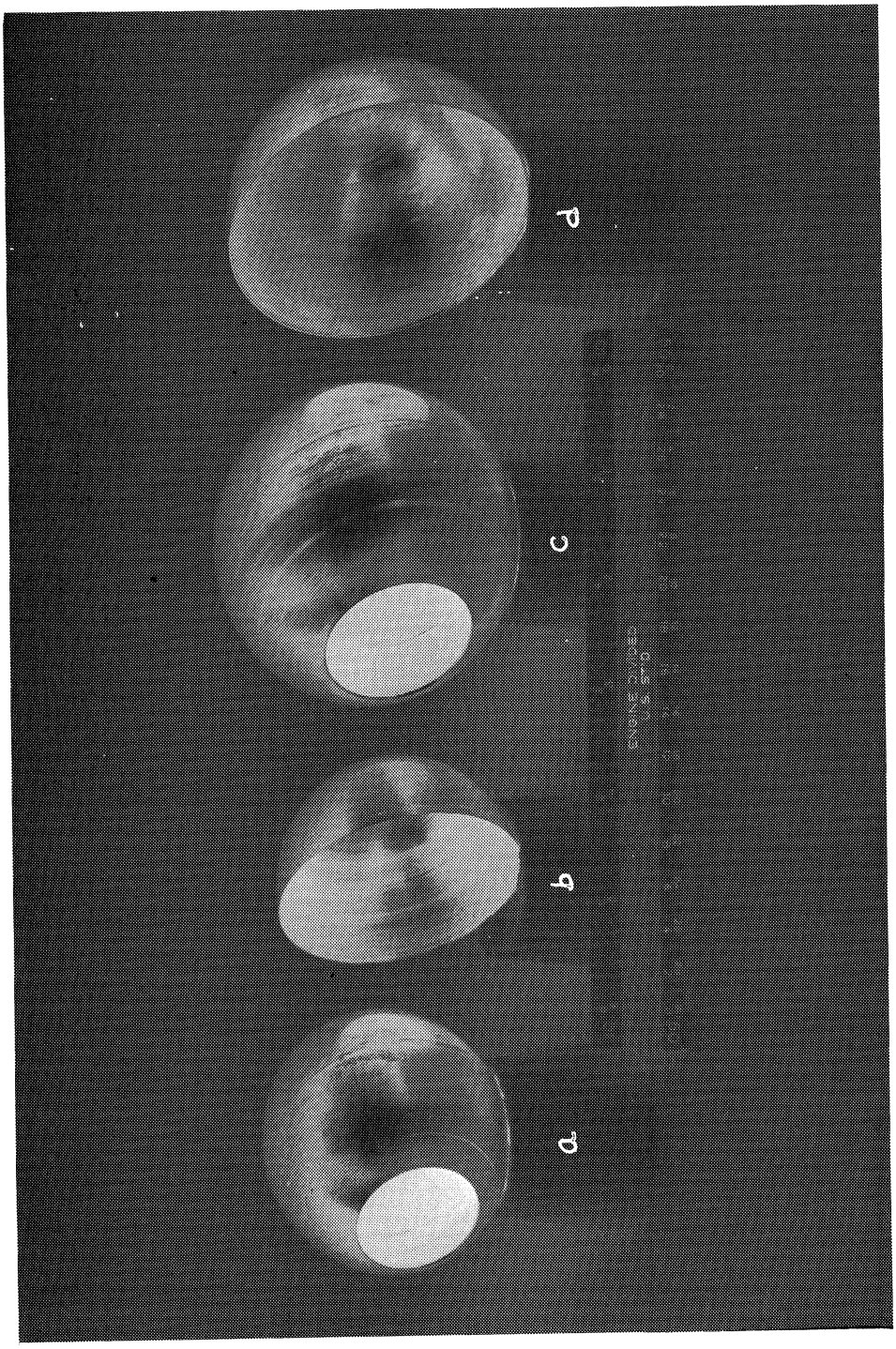

FIG. 4-1: EXPERIMENTAL MODELS. a) Diameter D = 2.55", Aperture Angle θ_o=30°, b) D=2.55", θ_o=90°, c) D=3.09", θ_o=30°, d) D = 3.09", θ_o=90°.

by a balsa wood tower, extends vertically through the ceiling. The mechanism is capable of moving the probe around a horizontal circle and in a direction specified by rectangular coordinates as well. The photograph in Fig. 4-2 shows a model being probed in the anechoic chamber as viewed from the position of the antenna. A detailed description of this surface field measurement facility has been given by Knott et al (1965). The performance of this facility is known to be quite reliable in the surface current measurements if the model is a perfectly conducting obstacle and the polarization of the incident field is horizontal. For other near field measurements, its performance is, often, not reliable, and the near field probing was therefore limited to the current measurements for horizontal polarization.

4.2 Backscattering Measurements

Backscattering measurements were made with all eleven models in the L- and S- band regions and were extended to the C-band region only for the 3.09 inch models. The corresponding covered ka ranges were:

$$ka = 0.70 \sim 1.10 \quad \text{(L-band)}$$
$$ka = 1.50 \sim 2.72 \quad \text{(S-band)}$$

for the 2.55 inch model, and

$$ka = 0.85 \sim 1.40 \quad \text{(L-band)}$$
$$ka = 2.18 \sim 3.20 \quad \text{(S-band)}$$
$$ka = 3.30 \sim 4.85 \quad \text{(C-band)}$$

for the 3.09 inch model.

The distance from the transmit-receive antenna to the supporting pedestal was 9 feet and the model was placed so that the plane of the aperture was parallel to the axis of the pedestal. When the aperture of the model was directed at the antenna ($\theta = 0$), the measurement for each model was repeated two to four times for the same ka value and the results were

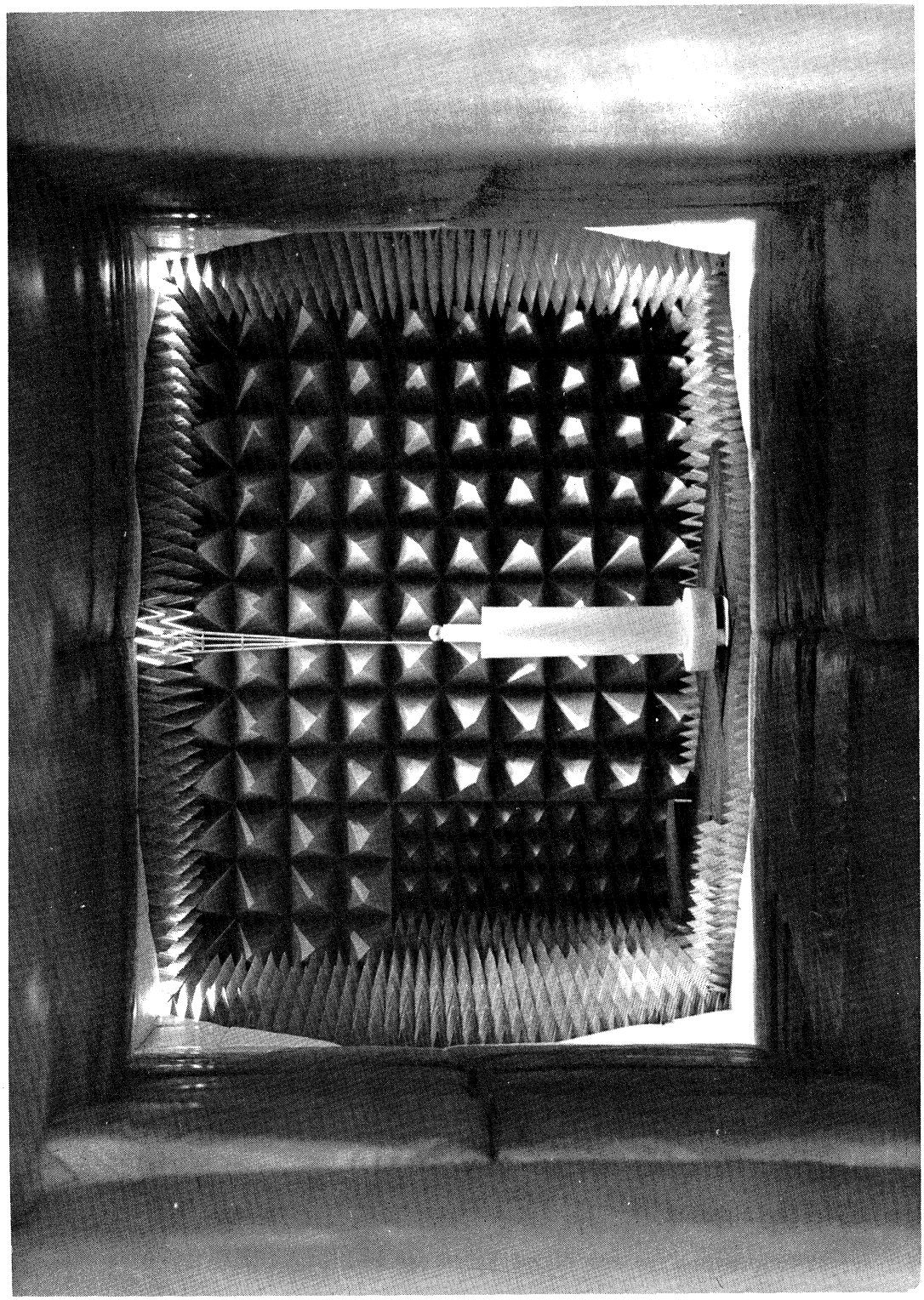

FIG. 4-2: SURFACE FIELD MEASUREMENT FACILITY AS VIEWED FROM THE POSITION OF THE ILLUMINATING ANTENNA.

averaged to give more reliable experimental data. The measured backscattering cross sections normalized to the geometrical cross section, πa^2, are shown in Figs. 4-3 through 4-7. In the regions $0.7 \leq ka \leq 1.1$ and $2.18 \leq ka \leq 2.72$ where the measurements with the different diameter models overlap, two sets of data are given. It is interesting to note that marked reductions in the backscattering are obtained in the vicinity of the resonant frequencies of a spherical cavity (lowest resonant mode in the spherical cavity occurs at $ka \cong 2.75$, the first root of $\psi_1'(ka) = 0$ and the next lowest mode at $ka \cong 3.87$, the first root of $\psi_2'(ka) = 0$, and the third at $ka \cong 4.49$, the first root of $\psi_1(ka) = 0$). These resonant effects are particularly strong for $\theta_o = 30^o$ and 45^o. For $\theta_o = 15^o$ it is presumed that the coupling through the small aperture is insufficient when $ka \cong 2.75$, and for $\theta_o > 45^o$ the detuning of the cavity resulting from the large size of the aperture can no longer be ignored.

Four complete backscattering cross section patterns in the E-plane ($\phi = 0$) for $ka = 1.0$, 2.0, 2.75, and 3.0 with $\theta_o = 30^o$ are given in Fig. 4-8. It is observed that when $ka = 1.0$ the spherical shell model has almost the same cross section as a solid sphere of the same size. As ka increases, however, the effect of the cavity becomes more apparent and the variations of the cross section as a function of θ increase. For $ka = 2.75$ the relative cross section is reduced to about -14 dB at $\theta = 0^o$.

4.3 Surface Field Measurements

The current components on the outside of the spherical shell were measured for 3.09 inch model with $\theta_o = 30^o$ at frequencies 2.432, 3.344 and 3.648 GHz, corresponding to $ka = 2.0$, 2.75 and 3.0 respectively. The measurements were made with the aperture of the spherical shell directed at the antenna ($\theta = 0$) at 5-degree intervals of θ along the conducting surface and normalized with respect to the theoretical values for a

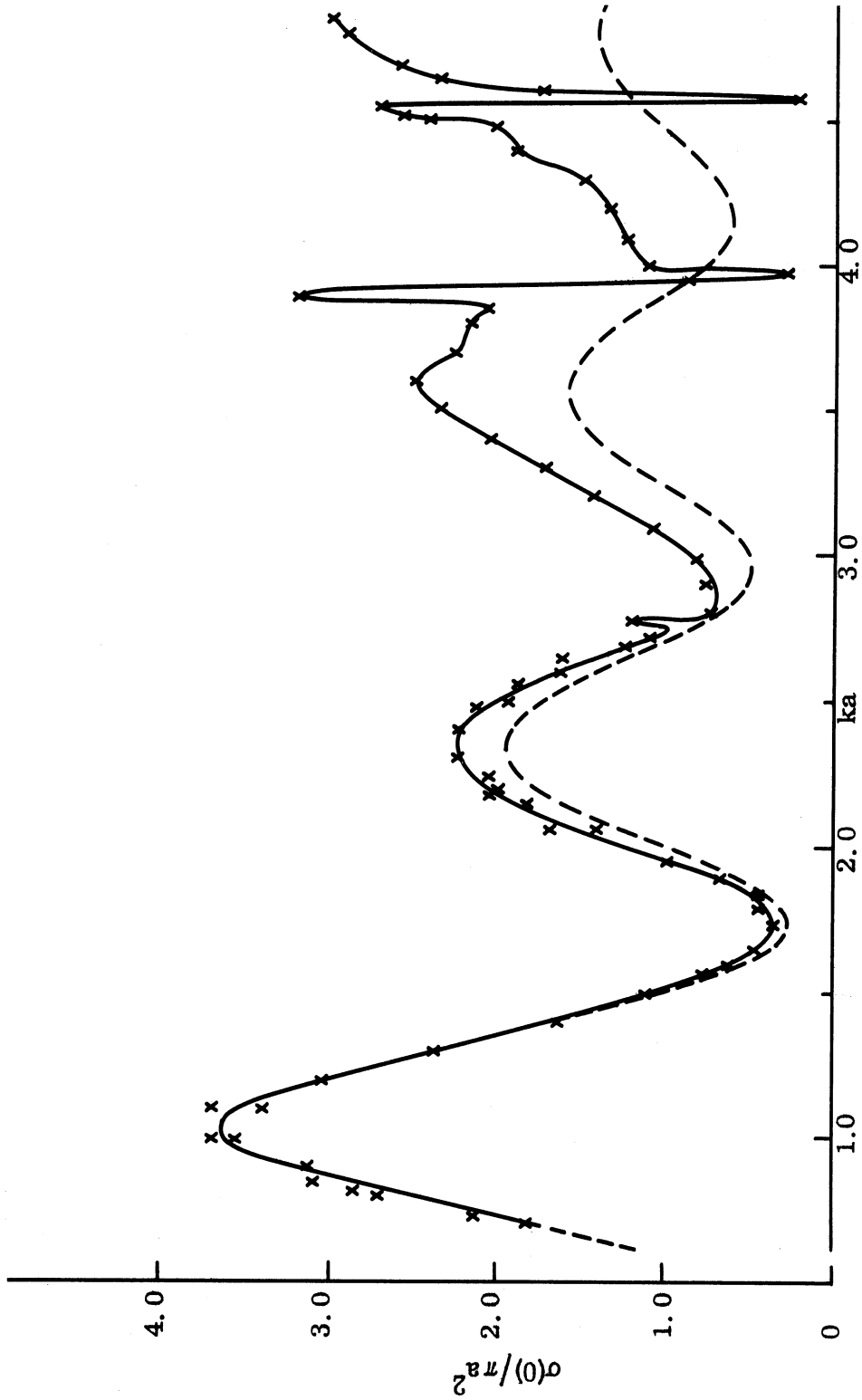

FIG. 4-3: MEASURED BACKSCATTERING CROSS SECTION OF A SPHERICAL SHELL WITH $\theta_o = 15^o$ (*-) AND THEORETICAL BACKSCATTERING CROSS SECTION OF A SOLID SPHERE (---) .

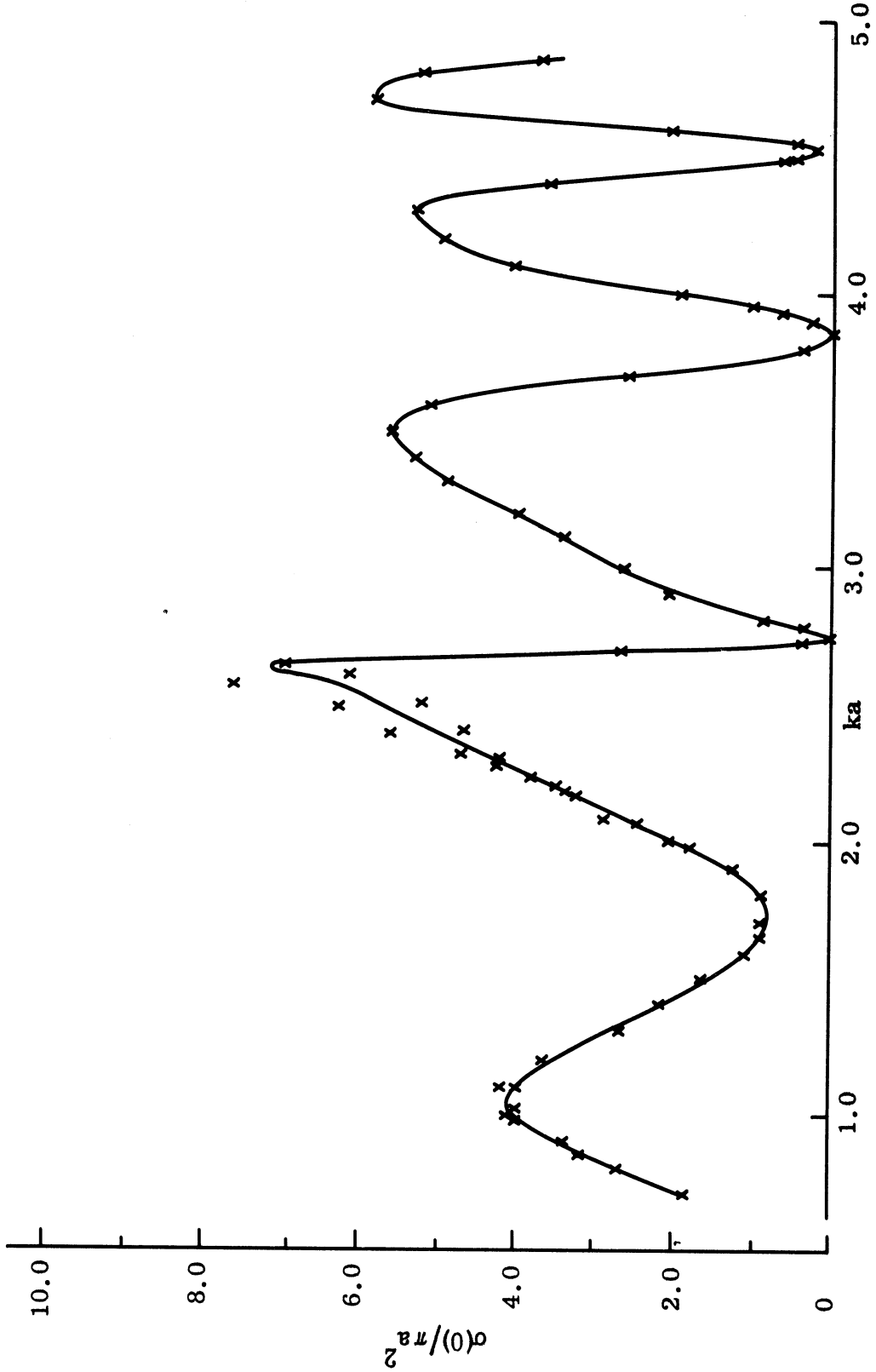

FIG. 4-4: MEASURED BACKSCATTERING CROSS SECTIONS OF A SPHERICAL SHELL WITH $\theta_o = 30^o$.

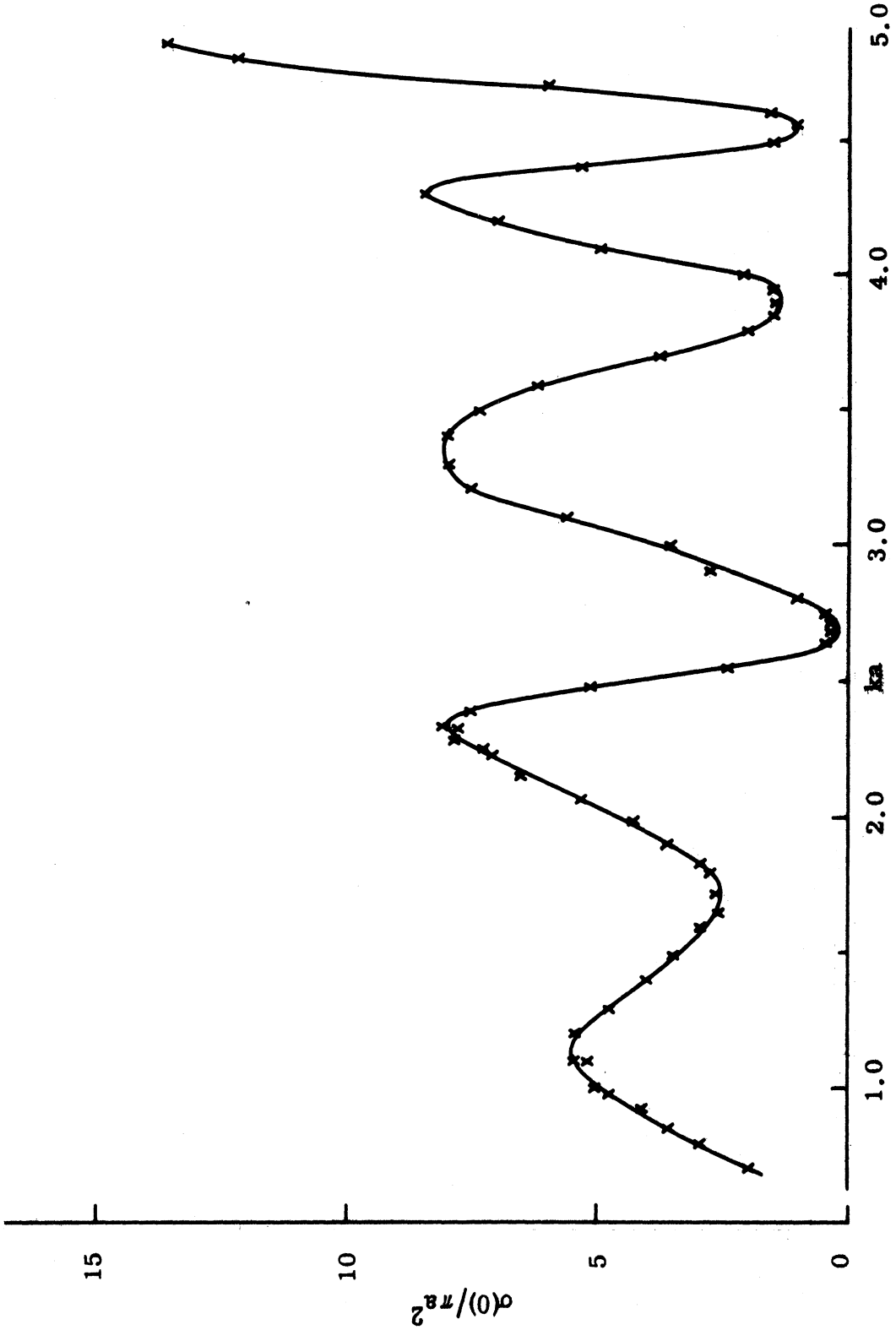

FIG. 4-5: MEASURED BACKSCATTERING CROSS SECTION OF A SPHERICAL SHELL WITH $\theta_o = 45^o$.

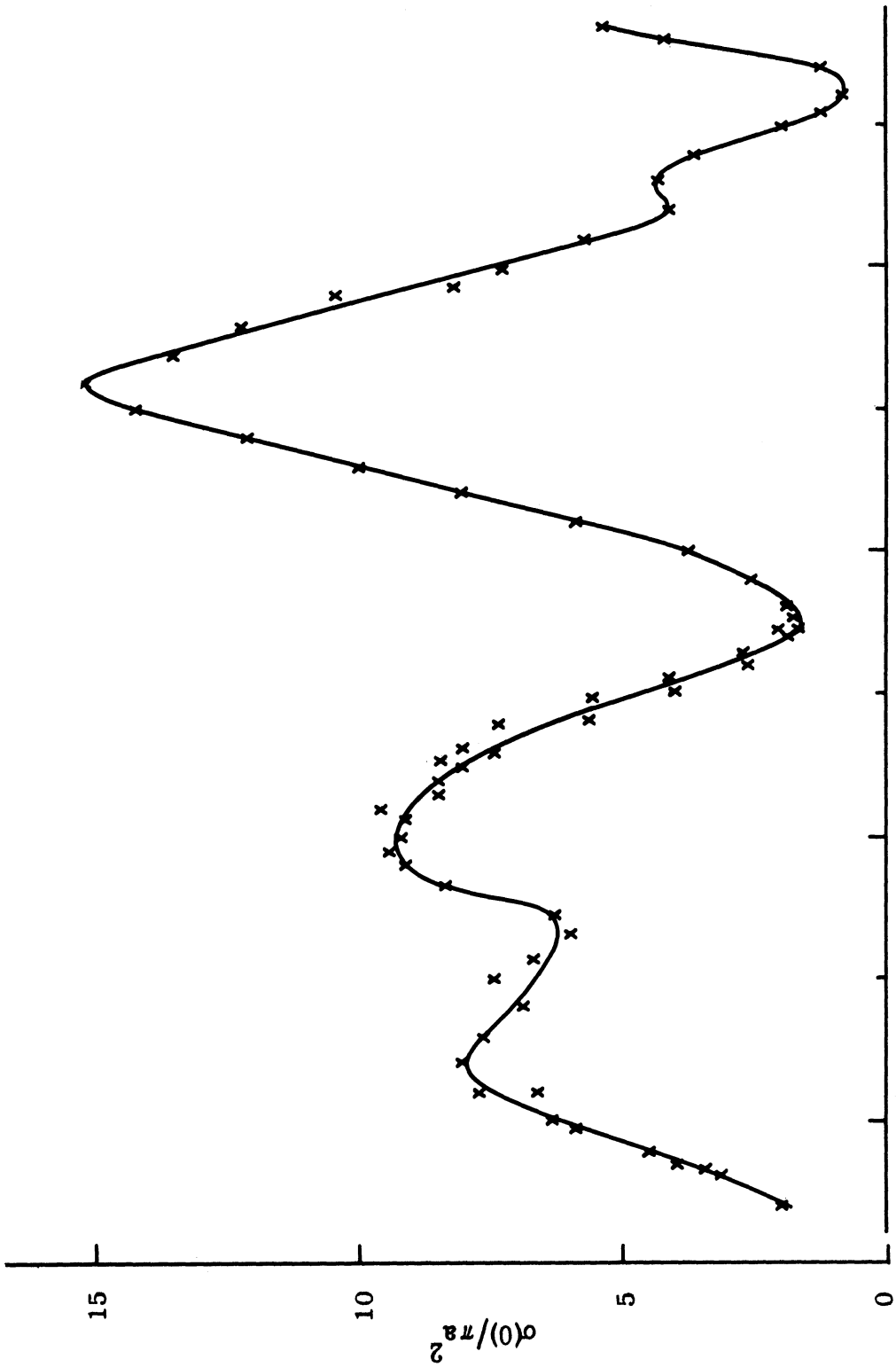

FIG. 4-6: MEASURED BACKSCATTERING CROSS SECTION OF A SPHERICAL SHELL WITH $\theta_o = 60^o$.

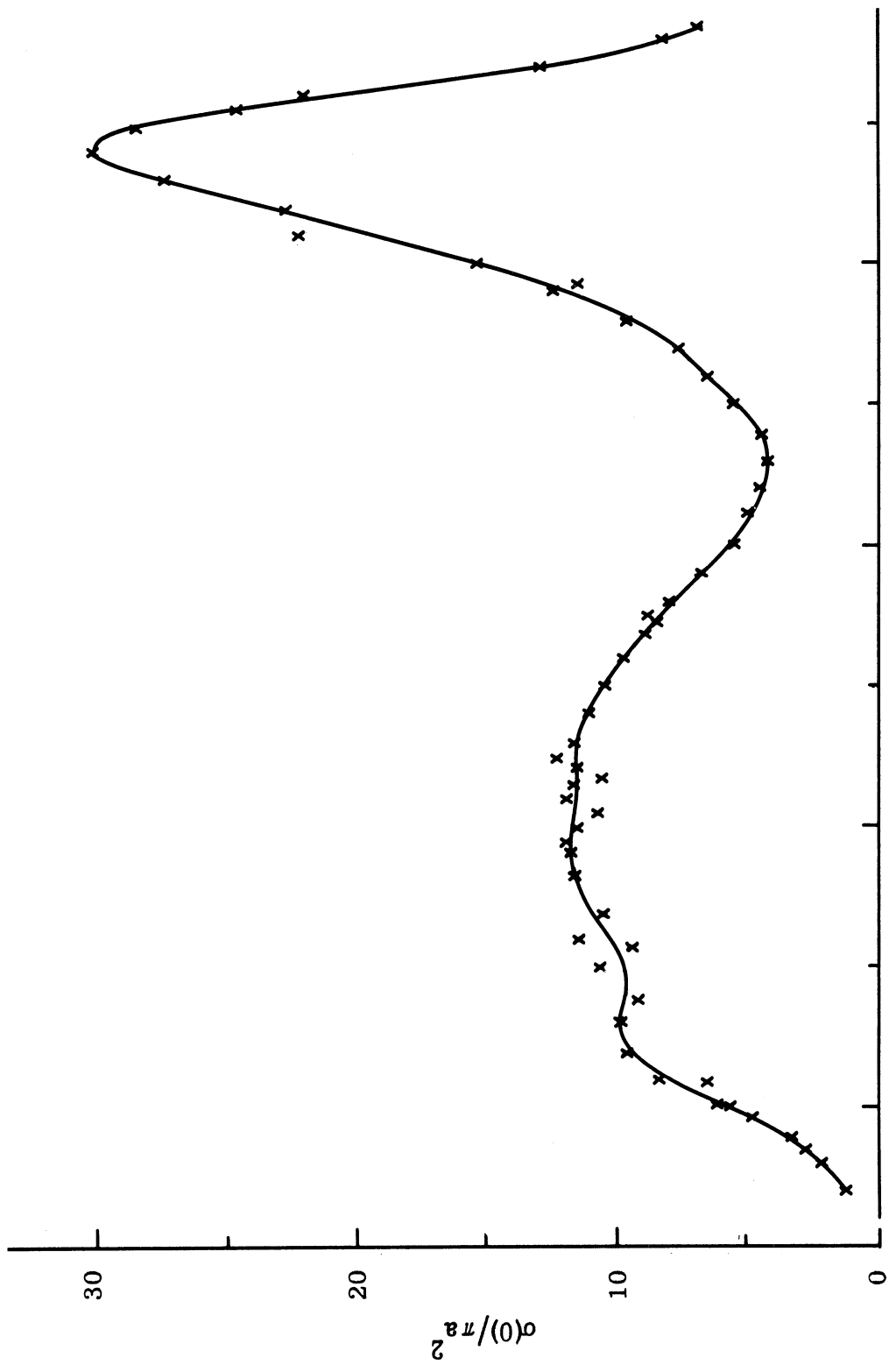

FIG. 4-7: MEASURED BACKSCATTERING CROSS SECTION OF A SPHERICAL SHELL WITH $\theta_o = 90^o$.

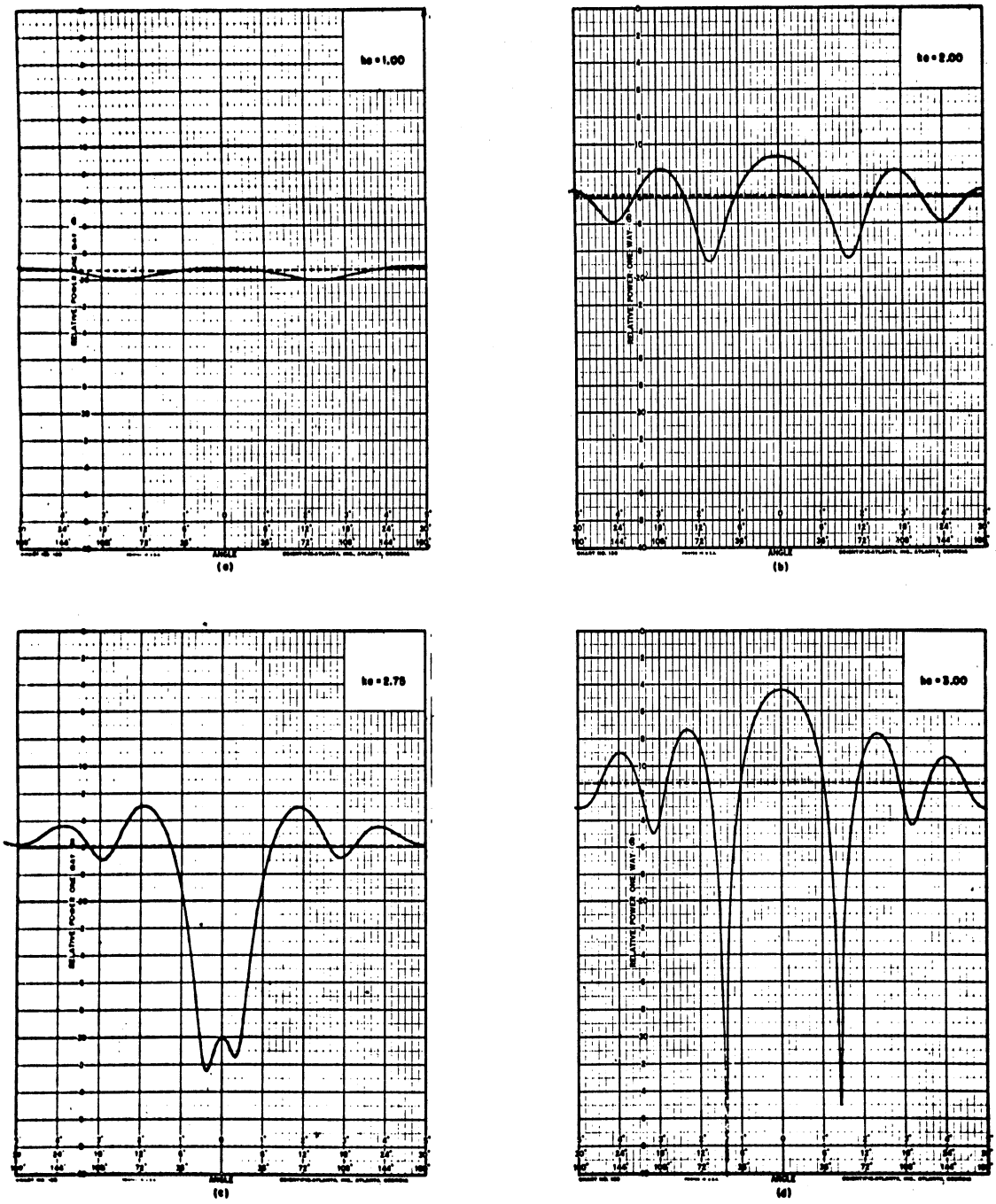

FIG. 4-8: BACKSCATTERING PATTERNS OF A SPHERICAL SHELL WITH $\theta_0 = 30^0$ (———) AND A SOLID SPHERE (- - -). HORIZONTAL POLARIZATION.

solid sphere at $\theta = 0^{o}$. A horizontal probe (bent about 1/4 inch from the end so that the plane of the loop is perpendicular to the lead) was scanned all the way around the spherical shell surface in a horizontal plane ($\phi = 0$) to measure the amplitude and phase of $T_2^{II}(\theta)$. The data was then averaged about the zero aspect to remove the asymmetrically induced error components in the probe. Since the probing mechanism is incapable of rotating the probe along the vertical plane ($\phi = \frac{\pi}{2}$), two separate measurements for $T_1^{II}(\theta)$ were taken along the upper half of the spherical shell surface for each ka. In the first a horizontal probe was used and next a vertical probe (with no bent portion). Of course, by taking the vector sum of these two measurements, the amplitude and phase of $T_1^{II}(\theta)$ were deduced.

The results are presented in Figs. 4-9 through 4-11 with the computed values for comparison. In Figs. 4-12a and b the measured and theoretical values of $T_1(\theta)$ and $T_2(\theta)$ for a sphere with ka = 3.0 are given to indicate the accuracy of the measurements taken for the spherical shell. Figs. 4-12a and b show that the experimental errors are about 0.6 dB in amplitude and 15 degrees in phase. The differences between measured and computed results in Figs. 4-9 through 4-11 are of the same order as those in Figs. 4-12a and b, except in the immediate vicinity of the edge where the discrepancies can be attributed to the interaction of the probe with the edge.

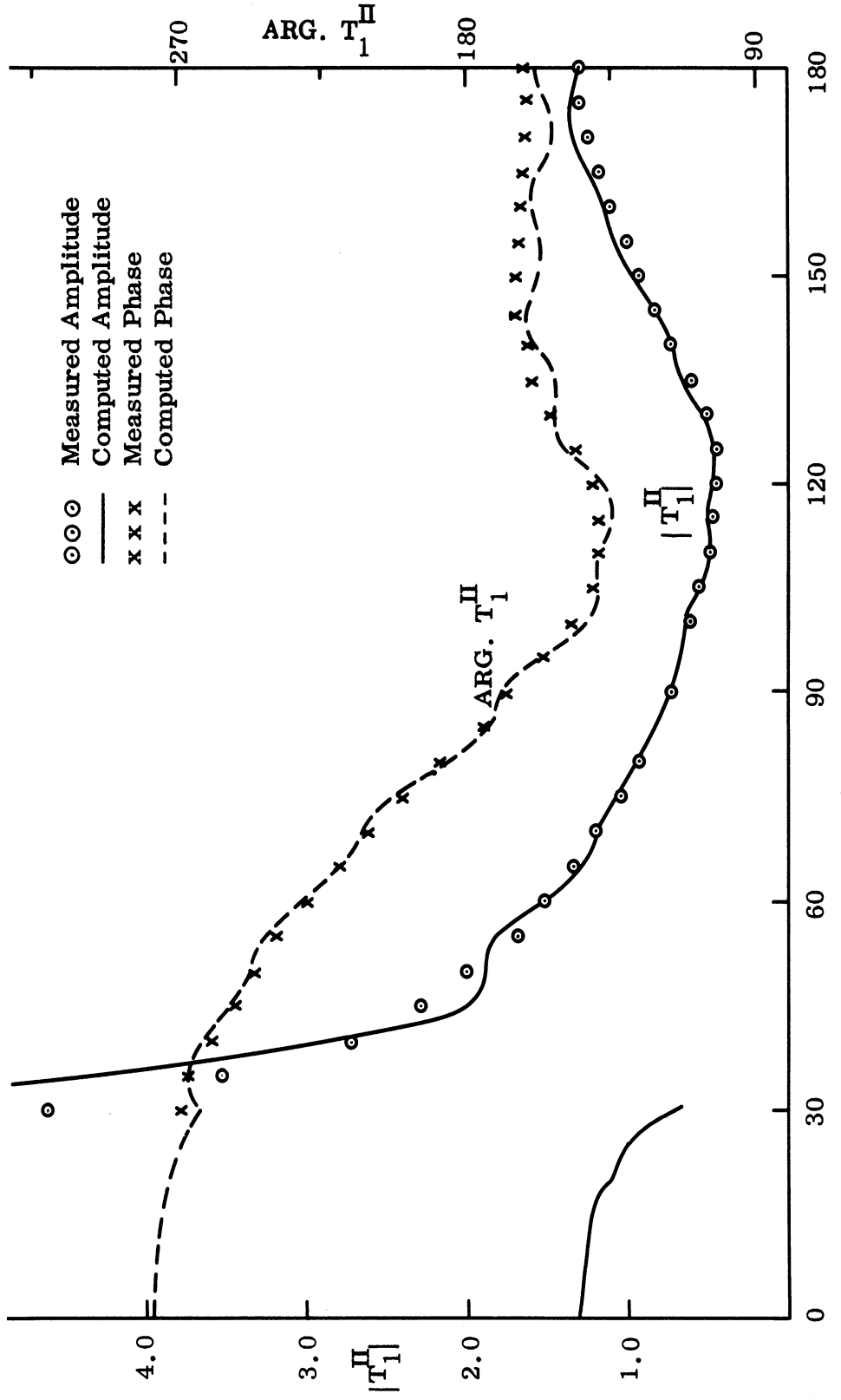

FIG. 4-9a: MEASURED AND COMPUTED $T_1^{II}(\theta)$ COMPONENT FOR ka = 2.0 WITH $\theta_o = 30^o$ AND M=20.

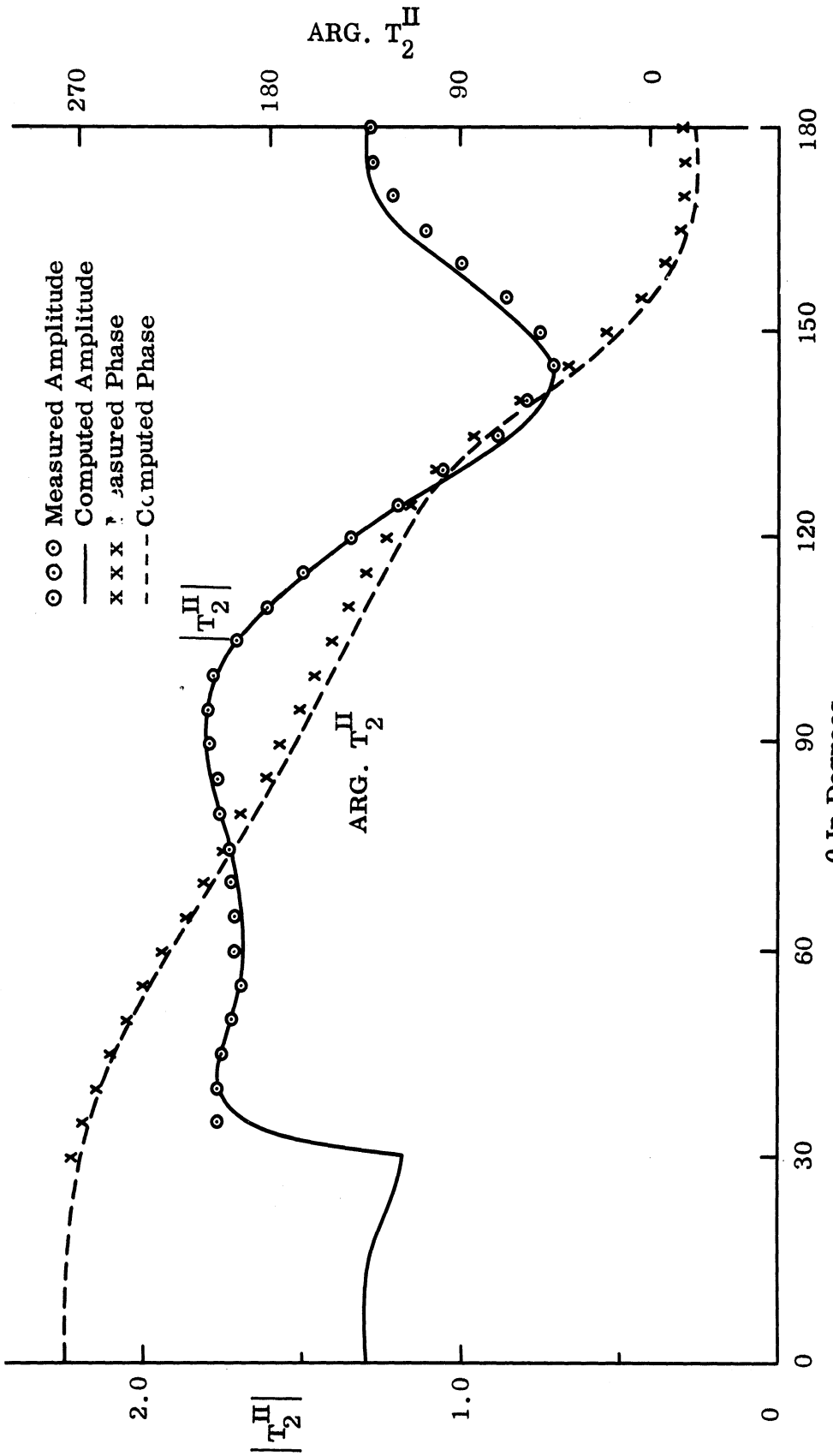

FIG. 4-9b: MEASURED AND COMPUTED $T_2^{II}(\theta)$ COMPONENT FOR ka=2.0 WITH $\theta_o=30^o$ AND M=20.

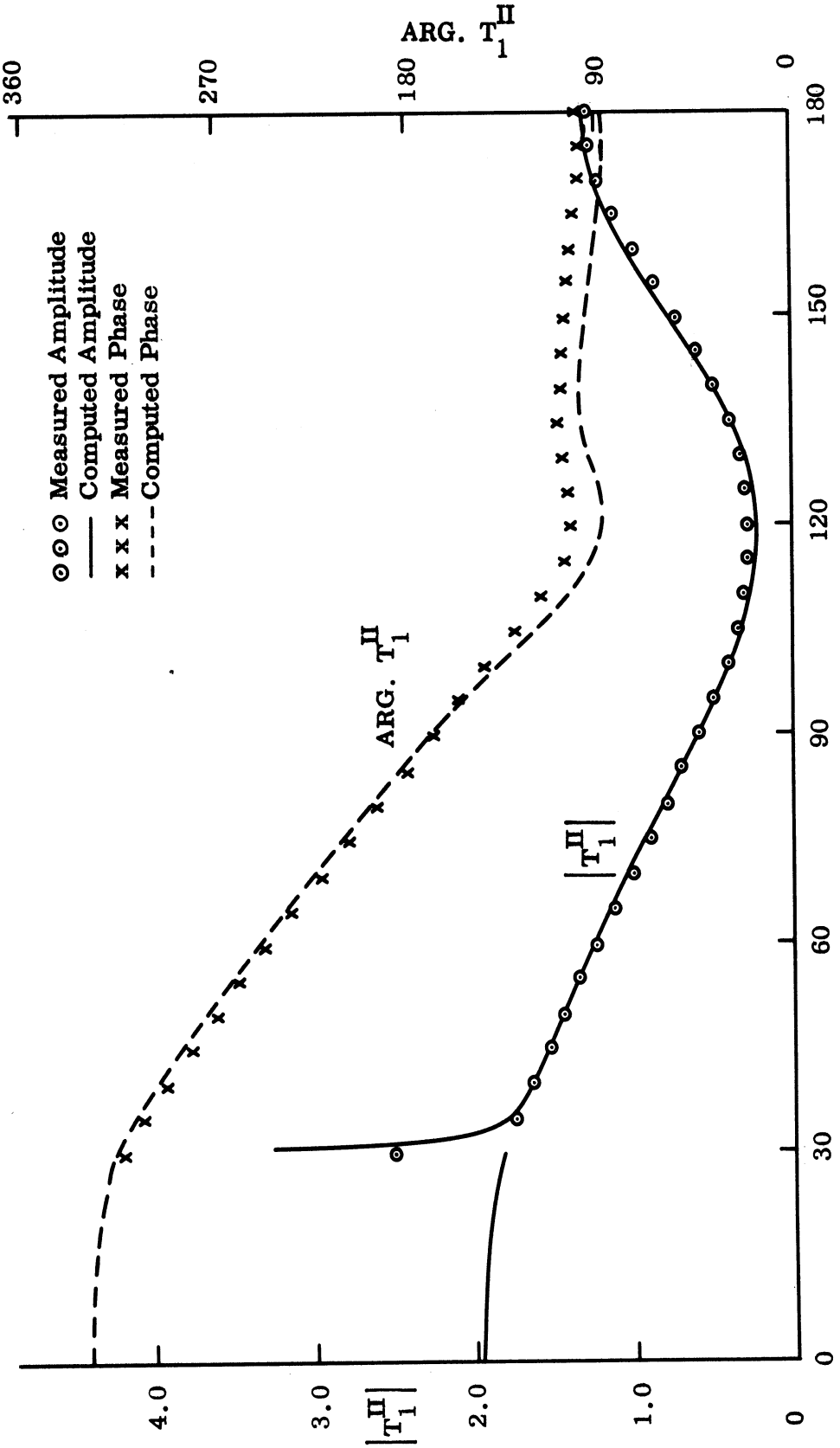

FIG. 4-10a: MEASURED AND COMPUTED $T_1^{II}(\theta)$ COMPONENT FOR ka = 2.75 WITH $\theta_o = 30^o$ AND M=20.

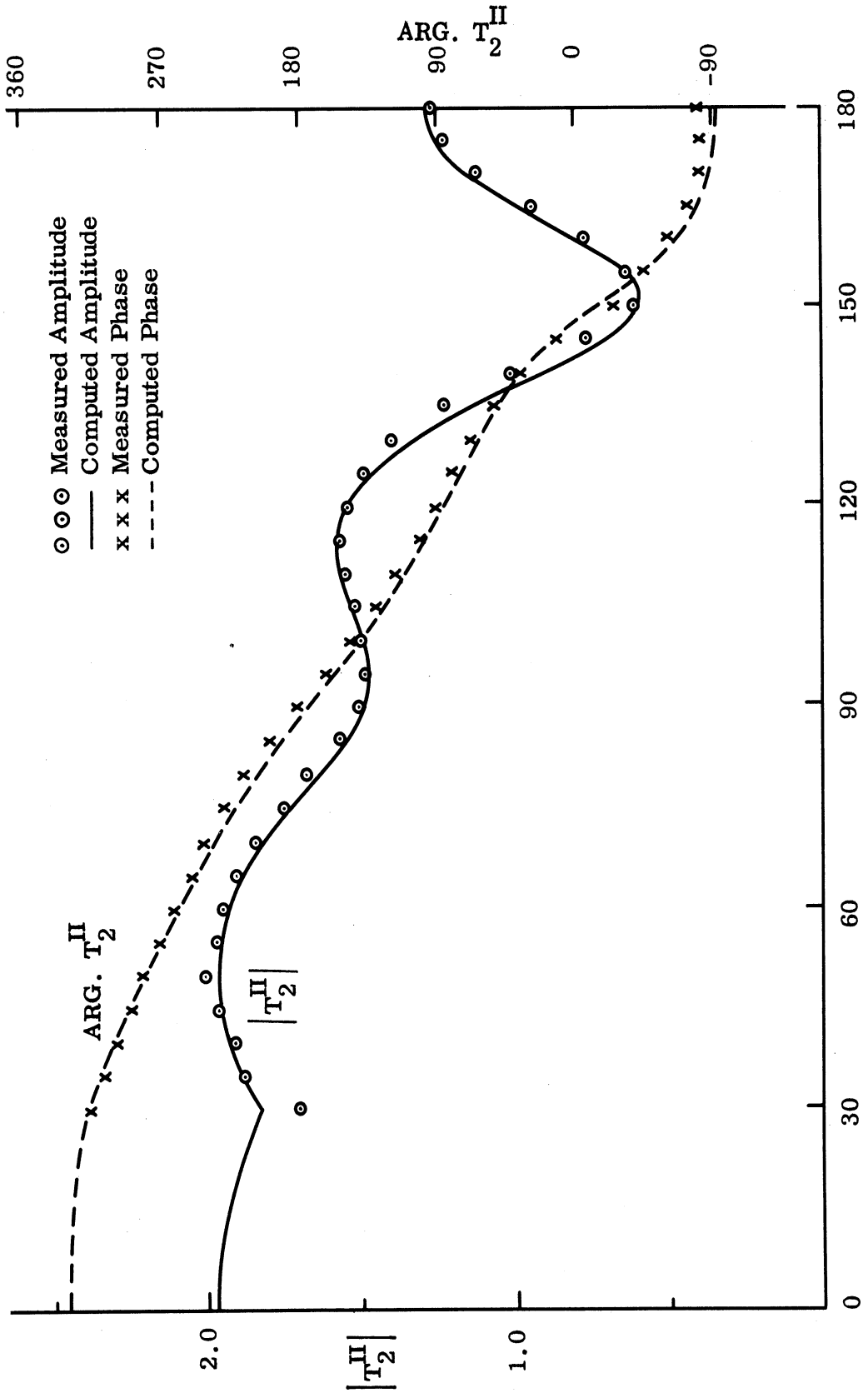

FIG. 4-10b: MEASURED AND COMPUTED $T_2^{II}(\theta)$ COMPONENT FOR ka = 2.75 WITH $\theta_o = 30^o$ AND M=20.

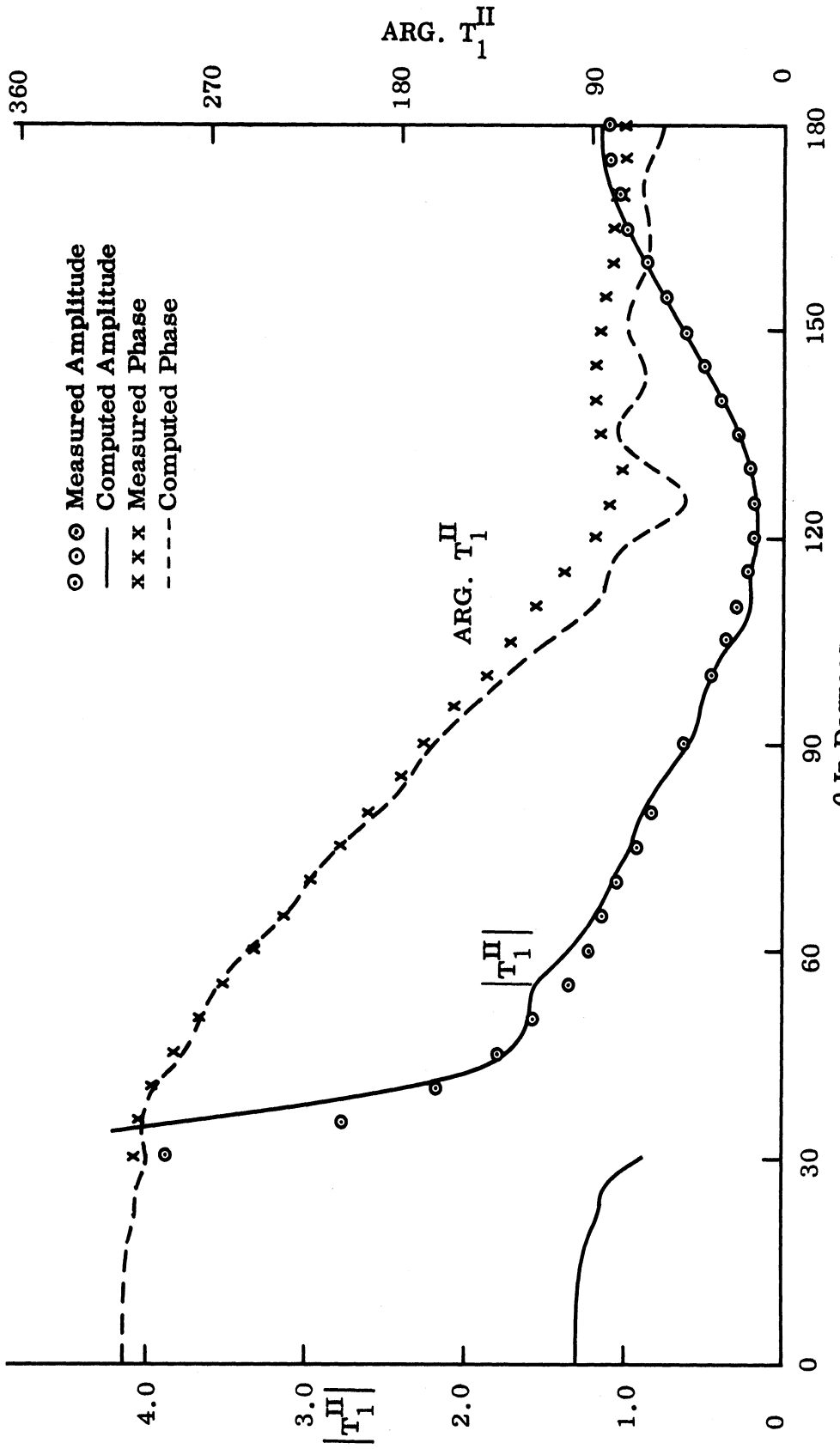

FIG. 4-11a: MEASURED AND COMPUTED $T_1^{II}(\theta)$ COMPONENT FOR ka = 3.0 WITH $\theta_o = 30^o$ AND M=20.

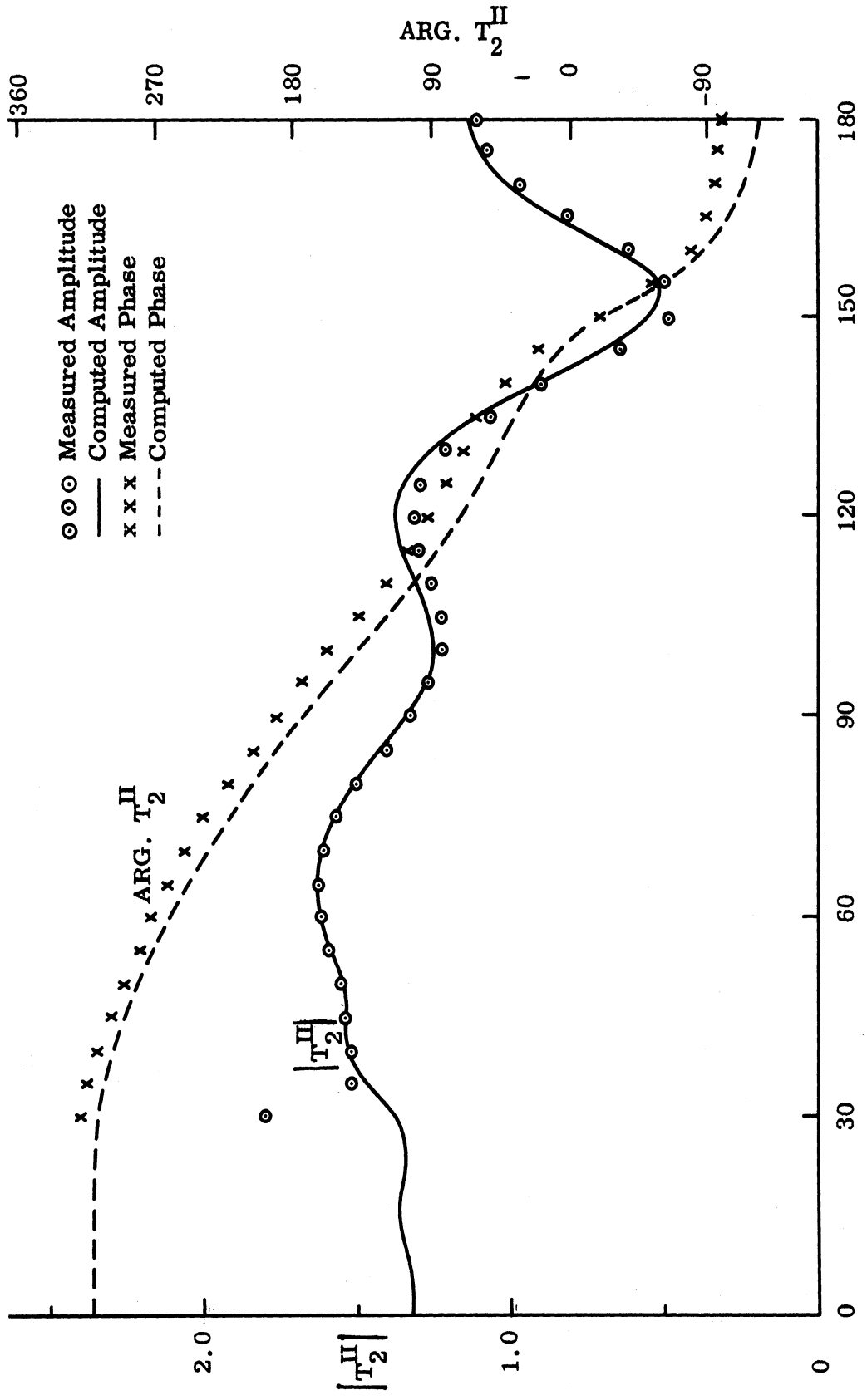

FIG. 4-11b: MEASURED AND COMPUTED $T_2^{II}(\theta)$ COMPONENT FOR ka = 3.0 WITH $\theta_o = 30^o$ AND M=20.

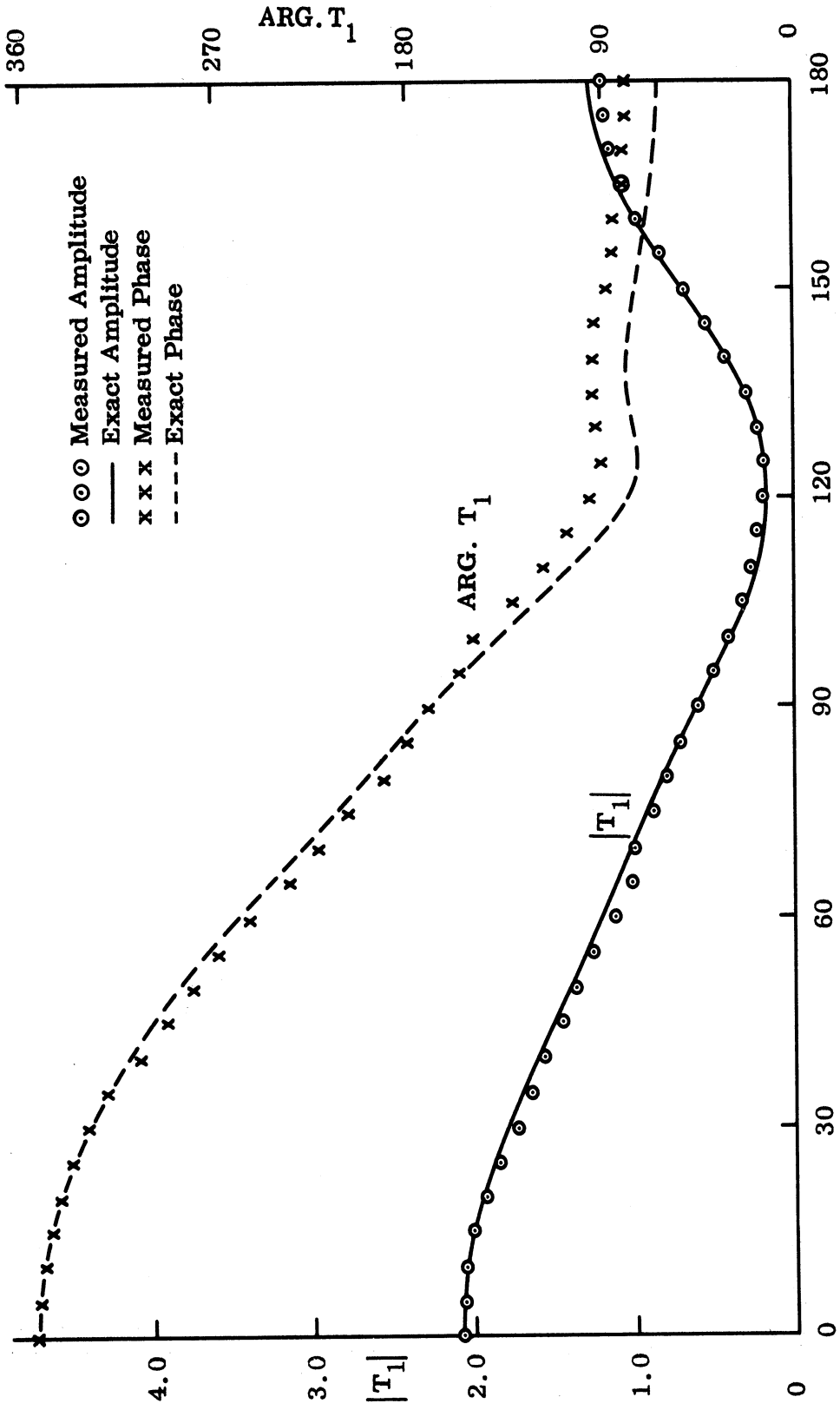

FIG. 4-12a: MEASURED AND EXACT $T_1(\theta)$ COMPONENT OF A SOLID SPHERE FOR ka = 3.0.

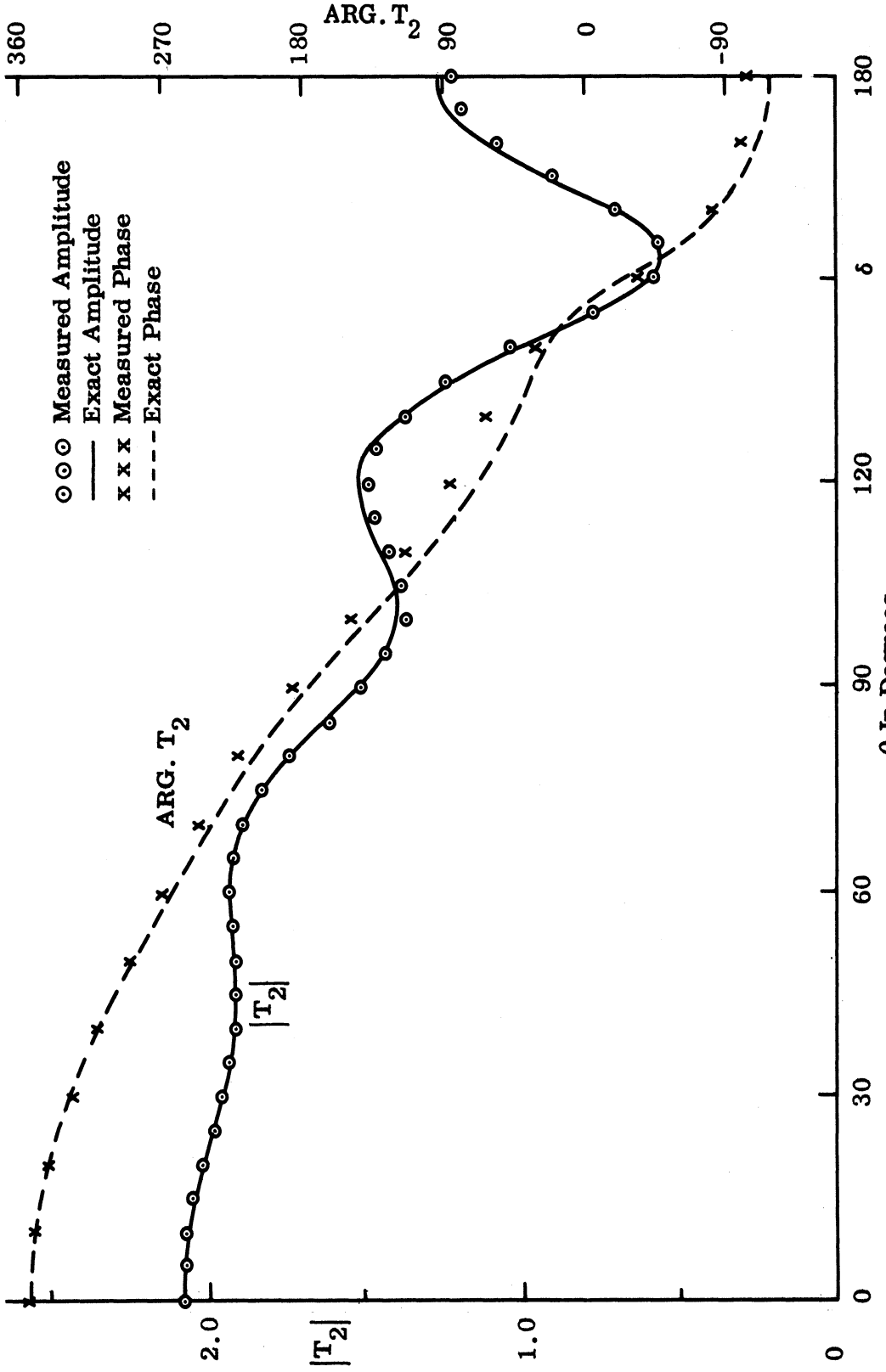

FIG. 4-12b: MEASURED AND EXACT $T_2(\theta)$ COMPONENT OF A SOLID SPHERE FOR ka = 3.0.

CHAPTER V

DISCUSSION

In order to confirm the theoretical predictions, the computed cross sections are compared with the experimental results for $\theta_o = 30^o$ and 90^o in Figs. 5-1 and 5-2 respectively. The agreement is very good, although we do observe that the experimental points lie somewhat higher than the predicted curve in the regions near to peaks and that the experimental points are, in general, shifted to the right about 2 percent in ka. This shift can be attributed to the fact that the shell of the experimental model has a finite thickness, while that used in the analysis is assumed to be infinitesimally thin. The shell thicknesses are, in fact, between 1.9 and 2.6 percent of the outside radius for the 3.09 inch diameter models used in the range $ka > 2.72$. If, therefore, the experimental data were plotted as a function of k times the radius of the cavity, the data would match the predicted curve as far as the shift is concerned (note that the outside radius is used in ka, Figs. 5-1 and 5-2). This implies that the cross section of a spherical shell depends more closely on the size of the cavity than on the outer dimension of the spherical shell.

In Chapter IV we observed marked reductions in the backscattering cross section at values of ka near to the resonant frequencies of a (closed) spherical cavity when the aperture is of moderate size. Hence, it must be true that the cavity itself plays quite a significant role in the modification of the scattering, and that the modification depends on the electrical size of the cavity. Unfortunately, the reason for the differences between the experimental and theoretical values near to the peaks is not precisely known. Although the deviations are less than 1.4 dB, it is interesting to note that

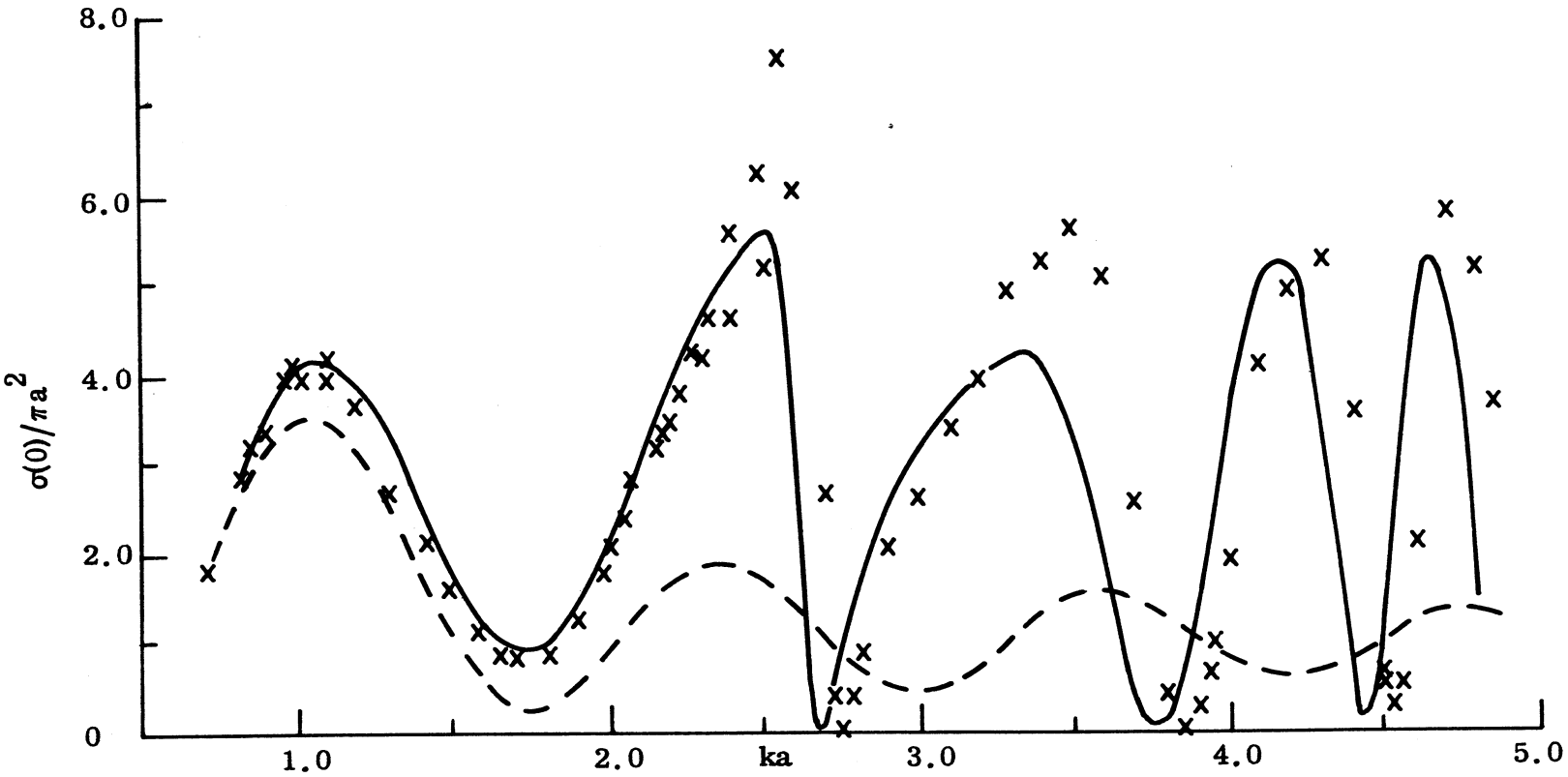

FIG. 5-1: COMPUTED (——) AND MEASURED (x x x) BACKSCATTERING CROSS SECTIONS OF A SPHERICAL SHELL FOR $\theta_o = 30^o$. DASHED LINE IS FOR A SOLID SPHERE.

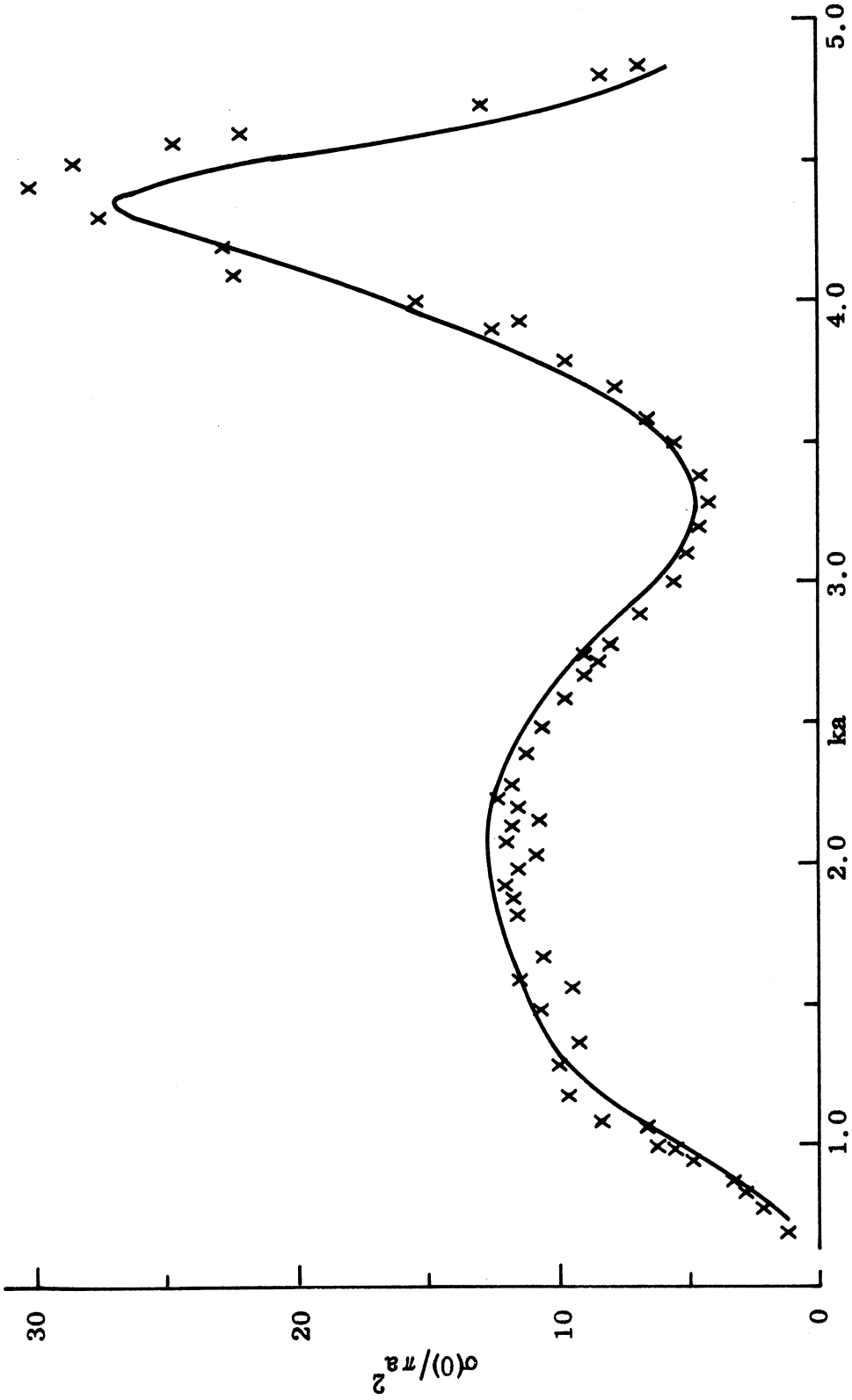

FIG. 5-2: COMPUTED (——) AND MEASURED (x x x) BACKSCATTERING CROSS SECTIONS OF A SPHERICAL SHELL FOR $\theta_o = 90^o$.

repeated measurements for the different diameter models produced uniform "curves" differing from each other by about 1 dB in the region of the first resonant peak for $\theta_o = 30^o$ (see Fig. 5-1). Since only the 3.09 inch diameter models were used for $ka > 2.72$, the existence of such deviations between the two models for $ka > 2.72$ is unknown. These experimental deviations could be attributed to one of the causes: the difference in the shell thickness between two models, non-uniformity of the shell thickness or even the unknown frequency sensitivity of the experimental facility.

Returning to the cavity resonance phenomenon, an examination of the computed and experimental data for the backscattering cross sections with various aperture angles reveals that the marked reductions and sharp peaks occur always at frequencies just below the free resonance frequencies of a spherical cavity. The decrease in the resonant frequency of the cavity can be explained by perturbation theory (Slater, 1950) if we regard the aperture as a perturbation applied to the closed spherical cavity. In such a case, power flows out through the aperture (wall) and a loss is introduced. Accordingly, we have a finite Q associated with the loss through the wall (Q_{wall}) and the resonant frequency of the perturbed cavity becomes smaller than that of the closed spherical cavity. A quantitative analysis of the perturbed frequency is, unfortunately, extremely difficult even for a small aperture size, and no such analysis has been attempted.

In the vicinity of the resonant frequencies of the cavity, the field quantities associated with the cavity are extremely sensitive to small changes in frequency. In particular, we would expect a rapid change in the phase of the field scattered (or reflected) from the cavity as the frequency of the incident field varies near the resonant frequency. This phase change produces a rapid change in scattering cross section from a maximum to a minimum

since the field scattered by the rest of the shell (e.g. the outside surface and edge of the shell) varies only slowly with frequency. The rapid change in cross section is especially evident at frequencies near to the cavity resonances when the aperture is of moderate size. Such a frequency sensitivity can be seen in all cases for which $15^{o} \leq \theta_{o} \leq 45^{o}$. Extreme instances are shown in Figs. 4-3 and 4-4. With $\theta_{o} = 15^{o}$, for example, the backscattering cross section has a sharp peak ($\sigma(0) \simeq 3.2\ \pi a^{2}$) at ka = 3.82, where a is here the cavity radius, but an increase in ka of only 0.03 is sufficient to reduce this to a "hull" where $\sigma \simeq 0.3\ \pi a^{2}$. As the aperture size increases ($\theta_{o} > 45^{o}$) the effect of the cavity resonance becomes insignificant, and no such rapid change in the scattering cross section now occurs. It is interesting to note that a spherical shell with aperture-on incidence has, in general, a higher backscattering cross section than a solid sphere except for ka near to a cavity resonance, and that the narrow band frequency characteristic near the resonance frequencies of the cavity is inherent in this type of geometry.

At this point it should be mentioned that ray optical techniques have been examined in an attempt to explain and clarify the scattering behavior. Such techniques are often valuable not only as a means of estimating scattering, but also because of the physical insight that they provide. With the present problem, however, the incorporation of effects due to edge diffraction, creeping waves, transmission through and reflection at the aperture, etc., failed to reproduce the main features of the scattering behavior as represented by the theoretical and experimental curves, and did so even for the larger values of ka where optical techniques are generally more accurate. This failure is probably attributable to the presence of the cavity, and tends to confirm the dominant role played by the cavity in determining the scattering.

Over the range $0.8 \leq \text{ka} \leq 4.85$, the numerical computations carried out using $M \leq 30$ for the matrix equation (2.85) produced good results as

measured by the parameter $\mathcal{E}_M$, the examination of the tangential E-field over the shell and the comparison with measured data for $\sigma(0)$ as well as $T_1^{II}(\theta)$ and $T_2^{II}(\theta)$. In low frequency region, $ka < 0.8$ (say), a choice of $M \leq 10$ should be enough for accurate computation, but as ka is increased into the high frequency region, we would expect to have to increase M at least in proportion, and for $ka > 4.85$, values in excess of 30 would be needed. Since the difficulty (and cost) of matrix inversion increases with the dimension of the matrix, it is obvious that the application of the present method is limited in the size of ka that can be handled. If ka is moderately large, say $ka > 10$, the Gauss-Seidel iterative method appears advantageous as regards computational labor and machine time in comparison with more conventional matrix inversion methods such as that used here. However, the relaxation parameter ω (see Appendix B) has to be chosen carefully in order to provide a reasonable rate of convergence in the iteration process. The optimum choice of ω is not known and considerable effort would be needed to obtain it.

Although the analysis in the preceding study was limited to the case of aperture-on incidence (angle of incidence, $\theta_i = 0$), the analysis can be extended to the case of a plane wave at arbitrary incidence with respect to the plane of the aperture. For the case of rear-on incidence ($\theta_i = 180^o$), the analysis would differ from that given here only in slight changes of functions $L_{mn}(\theta_o)$, $S_{mn}(\theta_o)$, $\gamma_n(\theta_o)$, $\delta_n(\theta_o)$ in Eq. (2.85).

As noted in the Introduction, one of the factors that motivated this study was the investigation of impedance (or reactive) loading as a means of controlling the scattering behavior of a body. Prior applications of this technique include that of loading a sphere using a circumferential slot, and though it was found that the backscattering cross section could be reduced to zero by appropriate choice of loading applied at the slot, any simple means

of realizing this load was extremely frequency sensitive. The resulting bandwidth obtained is, of course, a function of the loading device employed, and if a cavity is used for this purpose, it is possible that the shape of the cavity also plays a role. In searching for a cavity that could be appropriate for reducing the backscattering from a sphere, it seemed that a spherical cavity might be most desirable because of the similarity of the mode structures inside and outside such a region. The simplest model of the resulting structure is the spherical shell with a circular aperture that has been investigated here, and since the aperture in this model has dimensions determined solely by a and θ_o, it was felt that an exact (or accurate) solution for this problem would avoid any uncertainties caused by the assumption of a slot of infinitesimal width in the earlier studies of loaded spheres.

It was appreciated that our model, as it stands, does not have sufficient flexibility for controlling the scattering of a sphere of radius a in any pre-selected frequency range. The only parameter at our disposal is the aperture angle θ_o, and for θ_o small, not enough power penetrates into the cavity, whereas for θ_o large, the resonances of the cavity are overly degraded. Nevertheless, if this model were to display any real capability for reducing (or increasing) the scattering cross section over an extended range of ka, there are several possible generalizations of the model through which we might seek to transfer this frequency range to any pre-selected range of ka. We could, for example, fill our cavity with a dielectric or magnetic material. The analysis for this situation would be similar to that for our simple model, and on the assumption (which has been verified) that the electrical dimensions of the cavity are the main factor controlling the scattering, an appropriate choice of dielectric constant (> 1) could, for example, bring the region of cross section modification into the vicinity of $ka = 1$. Alternatively we could treat a thick shell whose internal radius b could be selected independent of a (providing $b < a$),

thereby producing an additional parameter, and if necessary insert a dielectric material into the cavity as well. And yet a third generalization of our model would be to insert a dielectric sphere of radius $b < a$ into our shell, thereby providing a spherical shell cavity.

All of these generalizations should yield to analyses of a similar nature to that which we have given, but because of the inherent complication of these more general structures, it was decided to treat the most simple case first. As we have seen, however, the simple model does not display any new capability for cross section control that would encourage us to believe in the practical utility of the more general forms. Only in the immediate vicinity of the frequencies at which the cavity resonates is there any marked reduction in the backscattering cross section of a solid sphere (or shell), and thus the bandwidth of this structure, regarded as a cross section reduction device, is limited. There is some indication of a more general enhancement of the scattering, but the amount is not sufficient to be of interest.

CHAPTER VI

CONCLUSIONS

This study has been devoted to a theoretical and experimental investigation of the scattering behavior of a spherical shell with a circular aperture for a plane wave at aperture-on incidence. Having postulated expansions of the field components in terms of spherical wave functions, the method of least square error has been applied in matching the field component at the boundary. In order to improve the convergence and accuracy of the solution in computation the method of least square error has been modified by separating out the correct surface field behavior at the edge of the aperture. A comparison of the numerical results obtained with the modified method with those computed by the original method shows the significant improvement provided by the modification.

In order to confirm the theoretical results, a series of surface and backscattering measurements were made in the range $0.7 \leq ka \leq 4.85$ using spherical shell models with aperture angle $\theta_o = 15^o$, 30^o, 45^o, 60^o and 90^o. It was observed that a spherical shell at aperture-on incident has, in general, a higher backscattering cross section than a solid sphere except in the vicinity of the cavity resonant frequencies, where marked reductions in the backscattering cross section occur within a narrow frequency band. For the surface field measurements, the amplitude and phase of $T_1^{II}(\theta)$ and $T_2^{II}(\theta)$ components were measured for ka = 2.0, 2.75, and 3.0 with $\theta_o = 30^o$. Good agreement between the measured and computed results for both the backscattering cross section and the surface field was obtained.

REFERENCES

Ås, B.O. and H.J. Schmitt (1958) "Back Scattering Cross Section of Reactively Loaded Cylindrical Antennas," Harvard University Cruft Laboratory Scientific Report No. 18.

Blore, W.E., and H.M. Musal, Jr. (1965) "The Radar Cross Section of Metal Hemispheres, Spherical Segments, and Partially Capped Spheres," IEEE Trans. AP-13 (478-479).

Carslaw, H.S. (1930) Fourier's Series and Integrals (Dover Publications, Inc., New York).

Chang, S. and T.B.A. Senior (1967) "Study of the Scattering Behavior of a Sphere with an Arbotrarily Placed Circumferential Slot," The University of Michigan Radiation Laboratory Report No. 5548-6-T.

Chen, K-M and V.V. Liepa (1964a) "The Minimization of the Backscattering of a Cylinder by Central Loading," IEEE Trans. AP-12 (576-582).

Chen, K-M and V.V. Liepa (1964b) "The Minimization of the Backscattering of a Cylinder by Central Loading," The University of Michigan Radiation Laboratory Report No. 5548-1-T.

Chen, K-M (1965) "Minimization of Backscattering of a Cylinder with a Moderate Radius by Loading Method," Michigan State University Technical Report No. 1, Contract AF 33(615)-1656.

Cole, W.J., E.R. Nagelberg and C.M. Nagel (1967) "Iterative Solution of Waveguide Discontinuity Problems," Bell Syst. Tech. Journ. XLVI (649-672).

Gerbes, W.W. and W.J. Kearns (1963) "Theoretical and Experimental Investigation of Backscattering from a Cavity-Loaded Monopole," USAF Cambridge Research Labs. Report AFCRL 66-355.

Guttman, L. (1946) "Enlargement Methods for Computing the Inverse Matrix," Annals of Math. Stat. 17 (336-343).

Iams, H.A. (1950) "Radio Wave Conducting Device," U.S. Patent No. 2,578,367.

Kazarinoff, N.D. and T.B.A. Senior (1962) "A Failure of Creeping Waves Theory," IRE Trans. AP-10 (634-638).

Knott, E.F., V.V. Liepa and T.B.A. Senior (1965) "A Surface Field Measurement Facility," Proc. IEEE 53 (1105-1107).

Liepa, V.V. and T.B.A. Senior (1966) "Theoretical and Experimental Study of the Scattering Behavior of a Circumferentially-Loaded Sphere," The University of Michigan Radiation Laboratory Report No. 5548-5-T.

Magnus, W., F. Oberhettinger and R.P. Soni (1966) Formulas and Theorems for the Special Functions of Mathematical Physics (Springer Verlag Inc., New York).

Meissner, A. (1929) "Transmitting Antennas for Broadcasting," Proc. IRE 17 (1178-1184).

Meixner, J. (1949) "Die Kantenbedingung in der Theorie der Beugung Electromagnetischer Wellen an Vollkommen Leitenden Ebene Schirmen," Ann. Physik 441 (2-9).

Mentzer, J.R. (1955) Scattering and Diffraction of Radio Waves (Pergamon Press, London and New York).

O'Neil, H.M. (1928) "Characteristics of Certain Broadcasting Antennas at South Schenectady Development Station," Proc. IRE 16 (872-889).

Raybin, D.M. (1965) "Radar Cross Section of Spherical Shell Segments," IEEE Trans. AP-13 (754-759).

Schwinger, J. (1947) "A Variational Principle for Scattering Problems," Phys. Rev. 72 (742).

Slater, J.C. (1950) Microwave Electronics (D. Van Nostrand Co., Inc., New York).

Sletten, C.J., P. Blacksmith, F.S. Holt, and B.B. Gorr (1964) "Scattering from Thick Reactively Loaded Rods," in "The Modification of Electromagnetic Scattering Cross Sections in the Resonance Region," A Symposium Record, 1, USAF Cambridge Research Laboratories Report No. AFCRL-64-727(I) (67-68).

Sommerfeld, A. (1949) Partial Differential Equations in Physics (Academic Press, New York and London).

Stratton, J.A. (1941) Electromagnetic Theory (McGraw-Hill Book Co., Inc., New York).

Tai, C.T. (1952) "Electromagnetic Back Scattering from Cylindrical Wires," J. Appl. Phys. 23 (909-916).

Thomas, D.P. (1963) "Diffraction by a Spherical Cap," Proc. Camb. Phil. Soc. 59 (197-209).

Tsu, R. (1961) "The Evaluation of Incomplete Normalization Integrals and Derivatives with Respect to the Order of Associated Legendre Polynomials," J. Math. and Phys. 40 (232-243).

Uslenghi, P.L.E. and R.S. Zich (1967) "The Scattering of a Plane Electromagnetic Wave by a Perfectly Conducting Spherical Shell with a Conical Hole," Electromagnetic Wave Theory, Symp. Proc., Delft (Pergamon Press, Oxford and New York).

Varga, R.S. (1962) Matrix Iterative Analysis (Prentice-Hall, Englewood Cliffs, New Jersey).

Williams, W.E. (1962) "The Reduction of Boundary Value Problems to Fredholm Integral Equations of the Second Kind," Z. Angew. Math. Phys. 13 (133-151).

Yen, J.L. (1959) "The Power Series Solution of Scattering Problems," The McGill Symposium on Microwave Optics, Part II., Diffraction and Scattering, AFCRC-TR-59-118(II), (237-242).

APPENDIX A

EVALUATION OF $L_{mn}(\theta_o)$ AND $S_{mn}(\theta_o)$.

From Eqs. (2.48) and (2.49) we have

$$L_{mn}(\theta_o) = \int_0^{\theta_o} \left(\frac{\partial P_m^1}{\partial \theta} \frac{\partial P_n^1}{\partial \theta} + \frac{P_m^1}{\sin\theta} \frac{P_n^1}{\sin\theta} \right) \sin\theta \, d\theta \quad , \tag{A.1}$$

$$S_{mn}(\theta_o) = \int_0^{\theta_o} \cdot \left(\frac{P_m^1}{\sin\theta} \frac{\partial P_n^1}{\partial \theta} + \frac{P_n^1}{\sin\theta} \frac{\partial P_m^1}{\partial \theta} \right) \sin\theta \, d\theta \quad , \tag{A.2}$$

which, on integrating by parts, become

$$L_{mn}(\theta_o) = \sin\theta \, P_m^1 \frac{\partial P_n^1}{\partial \theta} \Bigg]_{\theta=\theta_o} + n(n+1) \int_0^{\theta_o} P_m^1 P_n^1 \sin\theta \, d\theta \tag{A.3}$$

$$S_{mn}(\theta_o) = P_n^1 P_m^1 \Big]_{\theta=\theta_o} \quad . \tag{A.4}$$

The integral in Eq. (A.3) can be written as (Tsu, 1961)

$$\int_0^{\theta_o} P_m^1 P_n^1 \sin\theta \, d\theta = \begin{cases} \dfrac{\sin\theta_o}{(n-m)(n+m+1)} \left[P_n^1 \dfrac{\partial P_m^1}{\partial \theta} - P_m^1 \dfrac{\partial P_n^1}{\partial \theta} \right]_{\theta=\theta_o} \\ \qquad \text{for } m \neq n \qquad \text{(A.5a)} \\ \dfrac{\sin\theta_o}{(2n+1)} \left\{ \left(\dfrac{\partial P_\lambda^1}{\partial \lambda} \right)_{\lambda=n} \dfrac{\partial P_n^1}{\partial \theta} - P_n^1 \left[\dfrac{\partial}{\partial \lambda} \left(\dfrac{\partial P_\lambda^1}{\partial \theta} \right) \right]_{\lambda=n} \right\}_{\theta=\theta_o} \\ \qquad \text{for } m = n \qquad \text{(A.5b)} \end{cases}$$

and in the second of these the derivatives with respect to order, namely

$$\left(\frac{\partial P_\lambda^1}{\partial \lambda}\right)_{\lambda=n} \quad \text{and} \quad \left[\frac{\partial}{\partial \lambda}\left(\frac{\partial P_\lambda^1}{\partial \theta}\right)\right]_{\lambda=n} ,$$

can be evaluated in closed form by using the recurrence relations for the Legendre functions, starting with (Tsu, 1961)

$$\left[\frac{\partial}{\partial \lambda} P_\lambda(\cos\theta)\right]_{\lambda=0} = \ell n\ (\cos^2 \frac{\theta}{2})$$

and

$$\left[\frac{\partial}{\partial \lambda} P_\lambda(\cos\theta)\right]_{\lambda=1} = \cos\theta\left[\ell n(\cos^2\frac{\theta}{2}) + 1\right] - 1 .$$

However, in the following it is shown that a more direct and convenient recurrence relation for the integral itself can be found without evaluating the derivatives of the Legendre functions with respect to order.

Let us define

$$I_n^\ell(\theta_o) = \int_0^{\theta_o} \left[P_n^\ell(\cos\theta)\right]^2 \sin\theta\, d\theta \qquad (A.6)$$

$$(n, \ell = 0, 1, 2, \ldots, \ell \leq n) ,$$

and seek a recurrence relation for the $I_n^\ell(\theta_o)$. If we also define a function

$$Q_n^\ell(\theta) = \sin\theta\left\{\left(\frac{\partial P_\lambda^\ell}{\partial \lambda}\right)_{\lambda=n} \frac{\partial P_n^\ell}{\partial \theta} - P_n^\ell\left[\frac{\partial}{\partial \lambda}\left(\frac{\partial P_\lambda^\ell}{\partial \theta}\right)\right]_{\lambda=n}\right\} , \qquad (A.7)$$

then

$$I_n^{\ell}(\theta_o) = \frac{1}{2n+1} \quad Q_n^{\ell}(\theta_o) \tag{A.8}$$

and from the well known recurrence relation (Stratton, 1941)

$$\sin\theta \frac{\partial P_n^{\ell}}{\partial\theta} = n \cos\theta \, P_n^{\ell} - (n+\ell) \, P_{n-1}^{\ell} \tag{A.9}$$

by differentiating with respect to the order n, we obtain

$$\sin\theta \left[\frac{\partial}{\partial\lambda}\left(\frac{\partial P_\lambda^{\ell}}{\partial\theta}\right)\right]_{\lambda=n} = (\cos\theta \, P_n^{\ell} - P_{n-1}^{\ell}) + n \cos\theta \left(\frac{\partial P_\lambda^{\ell}}{\partial\lambda}\right)_n -$$

$$- (n+\ell)\left(\frac{\partial P_\lambda^{\ell}}{\partial\lambda}\right)_{n-1} . \tag{A.10}$$

Substitution of Eqs. (A.9) and (A.10) into (A.7) now gives

$$Q_n^{\ell}(\theta) = (n+\ell)\left[P_n^{\ell}\left(\frac{\partial P_\lambda^{\ell}}{\partial\lambda}\right)_{n-1} - P_{n-1}^{\ell}\left(\frac{\partial P_\lambda^{\ell}}{\partial\lambda}\right)_n\right] -$$

$$- \cos\theta \left[P_n^{\ell}\right]^2 + P_n^{\ell} \, P_{n-1}^{\ell} . \tag{A.11}$$

Similarly, starting with the recurrence relation

$$\sin\theta \frac{\partial P_n^{\ell}}{\partial\theta} = (n - \ell + 1) \, P_{n+1}^{\ell} - (n+1) \cos\theta \, P_n^{\ell} ,$$

we have

$$Q^{\ell}_{n-1}(\theta) = (n - \ell)\left[P^{\ell}_{n}\left(\frac{\partial P^{\ell}_{\lambda}}{\partial \lambda}\right)_{n-1} - P^{\ell}_{n-1}\left(\frac{\partial P^{\ell}_{\lambda}}{\partial \lambda}\right)_{n}\right] -$$

$$- P^{\ell}_{n-1} P^{\ell}_{n} + \cos\theta \left[P^{\ell}_{n-1}\right]^2 \quad , \qquad \text{(A.12)}$$

and hence, from Eqs. (A.11) and (A.12) with (A.8) the following recurrence relation for $I^{\ell}_{n}(\theta_o)$ results:

$$I^{\ell}_{n}(\theta_o) = \frac{1}{(2n+1)(n-\ell)} \left\{ (2n-1)(n+\ell)\, I^{\ell}_{n-1}(\theta_o) - \right.$$

$$\left. - \cos\theta \left[(n+\ell)(P^{\ell}_{n-1})^2 + (n-\ell)(P^{\ell}_{n})^2\right] + 2n\, P^{\ell}_{n-1} P^{\ell}_{n} \right\}$$

$$\text{for } n > \ell \quad . \qquad \text{(A.13)}$$

When $\ell = 1$, Eq. (A.13) becomes

$$I^{1}_{n}(\theta_o) = \frac{1}{(2n+1)(n-1)} \left\{ (2n-1)(n+1)\, I^{1}_{n-1}(\theta_o) \right.$$

$$\left. - \cos\theta \left[(n+1)(P^{1}_{n-1})^2 + (n-1)(P^{1}_{n})^2\right] + 2n P^{1}_{n-1} P^{1}_{n} \right\}$$

$$\text{for } n > 1 \, , \qquad \text{(A.14a)}$$

or, using Eq. (A.4),

$$I^{1}_{n}(\theta_o) = \frac{1}{(2n+1)(n-1)} \left\{ (2n-1)(n+1)\, I^{1}_{n-1}(\theta_o) \right.$$

$$\left. - \cos\theta \left[(n+1) S_{n-1,n-1} + (n-1) S_{n,n}\right] + 2n S_{n,n-1} \right\}$$

$$\text{for } n > 1 \, . \qquad \text{(A.14b)}$$

Since

$$I_1^1(\theta_o) = 1/3\,(2 - 3\cos\theta_o + \cos^3\theta_o) \tag{A.15}$$

by direct integration of Eq. (A.6), $I_n^1(\theta_o)$ can be evaluated for all n from the recurrence relation (A.14).

In summary, therefore, $L_{mn}(\theta_o)$ can be written as follows:

1) When $m \neq n$

$$L_{mn}(\theta_o) = \frac{\sin\theta_o}{(n-m)(n+m+1)}\left[n(n+1)\,P_n^1\,\frac{\partial P_m^1}{\partial\theta} - m(m+1)\,P_m^1\,\frac{\partial P_n^1}{\partial\theta}\right]_{\theta=\theta_o} \tag{A.16}$$

2) When $m = n$

$$L_{mn}(\theta_o) = \left[\sin\theta\,P_n^1\,\frac{\partial P_n^1}{\partial\theta}\right]_{\theta=\theta_o} + n(n+1)\,I_n^1(\theta_o) \tag{A.17}$$

where $I_n^1(\theta_o)$ is given by Eqs. (A.14) and (A.15).

APPENDIX B

APPLICATION OF THE GAUSS-SEIDEL ITERATIVE METHOD

Let us consider the application of the Gauss-Seidel iterative method to solve the matrix equation (2.63). Eq. (2.63) is repeated here for convenience with abbreviations, $B = [b_{pq}]$, $Y = y_q]$ and $G = g_p]$. Thus

$$BY = G, \quad (p, q = 1, 2, \ldots . 2M). \tag{B.1}$$

In order to solve iteratively the matrix Eq. (B.1), we express the matrix B as the matrix sum

$$B = D - L - U \tag{B.2}$$

where $D = \text{diag}\{b_{11}, b_{22}, \ldots . , b_{2M, 2M}\}$, and L and U are respectively strictly lower and upper triangular 2M x 2M matrices, whose entries are the negatives of the entries of B respectively below and above the main diagonal of B. Eq. (B.1) can then be written as

$$(D-L)\, Y = UY + G \tag{B.3}$$

which leads to the Gauss-Seidel iterative method, with the relaxation factor ω $(0 < \omega < 2)$,

$$(D-\omega L)\, Y^{(r+1)} = \{ (1-\omega) D + \omega U \}\, Y^{(r)} + \omega G , \tag{B.4}$$

$$(r = 0, 1, 2, \ldots .)$$

which can be written in terms of components as

$$b_{pp}\, y_p^{(r+1)} = (1-\omega)\, b_{pp}\, y_p^{(r)} - \omega \left\{ \sum_{q=1}^{p-1} b_{pq}\, y_q^{(r+1)} + \sum_{q=p+1}^{2M} b_{pq}\, y_q^{(r)} - g_p \right\}$$

$$(r = 0, 1, 2, \ldots) \tag{B.5}$$

where $Y^{(r)} = y_q^{(r)}]$, $\quad q = 1, 2, \ldots . , 2M$,

$$r = 0, 1, 2. \ldots .$$

$Y^{(o)}$ is an arbitrary, initial complex matrix approximation of the solution matrix Y of Eq. (B.1). If $Y^{(o)}$ is given, a sequence of matrix iterates $Y^{(r)}$ is successively defined by Eq. (B.4) or (B.5).

For a given Hermitian matrix H in the matrix equation HY = Z, the necessary and sufficient condition for the Gauss-Seidel iterative method to be convergent, i.e. $\lim_{r\to\infty} Y^{(r)} = Y$, is that the matrix H be positive definite (Varga, 1962). From Eq. (2.64) through (2.67) it is readily seen that $b_{pq} = b^*_{pq}$, i.e. the matrix $B = [b_{pq}]$ is Hermitian. The positive definiteness of the matrix B can be proved by showing that for any given matrix $\tilde{y}_p$ for p = 1,2,...., 2M,

$$\overline{\tilde{y}^*_p}\,[b_{pq}]\,\tilde{y}_p] = \int_{\theta_o}^{\pi} \left| \sum_{n=1}^{M} \left[\tilde{y}_{2n-1}\, \psi_n(ka)\, \frac{P_n^1(\cos\theta)}{\sin\theta} + \tilde{y}_{2n} \psi'_n(ka)\, \frac{\partial}{\partial\theta} P_n^1(\cos\theta) \right] \right|^2 \times$$

$$\times \sin\theta\, d\theta + \int_{\theta_o}^{\pi} \left| \sum_{n=1}^{M} \left[\tilde{y}_{2n-1} \psi_n(ka) \frac{\partial}{\partial\theta} P_n^1(\cos\theta) + \tilde{y}_{2n} \psi'_n(ka)\, \frac{P_n^1(\cos\theta)}{\sin\theta} \right] \right|^2 \sin\theta d\theta$$

$$+ \int_0^{\theta_o} \left| \sum_{n=1}^{M} \left[\tilde{y}_{2n-1}\, \frac{1}{\zeta_n(ka)}\, \frac{\partial}{\partial\theta} P_n^1(\cos\theta) + \tilde{y}_{2n}\, \frac{1}{\zeta'_n(ka)}\, \frac{P_n^1(\cos\theta)}{\sin\theta} \right] \right|^2 \sin\theta d\theta$$

$$+ \int_0^{\theta_o} \left| \sum_{n=1}^{M} \left[\tilde{y}_{2n-1}\, \frac{1}{\zeta_n(ka)}\, \frac{P_n^1(\cos\theta)}{\sin\theta} + \tilde{y}_{2n}\, \frac{1}{\zeta'_n(ka)}\, \frac{\partial}{\partial\theta} P_n^1(\cos\theta) \right] \right|^2 \sin\theta d\theta \,, \tag{B.6}$$

and whose right hand side is always greater than zero for $\theta_o > 0$ unless $\tilde{y}_1 = \tilde{y}_2 = \ldots = \tilde{y}_{2M} = 0$. Since the right hand side is never negative, it is sufficient to show that for $\theta_o \neq 0$,

$$\tilde{y}_1 = \tilde{y}_2 = \ldots \tilde{y}_{2M} = 0$$

is the only solution of equations:

$$\sum_{n=1}^{M}\left[\tilde{y}_{2n-1}\psi_n(ka)\frac{P_n^1(\cos\theta)}{\sin\theta}+\tilde{y}_{2n}\psi_n'(ka)\frac{\partial}{\partial\theta}P_n^1(\cos\theta)\right]=0\,, \qquad (B.7)$$

$$\theta_o<\theta<\pi\,,$$

$$\sum_{n=1}^{M}\left[\tilde{y}_{2n-1}\psi_n(ka)\frac{\partial}{\partial\theta}P_n^1(\cos\theta)+\tilde{y}_{2n}\psi_n'(ka)\frac{P_n^1(\cos\theta)}{\sin\theta}\right]=0\,, \qquad (B.8)$$

$$\theta_o<\theta<\pi\,,$$

$$\sum_{n=1}^{M}\left[\tilde{y}_{2n-1}\frac{1}{\zeta_n(ka)}\frac{\partial}{\partial\theta}P_n^1(\cos\theta)+\tilde{y}_{2n}\frac{1}{\zeta_n'(ka)}\frac{P_n^1(\cos\theta)}{\sin\theta}\right]=0\,, \qquad (B.9)$$

$$0<\theta<\theta_o\,,$$

$$\sum_{n=1}^{M}\left[\tilde{y}_{2n-1}\frac{1}{\zeta_n(ka)}\frac{P_n^1(\cos\theta)}{\sin\theta}+\tilde{y}_{2n}\frac{1}{\zeta_n'(ka)}\frac{\partial}{\partial\theta}P_n^1(\cos\theta)\right]=0\,, \qquad (B.10)$$

$$0<\theta<\theta_o\,,$$

which are the necessary and sufficient conditions for Eq. (B.6) to be zero.

By adding Eqs. (B.7) to (B.8), and (B.9) to (B.10), we have

$$\sum_{n=1}^{M}\left[\tilde{y}_{2n-1}\psi_n(ka)+\tilde{y}_{2n}\psi_n'(ka)\right]\left[\frac{P_n^1(\cos\theta)}{\sin\theta}+\frac{\partial}{\partial\theta}P_n^1(\cos\theta)\right]=0\,, \qquad (B.11)$$

$$\theta_o<\theta<\pi\,,$$

$$\sum_{n=1}^{M}\left[\tilde{y}_{2n-1}\frac{1}{\zeta_n(ka)}+\tilde{y}_{2n}\frac{1}{\zeta_n'(ka)}\right]\left[\frac{P_n^1(\cos\theta)}{\sin\theta}+\frac{\partial}{\partial\theta}P_n^1(\cos\theta)\right]=0\,, \qquad (B.12)$$

$$0<\theta<\theta_o\,.$$

respectively.

If we let

$$\phi_n(\theta) = \frac{P_n^1(\cos\theta)}{\sin\theta} + \frac{\partial}{\partial\theta} P_n^1(\cos\theta) \quad ,$$

all $\phi_n(\theta)$, $n = 1, 2, \ldots$ are continuous everywhere and their derivatives of all orders, $\frac{\partial}{\partial\theta}\phi_n(\theta)$, $(\partial^2/\partial\theta^2)\phi_n(\theta)$, ..., exist and are also continuous. Hence each of the left-hand sides of Eqs. (B.11) and (B.12), which is a finite sum of $\phi_n(\theta)$'s, has the same properties as the $\phi_n(\theta)$'s. Consequently, Eqs. (B.11) and (B.12) must be satisfied not only in each of the given intervals, but also throughout the entire domain of θ. Furthermore, $\{\phi_1(\theta), \phi_2(\theta), \ldots, \phi_M(\theta)\}$ is a set of orthogonal, linear independent functions. Therefore, each of the coefficients in Eqs. (B.11) and (B.12) must vanish. Thus, we have

$$\tilde{y}_{2n-1}\,\psi_n(ka) + \tilde{y}_{2n}\,\psi_n'(ka) = 0 \qquad \text{(B.13)}$$

$$\tilde{y}_{2n-1}\,\frac{1}{\zeta_n(ka)} + \tilde{y}_{2n}\,\frac{1}{\zeta_n'(ka)} = 0 \qquad \text{(B.14)}$$

$$\text{for } n = 1, 2, \ldots, M.$$

Similarly, by subtracting (B.8) from (B.7), and (B.9) from (B.10), we obtain

$$\sum_{n=1}^{M}\left[\tilde{y}_{2n-1}\,\psi_n(ka) - \tilde{y}_{2n}\psi_n'(ka)\right]\left[\frac{P_n^1(\cos\theta)}{\sin\theta} - \frac{\partial}{\partial\theta}P_n^1(\cos\theta)\right] = 0, \qquad \text{(B.15)}$$

$$\theta_o < \theta < \pi,$$

$$\sum_{n=1}^{M}\left[\tilde{y}_{2n-1}\,\frac{1}{\zeta_n(ka)} - \tilde{y}_{2n}\,\frac{1}{\zeta_n'(ka)}\right]\left[\frac{P_n^1(\cos\theta)}{\sin\theta} - \frac{\partial}{\partial\theta}P_n^1(\cos\theta)\right] = 0, \qquad \text{(B.16)}$$

$$0 < \theta < \theta_o,$$

from which we must have

$$\tilde{y}_{2n-1}\,\psi_n(ka) - \tilde{y}_{2n}\,\psi_n'(ka) = 0 \quad , \tag{B.17}$$

$$\tilde{y}_{2n-1}\,\frac{1}{\zeta_n(ka)} - \tilde{y}_{2n}\,\frac{1}{\zeta_n'(ka)} = 0 \quad . \tag{B.18}$$

for $n = 1, 2, \ldots, M$.

It is clear from Eqs. (B.14) and (B.18) that $\tilde{y}_1 = \tilde{y}_2 = \ldots = \tilde{y}_{2M} = 0$ is the only solution for any finite value of ka. However, it should be noted that when $\theta_o = 0$, Eqs. (B.9) and (B.10) are deleted and hence we have only Eqs. (B.13) and (B.17). Obviously the solution of these two equations is not unique when $\psi_n(ka) = 0$ or $\psi_n'(ka) = 0$, and there now exists a non-zero solution.

Since the matrix B is positive definite, the lower triangular matrix $(D-\omega L)$ is Eq. (B.4) is non-singular. We can therefore write

$$Y^{(r+1)} = HX^{(r)} + \omega(D-\omega L)^{-1} G, \quad (r = 0, 1, 2, \ldots), \tag{B.19}$$

where the matrix H, which is called the Gauss-Seidel matrix associated with the matrix B, is defined as

$$H = (D-\omega L)^{-1}\left\{(1-\omega)\, D+\omega U\right\} . \tag{B.20}$$

If we define error matrices $\Delta^{(r)} = \left[\delta_p^{(r)}\right]$, $(p = 1, 2, \ldots, 2M)$ by

$$\Delta^{(r)} = Y^{(r)} - Y \quad , \qquad r = 0, 1, 2, \ldots, \tag{B.21}$$

then from Eq. (B.4) we obtain

$$\Delta^{(r)} = H\Delta^{(r-1)} = \ldots = H^{(r)}\,\Delta^{(o)} \quad , \quad r = 0, 1, 2, \ldots \tag{B.22}$$

The matrix H is of course convergent $\lim_{r\to\infty} H^{(r)} = 0$ since $\lim_{r\to\infty} Y^{(r)} = Y$. However the rate of convergence is a function of ka, θ_o, M and ω, and due to its complicated expression, it is difficult to see its behavior until some actual results of the numerical computation are available. As we can see

from Eq. (B.22), the error matrix for r iterations depends not only on the matrix H but also on the initial error matrix $\Delta^{(o)}$, which is unknown. Eq. (B.22) is not therefore convenient for determining the number of iterations to give a reasonably good approximation to the solution of Eq. (B.1).

To determine the number of iterations desired for a certain error criterion, we consider the total square error $\mathcal{E}_M$. By using the same notation as in Eq. (2.63), Eq. (2.60) can be manipulated to give

$$\mathcal{E}_M = \frac{3}{8}\frac{1}{(ka)^2}\left\{(ka)^2\left(\frac{4}{3}+\cos\theta_o+\frac{1}{3}\cos^3\theta_o\right)\right.$$

$$\left.-\sum_{p=1}^{2M}\mathrm{Re}\left[y_p^*\left(2g_p-\sum_{q=1}^{2M}b_{pq}\,y_q\right)\right]\right\}. \qquad \text{(B.23)}$$

When the solution of Eq. (B.1) is approximated by the r^{th} iterative solution, the corresponding square error $\mathcal{E}_M^{(r)}$ follows from Eq. (B.23) on replacing the x_p's by $x_p^{(r)}$'s, and is

$$\mathcal{E}_M^{(r)} = \frac{3}{8}\frac{1}{(ka)^2}\left\{(ka)^2\left(\frac{4}{3}+\cos\theta_o+\frac{1}{3}\cos^3\theta_o\right)\right.$$

$$\left.-\sum_{p=1}^{2M}\mathrm{Re}\left[y_p^{(r)*}\left(2g_p-\sum_{q=1}^{2M}b_{pq}\,y_q^{(r)}\right)\right]\right\}. \qquad \text{(B.24)}$$

We are now able to specify the number of iterations by applying an error criterion to $\mathcal{E}_M^{(r)}$. Thus, for example, we might allow

$$0 \le \left(\mathcal{E}_M^{(r-1)}-\mathcal{E}_M^{(r)}\right)/\,\mathcal{E}_M^{(r-1)} < \alpha_1 \qquad \text{(B.25)}$$

where α_1 is a given small quantity by which the accuracy of the computed results can be decided.

APPENDIX C

SERIES REPRESENTATION OF EDGE SINGULARITY
Derivation of Eqs. (2.72) and (2.73)

In this appendix, Eqs. (2.72) and (2.73) are derived starting from the series expression (Magnus et al, 1966)

$$\Gamma\left(\frac{1}{2}-\mu\right) \sum_{n=0}^{\infty} P_n^{\mu}(\cos\theta) \cos\left[\left(n+\frac{1}{2}\right)\theta_o\right] = \begin{cases} \sqrt{\frac{\pi}{2}} \sin^{\mu}\theta (\cos\theta_o - \cos\theta)^{-\mu-1/2}, & 0 \le \theta_o < \theta \\ 0, & \theta < \theta_o < \pi \end{cases}$$

$$0 < \theta < \pi, \qquad \mathrm{Re}\{\mu\} < \frac{1}{2}. \tag{C.1}$$

When $\mu = -1$, using the relations

$$P_n^{-1}(\cos\theta) = \frac{1}{n(n+1)} P_n^1(\cos\theta),$$

$$\sin\theta\, P_o^{-1}(\cos\theta) = \int_{\cos\theta}^{1} P_o(x)\, dx,$$

Eq. (C.1) can be reduced to

$$\left(\frac{P_1^1}{\sin\theta} - \frac{P_2^1}{3\sin\theta}\right) \cos\frac{\theta_o}{2} + \sum_{n=1}^{\infty} \frac{1}{n(n+1)} \sin\theta\, P_n^1(\cos\theta) \cos\left[\left(n+\frac{1}{2}\right)\theta_o\right]$$

$$= \begin{cases} \sqrt{2(\cos\theta_o - \cos\theta)}, & 0 < \theta_o < \theta \\ 0, & \theta < \theta_o < \pi \end{cases} \tag{C.2}$$

$$0 < \theta < \pi.$$

Furthermore, substituting the recurrence relation

$$\frac{1}{n(n+1)} \sin\theta \; P_n^1(\cos\theta) = \frac{1}{2n+1}\left[\frac{2(2n+1)}{(2n-1)(2n+3)} \frac{P_n^1(\cos\theta)}{\sin\theta} - \right.$$

$$\left. - \frac{1}{2n-1} \frac{P_{n-2}^1(\cos\theta)}{\sin\theta} - \frac{1}{2n+3} \frac{P_{n+2}^1(\cos\theta)}{\sin\theta}\right],$$

into Eq. (C.2) and rearranging terms we obtain

$$\sum_{n=1}^{\infty} \gamma_n \frac{P_n^1(\cos\theta)}{\sin\theta} = \begin{cases} 0 & , \quad 0 < \theta < \theta_o \\ \sqrt{2(\cos\theta_o - \cos\theta)}, & \theta_o < \theta < \pi \end{cases} \tag{C.3}$$

where

$$\gamma_n = \frac{2}{(2n-1)(2n+3)} \cos\left(n+\frac{1}{2}\right)\theta_o - \frac{1}{(2n+5)(2n+3)} \cos\left(n+\frac{5}{2}\right)\theta_o$$

$$- \frac{1}{(2n-3)(2n-1)} \cos\left(n-\frac{3}{2}\right)\theta_o \tag{C.4}$$

$$n = 1, 2, \ldots$$

If Eq. (C.3) is differentiated term by term after multiplication by $\sin\theta$, we have

$$\sum_{n=1}^{\infty} \gamma_n \frac{\partial}{\partial\theta} P_n^1(\cos\theta) = \begin{cases} 0 & , \quad 0 < \theta < \theta_o \\ \cos\theta\sqrt{2(\cos\theta_o - \cos\theta)} + \dfrac{\sin^2\theta}{\sqrt{2(\cos\theta_o - \cos\theta)}}, & \theta_o < \theta < \pi . \end{cases} \tag{C.5}$$

However, the above differentiated series does not converge uniformly in the interval considered, and therefore Eq. (C.5) must be justified. When $\mu = 0$, Eq. (C.1) becomes

$$\sum_{n=0}^{\infty} P_n(\cos\theta)\cos\left[\left(n+\frac{1}{2}\right)\theta_o\right] = \begin{cases} 0 & , \quad 0<\theta<\theta_o \\ \dfrac{1}{\sqrt{2(\cos\theta_o-\cos\theta)}}, & \theta_o<\theta<\pi \end{cases} \quad (C.6)$$

from which, together with Eq. (C.3) we can write

$$\cos\theta \sum_{n=1}^{\infty} \gamma_n \frac{P_n^1(\cos\theta)}{\sin\theta} + \sin^2\theta \sum_{n=0}^{\infty} P_n(\cos\theta)\cos\left[\left(n+\frac{1}{2}\right)\theta_o\right]$$

$$= \begin{cases} 0 & , \quad 0<\theta<\theta_o \\ \cos\theta\sqrt{2(\cos\theta_o-\cos\theta)} + \dfrac{\sin^2\theta}{\sqrt{2(\cos\theta_o-\cos\theta)}}, & \theta_o<\theta<\pi. \end{cases} \quad (C.7)$$

Again, by making use of the recurrence relations

$$\sin^2\theta\, P_n(\cos\theta) = -\frac{1}{2n+1}\left[\frac{2(2n+1)}{(2n-1)(2n+3)} P_n^2(\cos\theta) - \frac{1}{2n-1} P_{n-2}^2(\cos\theta) - \frac{1}{2n+3} P_{n+2}^2(\cos\theta)\right],$$

$$P_n^{m+1}(\cos\theta) = m\cos\theta \frac{P_n^m(\cos\theta)}{\sin\theta} - \frac{\partial}{\partial\theta} P_n^m(\cos\theta),$$

it can be shown that the left-hand side of Eq. (C.7) reduces to that of Eq. (C.5), and, hence, Eq. (C.5) is verified. In the neighborhood of $\theta = \theta_o$, Eq. (C.5) behaves as $0\left(1/\sqrt{\theta-\theta_o}\right)$ if $\theta > \theta_o$, and the series is properly divergent at $\theta = \theta_o$.

Let us now replace θ_o and θ, respectively by $\pi-\theta_o$ and $\pi-\theta$, and substitute into Eqs. (C.3) and (C.5). Since

$$\cos\left[\left(n+\frac{1}{2}\right)(\pi-\theta_o)\right] = (-1)^n \sin\left[\left(n+\frac{1}{2}\right)\theta_o\right]$$

and

$$P_n^1\left[\cos(\pi-\theta)\right] = (-1)^{n+1}\ P_n^1(\cos\theta)\ ,$$

Eqs. (C.3) and (C.5) lead to, respectively,

$$\sum_{n=1}^{\infty} \delta_n \frac{P_n^1(\cos\theta)}{\sin\theta} = \begin{cases} -\sqrt{2(\cos\theta - \cos\theta_o)}, & 0 < \theta < \theta_o \\ 0 \quad , & \theta_o < \theta < \pi \ , \end{cases} \tag{C.8}$$

$$\sum_{n=1}^{\infty} \delta_n \frac{\partial}{\partial\theta} P_n^1(\cos\theta) = \begin{cases} -\cos\theta\sqrt{2(\cos\theta-\cos\theta_o)} + \dfrac{\sin^2\theta}{\sqrt{2(\cos\theta-\cos\theta_o)}}, \\ \qquad\qquad 0 < \theta < \theta_o \\ 0 \quad , \qquad \theta_o < \theta < \pi \ , \end{cases} \tag{C.9}$$

where

$$\delta_n = \frac{2}{(2n-1)(2n+3)} \sin\left(n+\frac{1}{2}\right)\theta_o - \frac{1}{(2n+5)(2n+3)} \sin\left(n+\frac{5}{2}\right)\theta_o$$

$$- \frac{1}{(2n-3)(2n-1)} \cos\left(n-\frac{3}{2}\right)\theta_o \tag{C.10}$$

$$n = 1, 2, \ldots$$

APPENDIX D

COMPUTER PROGRAM

1. Main Computer Program

This program computes:

a) all the matrix elements a_{pq}'s and f_p's $(p,q = 1,2,\ldots,2M+2)$ in Eq. (2.85),

b) x_q's $(q = 1,2,\ldots, 2M+2)$ after inverting the matrix $[a_{pq}]$ by enlargement method (Guttman, 1946),

c) the total tangential electric field components $E_\theta(a,\theta,0)$ and $E_\phi(a,\theta,\frac{\pi}{2})$, and the surface field components $T_1^{II}(\theta)$ and $T_2^{II}(\theta)$ for $\theta = 0\ (5)\ 180$ degrees,

and d) the backscattering cross section and error, ε_M,

for given θ_o, M, ka and IDM, where IDM is the maximum number of terms retained in the computation of the matrix elements, a_{pq}'s and f_p's. All the computations in the main and related subroutines are carried out in double-precision mode.

List of the Main Program

```
$RUN *FORTRAN PAR=MAP
      IMPLICIT REAL*8 (A-Z)
      COMMON/DIM/IAX
      INTEGER N,IDM,IDM2,INVAL,M,M1,M2,N2,IRW,NO,IER,J1,IAX,MEXACT
      COMPLEX*16 T1TEMP,T2TEMP,T1,T2,TEMP1,SUM1,SUM2,SUM3,SUM4
      COMPLEX*16 XPZP(40),XPPZ(40),GPZPI(200),DZZP(200)
      COMPLEX*16 AX(82,82),ANVRS(82,82),SSUM1,SSUM2,S1S,GPZ(200)
       COMPLEX*16 FV(82),CTERM,TT,AN(200),ZET(200),ZETP(200),X(82)
      COMPLEX*16 TEMP,EST,ESP,MINUSI,ESUM1,ESUM2,XPZ(40),XPPZP(40)
      DIMENSION P1(200),DP1(200),LX(200,200), IN(200)
      DIMENSION PSIN(200),PSINP(200)
      COMPLEX*16 ETT,ETP
      LOGICAL BOOD,BOOZ,BOOF,BOOB
      NAMELIST /NAM/ M,IDM,IDM2
      NAMELIST /LOG/BOOD,BOOF,BOOB
      NAMELIST /JKA/ KA,M,BOOZ,BOOF
      NAMELIST/LUP/M,IRW,NO
      DATA PI/3.14159265358979/
      IAX=82
C
      MINUSI=DCMPLX(0.D0,-1.D0)
C     PHI=0.
      BOOD=.FALSE.
      BOOF=.FALSE.
      BOOF=.FALSE.
      BOOB=.FALSE.
      BOOZ=.FALSE.
      DP=3.14159265358979/180.D0
      TTA=30.D0
      READ (5,LOG)
 10   CONTINUE
      READ (5,NAM)
      WRITE (6,NAM)
```

```
      INVAL=1
      THETA =TTA*DP
      COSO=DCOS(THETA)
C
9     READ (5,JKA,END=8)
      WRITE (6,JKA)
      CALL DATA(THETA,M,IDM,P1,DP1,IN,LX,BOOD)
C
      CALL FSH(KA,THETA,MEXACT,IDM,ZET,ZETP,PSIN,PSINP, W,W1,BOOZ)
      CALL ACOEF(AN,THETA,IDM)
C
      M2=2*M +2
      M1=2*M+1
C
      IF (BOOF) WRITE (6,720) M2
720   FORMAT (' FV(1)...FV('I2,')')
      CALL FFUN(FV,1.D-8, M,IDM,MEXACT,PSIN,PSINP,P1,LX,BOOF,AN,ZET,&8)
C
89    READ (5,LUP,END=88)
      WRITE (6,LUP)
      CALL AMTRX(AX,MEXACT,M,IDM,IDM2,PSIN,PSINP,ZET,ZETP,LX,AN,P1,
     C BOOB)
      NO=0
      CALL DCIBYE(AX,ANVRS,IRW,IAX,NO,IER)
750   FORMAT ('  AX('I2,','I2,')='2D18.9,'   AX('I2,','I2,')='2D18.9)
      DO 70 N=1,IDM2
      X(N)=(0.D0,0.D0)
```

```
      DO 70 J1=1,IDM2
70    X(N)= X(N)+ANVRS(N,J1)*FV(J1)
      PRINT 498,IDM2
498   FORMAT ('     X(1)...X('I2,')')
      DO 100 N=1,IDM2,2
      N2=N+1
      PRINT 499,N,X(N),N2,X(N2)
499   FORMAT ('       ',I2,2D20.9,5X,I2,2D20.9)
100   CONTINUE
C     COMPUTATIN OF E S THETA AND E S PHI
      DO 315 N=1,MEXACT
      N2=N*2
      GAM=AN(N)
      IF (N.GT. M) GO TO 3155
      XPZ(N)=X(2*N-1)*PSIN(N)*ZET(N)
      XPPZP(N)= X(2*N)*PSINP(N)*ZETP(N)
      XPZP(N)=X(N2-1) *PSIN(N)*ZETP(N)
      XPPZ(N)=X(N2)*PSINP(N)*ZET(N)
3155  GPZ(N)=GAM*PSIN(N)*ZET(N)
      GPZPI(N)=GAM*(PSIN(N)*ZETP(N)+DCMPLX(0.D0,.5D0))
      DEL=AN(N)*MINUSI
      DZZP(N)=DEL*ZET(N)/ZETP(N)
315   CONTINUE
      NO=MEXACT+1
      DO 316 N=NO,IDM
      GAM=AN(N)
316   GPZ(N)=GAM*MINUSI*ZET(N)
      PRINT 504
504   FORMAT('0',3X,'THETA',7X,'MOD ETT',7X,'MOD ETP',7X,'MOD T1',7X,'PH
     CASE T1',7X,'MOD T2',7X,'PHASE T2')
      THETA=0.D0
      KA2=KA*KA
      DO 80 J1=1,37
```

```
      ANG=THETA*DP
      SINE=DSIN(ANG)
      COSINE=DCOS(ANG)
      PREV=0.D0
      SSUM1=(0.D0,0.D0)
      SSUM2=SSUM1
      ESUM1=SSUM1
      ESUM2=SSUM1
      SUM1=(0.D0,0.D0)
      SUM2=(0.D0,0.D0)
      SUM3=(0.D0,0.D0)
      SUM4=(0.D0,0.D0)
      T1TEMP=(0.D0,0.D0)
      T2TEMP=(0.D0,0.D0)
      TSUM1=0.D0
      TSUM2=0.D0
      TSUM3=0.D0
      TSUM4=0.D0
      DO 81 N=1,IDM
      EN=N
      N2=2*N
      FN2=N2
      CALL LEGEN(N,ANG,P,P1N)
      IF (ANG.EQ.0.D0) GO TO 82
      IF (DABS(ANG-PI).LE.1.D-8) GO TO 83
      P1SIN=P1N/SINE
      DP1N=EN*COSINE*P1SIN-(EN+1.D0)*PREV
```

```
      GO TO 84
82    DP1N=EN*(EN+1.D0)/2.D0
      P1SIN=DP1N
      GO TO 84
83    DP1N=((-1)**N)*EN*(EN+1.D0)/2.D0
      P1SIN=-DP1N
84    PREV=P1SIN
      IF (N.GT.M) GO TO 85
      SSUM1=XPZ(N)*P1SIN+XPPZP(N)*DP1N+SSUM1
      ESUM1=XPZ(N)*DP1N+XPPZP(N)*P1SIN+ESUM1
      T1TEMP=T1TEMP+XPZP(N)*DP1N-XPPZ(N)*P1SIN
      T2TEMP=T2TEMP+XPZP(N)*P1SIN-XPPZ(N)*DP1N
85    SSUM2=GPZ(N)*P1SIN+SSUM2
      ESUM2=ESUM2+GPZ(N)*DP1N
      IF (N.GT.MEXACT) GO TO 861
      SUM1=SUM1+GPZPI(N)*DP1N
      SUM2=SUM2+DZZP(N)*P1SIN
      SUM3=SUM3+GPZPI(N)*P1SIN
      SUM4=SUM4+DZZP(N)*DP1N
      GO TO 81
861   GAM=AN(N)
      TERM =GAM/(FN2+1.D0)*(.5D0+3.D0*KA2/(( FN2-1.D0) *(FN2+3.D0)) *
     C (1.D0+5.D0*KA2/((FN2-3.D0)*(FN2+5.D0))))
      TSUM1=TSUM1+TERM*DP1N
      TSUM3=TSUM3+TERM*P1SIN
      DEL=AN(N)*MINUSI
      TERM=DEL/EN*(1.D0 +KA2/(2.D0*EN*EN-EN) *(1.D0+3.D0*(EN-1.D0) *KA2/
     C (EN*(FN2-1.D0)*(FN2-3.D0))))
      TSUM2=TSUM2+TERM*P1SIN
      TSUM4=TSUM4+TERM*DP1N
81    CONTINUE
       CTERM=(0.D0,0.D0)
      TEMP=CTERM
```

```
      IF (THETA .GE. TTA) GO TO 90
      ROOT=DSQRT(2.D0*(COSINE-COSO))
      CTERM=X(M2)*(SINE*SINE/ROOT-COSINE*ROOT)
      TEMP=X(M2)*ROOT
90    EST=(SSUM1+X(M1)*SSUM2+CTERM)/KA
      ESP=-(ESUM1+X(M1)*ESUM2-TEMP)/KA
      ANG=KA*COSINE
      TEMP=DCMPLX(DCOS(ANG),DSIN(ANG))
      ETT=COSINE*TEMP+EST
      ETP=ESP-TEMP
      REAL=ETT
      IMAG=ETT*MINUSI
      MOD1=DSQRT(REAL*REAL+IMAG*IMAG)
      REAL=ETP
      IMAG=ETP*MINUSI
      MOD2=DSQRT(REAL*REAL+IMAG*IMAG)
505   FORMAT (' ',F8.0,2(2X,2D18.9,F10.5))
      CTERM=(0.D0,0.D0)
      TEMP1=(0.D0,0.D0)
      IF (THETA .LE. TTA) GO TO 901
      ROOT=DSQRT(2.D0*(COSO-COSINE))
      CTERM=DCMPLX(0.D0,.5D0)*(COSINE*ROOT+SINE*SINE/ROOT)
      TEMP1=DCMPLX(0.D0,.5D0)*ROOT
901   SUM1=SUM1+DCMPLX(0.D0,1.D0)*TSUM1-CTERM
      SUM2=SUM2-KA*TSUM2
      SUM3=SUM3+DCMPLX(0.D0,1.D0)*TSUM3-TEMP1
      SUM4=SUM4-KA*TSUM4
```

```
      T1=-COSINE*TEMP+DCMPLX(0.D0,1.D0)*(T1TEMP+  X(M1)*SUM1-X(M2)
     C *SUM2)/KA
      T2=-TEMP+DCMPLX(0.D0,1.D0)*(T2TEMP+ X(M1)*SUM3-X(M2)*SUM4)/KA
      REAL =T1
      IMAG=T1*MINUSI
      MODT1=DSQRT(REAL*REAL+IMAG*IMAG)
      PHASE1=DATAN2(IMAG,REAL)*180.D0/PI
      REAL=T2
      IMAG=T2*MINUSI
      MODT2=DSQRT(REAL*REAL+IMAG*IMAG)
      PHASE2=DATAN2(IMAG,REAL)*180.D0/PI
      PRINT 506,THETA,MOD1,MOD2,MODT1,PHASE1,MODT2,PHASE2
  506  FORMAT (' ',F8.0,3(5X,F10.5),5X,F8.3,5X,F10.5,5X,F8.3)
  80  THETA=THETA+5.D0
  C   COMPUTATION OF SIGMA/(PI*A*A)
      SSUM1=(0.D0,0.D0)
      SSUM2=SSUM1
      TT=(1.D0,0.D0)
      DO 313 N=1,MEXACT
      EN=N
      TT=TT*(0.D0,1.D0)
      EN1=EN*(EN+1.D0)/2.D0
      GAM=AN(N)
      DEL=AN(N)*DCMPLX(0.D0,-1.D0)
      CTERM=X(M1)*GAM*PSIN(N)    ,
      TEMP=X(M2)*DEL/ZETP(N)
      SSUM2=SSUM2+TT*EN1*(CTERM-TEMP*DCMPLX(0.D0,1.D0))
      IF (N.GT. M) GO TO 313
      N2=2*N
      CTERM=X(N2-1)*PSIN(N)
      TEMP=X(N2)*PSINP(N)
      SSUM1=SSUM1+TT*EN1*(CTERM-TEMP*DCMPLX(0.D0,1.D0))
  313 CONTINUE
```

```
      S1S=SSUM1+SSUM2
      TERMR=S1S
      TERMI=S1S*DCMPLX(0.D0,-1.D0)
      SIGPI=4.D0*(TERMR*TERMR+TERMI*TERMI)/(KA*KA)
C     COMPUTATION OF EM
      SUM=0.D0
      DO 314 N=1,M
      N2=N*2
      CTERM=X(N2-1)*PSIN(N)*ZET(N)*DCONJG(FV(N2-1))+X(N2)*PSINP(N)
     C *ZETP(N)*DCONJG(FV(N2))
      TERMR=CTERM
      SUM=SUM+TERMR
314   CONTINUE
      CTERM=X(M1)*DCONJG(FV(M1))
      TERMR=CTERM
      EM=W*(1.0D0/W1 -(SUM+TERMR))
      PRINT 500,SIGPI,EM
500   FORMAT ('0      SIGMA ='D17.9,'     EM ='D17.9)
88    GO TO 10
C
8     CONTINUE
      CALL SYSTEM
      END
$ENDFILE
$RUN -LOAD#+S446:CHNGSUBOBJ+S446:SUBOBJ+S446:SUMS+S446:LEGN MAP *SINK*
5=*SOURCE* 6=*SINK* 7=*SINK*
 &LOG BOOD=.FALSE., BOOB=.FALSE. &END
 &NAM M=10, IDM=200, IDM2=22 &END
 &JKA KA=1.D0, M=10, BOOZ=.FALSE. &END
 &LUP M=10,IRW=22,NO=0 &END
$ENDFILE
$SIG
```

2. Subroutines

Subroutines used are as follows:

a) SUBROUTINE DATA

This gives $P_n^1(\cos\theta_o)$, $L_{mn}(\theta_o)$ and $I_n^1(\theta_o)$ for all n, m = 1, 2, ...IDM.

b) SUBROUTINE FSH

$\psi_n(ka)$, $\psi_n'(ka)$, $\xi_n(ka)$ and $\xi_n'(ka)$ are computed from the spherical Hankel functions (calling SUBROUTINE HANKLF) for all n such that $\left|\mathcal{J}_n(ka)\right| > 10^{-50}$. For larger values of n up to n = IDM, $\left[j\psi_n(ka)\xi_n(ka)\right]$ and $\left[j\psi_n'(ka)\xi_n'(ka)\right]$ are approximated by

$$\left[j\psi_n(x)\xi_n(x)\right] \sim \frac{x}{2n+1}\left\{1 - \frac{1}{1!(2n+3)}\left(\frac{x^2}{2}\right) + \frac{1}{2!(2n+3)(2n+5)}\left(\frac{x^2}{2}\right)^2 - \right.$$

$$\left. - \frac{1}{3!(2n+3)(2n+5)(2n+7)}\left(\frac{x^2}{2}\right)^3\right\} \times$$

$$\times\left\{1 + \frac{1}{1!(2n-1)}\left(\frac{x^2}{2}\right) + \frac{1}{2!(2n-1)(2n-3)}\left(\frac{x^2}{2}\right)^2 + \right.$$

$$\left. + \frac{1}{3!(2n-1)(2n-3)(2n-5)}\left(\frac{x^2}{2}\right)^3\right\},$$

and

$$\left[j\psi_n'(x)\,\xi_n'(ka)\right] \sim -\frac{1}{(2n+1)}\left\{(n+1) - \frac{(n+3)}{1!(2n+3)}\left(\frac{x^2}{2}\right) + \frac{(n+5)}{2!(2n+3)(2n+5)}\left(\frac{x^2}{2}\right)^3 - \right.$$

$$\left. - \frac{(n+7)}{3!(2n+3)(2n+5)(2n+7)}\left(\frac{x^2}{2}\right)^3\right\} \times$$

$$\times\left\{n + \frac{(n-2)}{1!(2n-1)}\left(\frac{x^2}{2}\right) + \frac{(n-4)}{2!(2n-1)(2n-3)}\left(\frac{x^2}{2}\right)^2 + \right.$$

$$\left. + \frac{(n-6)}{3!(2n-1)(2n-3)(2n-5)}\left(\frac{x^2}{2}\right)^3\right\} .$$

c) SUBROUTINE ACOEF

This computes γ_n and δ_n ($n = 1, 2, \ldots$ IDM) given in Eqs. (C.4) and (C.10) respectively.

d) SUBROUTINE AMTRX and SUBROUTINE FFUN

Subroutines AMTRX and FFUN give the matrix elements a_{pq}'s and f_p's, respectively, for $p, q = 1, 2, \ldots$ 2M+2. The maximum number of terms retained in the sum is given by IDM.

e) SUBROUTINE DCIBYE, SUBROUTINE LEGEN and SUBROUTINE HANKLF.

Subroutine DCIBYE inverts a given complex matrix by enlargement method. Subroutines LEGEN and HANKLF give the Legendre functions, $P_n(\cos\theta)$ and $P_n^1(\cos\theta)$, and spherical Hankel functions (the first or the second kind) respectively. All three subroutines were previously developed at the Radiation Laboratory, University of Michigan and had been used as standard subroutines. The list of those three subroutines is therefore not given here.

List of Subroutines

```
      SUBROUTINE DATA(THTA,M,IDM,P1,DP1,IN,LX,BOO)
C
      IMPLICIT REAL*8 (A-Z)
      INTEGER M,I,L,ILD,FILD,JLD ,IDM
      LOGICAL BOO
      DIMENSION LX(IDM,IDM),            P1(IDM),DP1(IDM),IN(IDM)
C
      X=DCOS(THTA)
      SN=DSIN(THTA)
      HLD=0.D0
      DO 1 I=1,IDM
      FI=I
      CALL LEGEN(I,THTA,PN,P1(I))
       IF (THTA .EQ. 0.D0) GO TO 10
      IF(DABS(THTA-3.14159265358979) .LE. 1.D-8) GO TO 11
      PP=P1(I)/SN
      DP1(I)=FI*X*PP-(FI+1.)*HLD
      GO TO 9
10    DP1(I)=I*(I+1.D0)/2.D0
      GO TO 9
11    DP1(I)=((-1)**I)*I*(I+1.D0)/2.D0
9     IF (BOO) WRITE (6,600) I,P1(I),DP1(I)
1     HLD=PP
600   FORMAT ('      I='I2,' P1='D16.9,'  DP1='D16.6)
C
      IN(1)=(2.-3.*X+X*X*X)/3.
      DO 3 I=2,IDM
      FI=I
      ILD=I+1
      FILD=ILD
      JLD=I-1
      FJLD=JLD
      IN(I)=((2.*FI-1.)*FILD*IN(JLD)-X*(FILD*P1(JLD)*P1(JLD)+FJLD*P1(I)
```

```
     C *P1(I))+2.*FI*P1(I)*P1(JLD))/((2.*FI+1.)*FJLD)
3    CONTINUE
     IF (BOO) WRITE (6,615) IDM
615  FORMAT ('-IV(1)...IV('I2,')')
     IF (BOO) WRITE (6,610)(IN(I),I=1,IDM)
610  FORMAT (' '3D19.9)
C
     DO 4 I=1,IDM
     FI=I
     DO 4 L=1,I
     FL=L
     IF (I.EQ.L) GO TO 5
     LX(I,L)=SN*(FI*(FI+1.)*P1(I)*DP1(L)-FL*(FL+1.)*P1(L)*DP1(I))/((FI-
    1FL)*(FI+FL+1.))
     LX(L,I)=LX(I,L)
     GO TO 4
5    LX(I,I)=SN*P1(I)*DP1(I)+FI*(FI+1.)*IN(I)
4    CONTINUE
     IF (BOO) WRITE (6,625) IDM,IDM
625  FORMAT ('-LX(1,1)...LX('I2,','I2,')')
     IF (BOO) WRITE (6,610)((LX(I,L),L=1,IDM),I=1,IDM)
C
     RETURN
     END
```

```
      SUBROUTINE FSH(KA,THETA,M,IDM,ZET,ZETP,PSIN,PSINP,W,W1,BOO)
C
      IMPLICIT REAL*8 (A-Z)
      INTEGER M,IDM,I
      INTEGER N,NN
      COMPLEX*16 ZET,ZETP
      LOGICAL BOO
      DIMENSION ZET(IDM),ZETP(IDM),PSIN(IDM),PSINP(IDM)
C
      KA22=KA*KA/2.DO
      HLDJ=DSIN(KA)/KA
      HLDY=-DCOS(KA)/KA
      DO 6 I=1,IDM
      FI=I
      CALL HANKLF(2,I,KA,JV,YV)
      IF (DABS(JV) .LE. 1.D-50) GO TO 91
      ZET(I)=KA*DCMPLX(JV,-YV)
      PSIN(I)=KA*JV
      PSINP(I)=KA*HLDJ-FI*JV
      ETANP=-KA*HLDY+FI*YV
      ZETP(I)=DCMPLX(PSINP(I),ETANP)
      IF (BOO) WRITE (6,630) I,ZET(I),ZETP(I)
630   FORMAT ('0I='I2,'  ZET(I)='2D17.9,/'        ZETP(I)='2D17.9)
      HLDJ=JV
6     HLDY=YV
91    M=I-1
      PRINT 399,M,ZET(M),ZETP(M)
399   FORMAT ('0',1X,'LAST EXACT N ='I4,2X,'  ZET(N) =',2D18.10,2X,
     C '  ZETP(N) ='2D18.10)
      DO 95 N=I,IDM
      EN=N
      TERM1=1.DO
      TERM2=1.DO
```

```
      SIGN=-1.D0
      SUM1=1.D0
      SUM2=1.D0
      SUM3=EN+1.D0
      SUM4=EN
      DO 92 NN=1,3
      EP=2.D0*NN+1.D0
      EM=2.D0*NN-1.D0
      TERM1=TERM1*KA22/(NN*(2.D0*EN+EP))
      SUM1=SUM1+SIGN*TERM1
      SUM3=SUM3+SIGN*(EN+EP)*TERM1
      SIGN=-SIGN
      TERM2=TERM2*KA22/(NN*(2.D0*EN-EM))
      SUM2=SUM2+TERM2
      SUM4=SUM4+(EN-2.*NN)*TERM2
      SIGN=SIGN
92    CONTINUE
        ZET(N)=DCMPLX(       KA*SUM1*SUM2/(2.D0*EN+1.D0),0.D0)
        ZETP(N)=DCMPLX(      -SUM3*SUM4/(KA*(2.D0*EN+1.D0)),0.D0)
      IF (N.EQ. I) PRINT 400,N,ZET(N),ZETP(N)
400   FORMAT ('0',1X,'FIRST APPROXIMATE N ='I4,2X,'PSIRO(N) =',2D18.10,
     C2X,'PSIROP(N) ='2D18.10)
95    CONTINUE
C
      X=DCOS(THETA)
      X3=X*X*X
      W=3.D0/(8.D0*KA*KA)
      W1=KA*KA*(4.D0+3.D0*X+X3)
      W1=3.D0/W1
      IF (BOO) WRITE (6,640) W,W1
640   FORMAT ('- W='D19.10,' W1='D19.10)
      RETURN
      END
```

```
      SUBROUTINE ACOEF(A,THETA0,LIM)
      IMPLICIT REAL*8(A-H,O-Z)
      COMPLEX*16 A(LIM),TERM,B0 ,B(1000)
      DATA PI/3.141592653589 79/
      ANG0=THETA0/2.D0
      B0=DCMPLX(DCOS(ANG0),DSIN(ANG0))
      ANG0=-ANG0
      TERM=DCMPLX(DCOS(ANG0),DSIN(ANG0))
      NN0=LIM-2
      DO 20 N=1,NN0
      EN=N
      EN2=2.D0*EN
      EN23=EN2+3.D0
      IF (N.GT. (NN0-2)) GO TO 100
      ANG0=THETA0*(EN+2.5D0)
      B(N+2)=DCMPLX(DCOS(ANG0),DSIN(ANG0))
      IF (N.GT. 2) GO TO 99
      IF (N.EQ. 2) TERM=B0
      ANG0=(EN+.5D0)*THETA0
      B(N  )=DCMPLX(DCOS(ANG0),DSIN(ANG0))
      A(N)=DCMPLX(2.D0,0.D0)*B(N)/((EN2-1.D0)*EN23)-B(N+2)/((EN2+5.D0)*
     C EN23)-TERM/((EN2-3.D0)*(EN2-1.D0))
      GO TO 20
 99   A(N)= DCMPLX(2.D0,0.D0) *B(N)/((EN2-1.D0)*EN23) -B(N+2)/((EN2+5.D0
     C)*EN23)-B(N-2)/((EN2-3.D0)* (EN2-1.D0))
      GO TO 20
 100  A(N)= DCMPLX(2.D0,0.D0)*B(N)/((EN2-1.D0)*EN23) -B(N-2) /((EN2-3.D0
     C )*(EN2-1.D0))
      A(N+2) =-B(N)/((EN2+1.D0)*EN23)
 20   CONTINUE
      RETURN
      END
```

```
      SUBROUTINE AMTRX(AX,MEXACT,M,LIM,IDM2,PSIN,PSINP,ZET,ZETP,LX,
     C A,P1,BOO2)
      IMPLICIT REAL*8 (A-H,O-Z)
      COMMON/DIM/IAX
      REAL*8 LX
      COMPLEX*16 ZET(LIM),ZETP(LIM),CCP,CCP1,CCPZ,CCPZ1,CG,CGP,
     C PAR, PAR1, AX(IAX,IAX), A(LIM),PZ,PZP,DELC,KOEFC
      COMPLEX*16 TERM(1002),TERML(1002),TERMJ(1002),TERMP(1002)
      DIMENSION PSIN(LIM),PSINP(LIM),LX(LIM,LIM),P1(LIM)
      COMPLEX*16 SUM21,SUM22,SUMP,SUMD,CON1,CON2,CON,MINUSI
      LOGICAL BOO2
C
      MINUSI=DCMPLX(0.DO,-1.DO)
      M21=2*M+1
      M22=2*M+2
      DO 5 L=1,MEXACT
      GAM=A(L)
      DEL=A(L)*MINUSI
      DELC=DCMPLX(DEL,0.DO)
      TERML(L)=GAM*PSIN(L)*ZET(L)
      TERMP(L)=DELC/(PSINP(L)*ZETP(L))
      TERMJ(L)=DCONJG(TERML(L))
      TERM(L)=DCONJG(TERMP(L))
5     CONTINUE
      M1E=MEXACT+1
      DO 6 L=M1E,LIM
      GAM=A(L)
      DEL=A(L)*MINUSI
      ZETR=ZET(L)
      ZETPR=ZETP(L)
      TERML(L)=DCMPLX(0.DO,-GAM*ZETR)
      TERMP(L)=DCMPLX(0.DO,DEL/ZETPR)
      TERMJ(L)=-TERML(L)
```

```
      TERM(L)=-TERMP(L)
6     CONTINUE
      SUMP=DCMPLX(0.D0,0.D0)
      SUMD=DCMPLX(0.D0,0.D0)
      SUM21=DCMPLX(0.D0,0.D0)
      SUM22= DCMPLX(0.D0,0.D0)
      LIM1=LIM-1
      DO 25 L=1,LIM1
      EL=L
      SUMP=SUMP+TERML(L)*PI(L)
      SUMD=SUMD+TERM(L)*PI(L)
      TERMR=TERML(L)
      TERMI=TERML(L)*MINUSI
      CON1=(TERMR*TERMR+TERMI*TERMI)*(2.D0*EL*EL*(EL+1.D0)*(EL+1.D0)
     C /(2.D0*EL+1.D0)-LX(L,L))
      TERMR=TERMP(L)
      TERMI=TERMP(L)*MINUSI
      CON2=(TERMR*TERMR+TERMI*TERMI)*LX(L,L)
      SUMJ2=0.D0
      SUMJ=0.D0
      JAY=L+1
      DO 255 J=JAY,LIM
      CON=TERML(L)*TERMJ(J)*LX(J,L)
      TERMR=CON
      SUMJ=SUMJ+TERMR
      CON=TERMP(L)*TERM(J)*LX(J,L)
      TERMR=CON
```

```
      SUMJ2=SUMJ2+TERMR
255   CONTINUE
      SUM21=SUM21+CON1-2.D0*SUMJ
      SUM22=SUM22+CON2+2.D0*SUMJ2
25    CONTINUE
C   A(2M+1,2M+1)
      AX(M21,M21)=SUM21
C   A(2M+2,2M+2)
      AX(M22,M22)=SUM22
C   A(2M+1,2M+2)
      AX(M21,M22)=DCMPLX(0.D0,0.D0)
C   A(2M+2,2M+1)
      AX(M22,M21)=AX(M21,M22)
      DO 22 IM=1,M
      FM=IM
      MB=2 *IM
      MB1=MB-1
      CC=2.D0*FM*FM*(FM+1.D0)*(FM+1.D0)/(2.D0*FM+1.D0)
      CCPZ1=CC*PSIN(IM)*ZET(IM)
      CCPZ=CC*PSINP(IM)*ZETP(IM)
      CG=DCONJG(ZET(IM))
      CGP=DCONJG(ZETP(IM))
      KOEFC=DCMPLX(1.0D0,0.0D0)
      CON1=KOEFC/(PSIN(IM)*CG)
      CON2=KOEFC/(PSINP(IM)*CGP)
      SUM21=DCMPLX(0.D0,0.D0)
      DO 26 L=1,LIM
      SUM21=SUM21+TERML(L)*LX(IM,L)
26    CONTINUE
      GAM=A(IM)
C   A(2M-1,2M+1)
      AX(MB1,M21)=CCPZ1*GAM-SUM21
C   A(2M,2M+1)
```

```
      AX(MB,M21)=-P1(IM)*SUMP
      DO 21 N=1,M
      NB=2*N
      NB1=NB-1
      CCP=0.DO
      CCP1=0.DO
      IF (N.NE.IM) GO TO 23
      CCP=CCPZ
      CCP1=CCPZ1
   23 CONTINUE
      PZ=PSIN(N)*ZET(N)
      PZP=PSINP(N)*ZETP(N)
      PAR1=LX(IM,N)*(CON1-PZ)
      PAR=LX(IM,N)*(CON2-PZP)
C     A(2M-1,2N-1)
      AX(MB1,NB1)=CCP1+PAR1
C     A(2M,2N)
      AX(MB,NB)=CCP+PAR
C     A(2M-1,2N)
      AX(MB1,NB)=P1(IM)*P1(N)*(CON1-PZP)
C     A(2M,2N-1)
      AX(MB,NB1)=P1(IM)*P1(N)*(CON2-PZ)
C     A(2M+2,2N-1)
      AX(M22,NB1)=P1(N)*SUMD
C     A(2M+2,2N)
      SUM22=DCMPLX(0.DO,0.DO)
      DO 28 L=1,LIM1
```

```
      SUM22=SUM22+TERM(L)*LX(N,L)
 28   CONTINUE
      AX(M22,NB)=SUM22
C     A(2M+1,2N-1)
      AX(M21,NB1)=PZ*DCONJG(AX(NB1,M21))
C     A(2M+1,2N)
      AX(M21,NB)=PZP*DCONJG(AX(NB,M21))
 21   CONTINUE
C     A(2M,2M+2)
      AX(MB,M22)=CON2*DCONJG(AX(M22,MB))
C     A(2M-1,2M+2)
      AX(MB1,M22)=CON1*DCONJG(AX(M22,MB1))
 22   CONTINUE
      IF (.NOT. BOO2) GO TO 999
      DO 998 I=1,IDM2
      DO 998 J=1,IDM2,2
      J1=J+1
      PRINT 750,I,J,AX(I,J),I ,J1,AX(I ,J1)
 750  FORMAT ('  AX('I2,','I2,')='2D18.9,'    AX('I2,','I2,')='2D18.9)
 998  CONTINUE
 999  CONTINUE
      RETURN
      END
```

```
      SUBROUTINE FFUN(FV,ACC,M,IDM,MEXACT,PSIN,PSINP,P1,LX,BOOF,A,ZET,*)
C***FFUN COMPUTES FV(2*IM) AND FV(2*IM-1)
      IMPLICIT REAL*8 (A-H,O-Z)
      REAL*8 LX
      COMPLEX*16 A(IDM),ZET(IDM),FMSUM,SUM
      COMPLEX*16 FV,CTERM,CTERM1,TT,COEF,TERM,TERM1
      COMPLEX*16 TERMP,TERM1P
      LOGICAL BOOF
      DIMENSION FV(1),PSIN(IDM),PSINP(IDM),LX(IDM,IDM),P1(1)
C
      M21=2*M+1
      M22=M21+1
      FMSUM=(0.D0,0.D0)
      DO 100 IM=1,M
      FM=IM
      CTERM=(0.D0,0.D0)
      CTERM1=CTERM
      TERMP=(0.D0,0.D0)
      TERM1P=TERMP
      TT=(1.D0,0.D0)
C***MAKE SURE HAVE ENOUGH PSIN S ETC FOR THE SERIES
      DO 11 N=1,25
      FN=N
      TT=TT*(0.D0,1.D0)
      COEF=(2.*FN+1.)/(FN*(FN+1.))*TT
      FT=0.D0
      IF (IM.NE.N) GO TO 12
      FT=2.*FM*FM*(FM+1.)*(FM+1.)/(2.*FM+1.)
12    FT=FT-LX(IM,N)
      TERM1=       COEF*DCMPLX(PSIN(N)*FT,PSINP(N)* P1(IM)*P1(N))
      CTERM1=CTERM1+TERM1
      TERM =      COEF*DCMPLX(PSIN(N)*P1(IM)*P1(N),PSINP(N)*FT)
      CTERM=CTERM+TERM
```

```
      IF (((CDABS(TERM1P)+CDABS(TERM1))/CDABS(CTERM1) +(CDABS(TERMP)+
     C CDABS(TERM))/CDABS(CTERM)).LT. ACC) GO TO 60
      TERM1P=TERM1
      TERMP=TERM
 11   CONTINUE
           WRITE (6,775)
 775       FORMAT (' SERIES FOR F NOT CONVERGING')
           GO TO 8
 60   ISB=2*IM
      ISB1=ISB-1
      FV(ISB1)=-CTERM1
      FV(ISB)=CTERM
      IF (BOOF) WRITE (6,730) N,FV(ISB1),FV(ISB)
 730  FORMAT (' ',I2,' ',2D20.9,'   '2D20.9)
      GAM=A(IM)
      FMSUM=FMSUM+GAM*PSIN(IM)*DCONJG(ZET(IM))*FV(ISB1)
 100  CONTINUE
      MC=M+1
        SUM=(0.D0,0.D0)
      DO 101 IM=MC,IDM
      FM=IM
      TT=(1.D0,0.D0)
      CTERM1=(0.D0,0.D0)
      DO 13 N=1,MEXACT
      FN=N
      TT=TT*(0.D0,1.D0)
      COEF=(2.*FN+1.)/(FN*(FN+1.))*TT
```

```
      FT=0.D0
      IF (IM.NE.N) GO TO 14
      FT=2.*FM*FM*(FM+1.)*(FM+1.)/(2.*FM+1.)
14    FT = FT-LX(IM,N)
      TERM1=          COEF*DCMPLX(PSIN(N)*FT,PSINP(N)* P1(IM)*P1(N))
      CTERM1=CTERM1+TERM1
13    CONTINUE
      GAM=A(IM)
      IF (IM .GT. MEXACT) GO TO 95
      SUM=SUM+GAM*PSIN(IM)*DCONJG(ZET(IM))*CTERM1
      GO TO 101
95    SUM=SUM+GAM*DCMPLX(0.D0,1.D0)*ZET(IM)*CTERM1
101   CONTINUE
      FV(M21)=FMSUM-SUM
      FV(M22)=(0.D0,0.D0)
      IF (BOOF) WRITE (6,730) M21,FV(M21),FV(M22)
      RETURN
8     CONTINUE
      RETURN 1
      END
```

Unclassified

Security Classification

DOCUMENT CONTROL DATA - R & D

(Security classification of title, body of abstract and indexing annotation must be entered when the overall report is classified)

1. ORIGINATING ACTIVITY *(Corporate author)*
The University of Michigan Radiation Laboratory, Dept. of Electrical Engineering, 201 Catherine Street, Ann Arbor, Michigan 48108

2a. REPORT SECURITY CLASSIFICATION
UNCLASSIFIED

2b. GROUP
NA

3. REPORT TITLE
SCATTERING BY A SPHERICAL SHELL WITH A CIRCULAR APERTURE

4. DESCRIPTIVE NOTES *(Type of report and inclusive dates)*
Scientific Interim

5. AUTHOR(S) *(First name, middle initial, last name)*
Seichoong Chang
Thomas B. A. Senior

6. REPORT DATE
April 1969

7a. TOTAL NO. OF PAGES
137

7b. NO. OF REFS
32

8a. CONTRACT OR GRANT NO.
F19628-68-C-0071

b. PROJECT NO., Task, and Work Unit Nos.
5635-02-01

c. Dod Element 61102F

d. Dod Subelement 681305

9a. ORIGINATOR'S REPORT NUMBER(S)
1363-5-T
Scientific Report No. 5

9b. OTHER REPORT NO(S) *(Any other numbers that may be assigned this report)*
AFCRL-69-0203

10. DISTRIBUTION STATEMENT Nr. 1
1-Distribution of this document is unlimited. It may be released to the Clearinghouse, Department of Commerce, for sale to the general public.

11. SUPPLEMENTARY NOTES
Submitted in partial fulfillment of the requirements for a Doctorate in Electrical Engineering at The University of Michigan

12. SPONSORING MILITARY ACTIVITY
Air Force Cambridge Research Laboratories (CRD)
L. G. Hanscom Field
Bedford, Massachusetts 01730

13. ABSTRACT

The electromagnetic scattering behavior of a spherical shell with a circular aperture is studied. The shell is assumed to be perfectly conducting and infinitesimally thin, and is illuminated by a plane wave symmetrically incident upon the aperture. The application of the method of least square error, as well as of a modified version is fully discussed. The modification consists of the separating out of the appropriate surface field behavior near to the edge of the aperture, and was carried out to overcome the slow convergence and marginal accuracy of the original approach. The marked improvement provided by the modification is clearly evident.

The numerical study is limited to the frequency range corresponding to $0.8 \leq ka \leq 4.85$, where a is the radius of the spherical shell, and numerical values of the backscattering cross sections for the aperture angle $\theta_0=30^0$ and 90^0, as well as for the tangential field components over the boundary surface for $\theta_0=30^0$, are presented. To verify these results and to obtain more physical insight into the scattering behavior, experimental measurements of the backscattering cross sections for $\theta_0=15^0, 30^0, 45^0, 60^0$ and 90^0, and of the current components for $\theta_0=30^0$, are obtained using two sets of spherical shell models. It is observed that a spherical shell with aperture-on incidence has, in general, a higher backscattering cross section than a solid sphere except at values of ka near to the cavity resonances, where marked reductions occur. A comparison of the numerical and experimental results is made.

DD FORM 1 NOV 65 1473

Unclassified

Security Classification

14. KEY WORDS	LINK A		LINK B		LINK C	
	ROLE	WT	ROLE	WT	ROLE	WT
Electromagnetic Scattering						
Spherical Shell						
Aperture						
Cavity						
Impedance Loading						